Rhenium Platforms Supporting Ancillary BODIPY Moieties for the Conversion of CO_2 to CO

by

Justin James Teesdale

A thesis submitted to the Faculty of the University of Delaware in partial fulfillment of the requirements for the degree of Bachelor of Science in Chemistry with Distinction

Spring 2013

Rhenium Platforms Supporting Ancillary BODIPY Moieties for the Conversion of CO_2 to CO

by

Justin James Teesdale

Approved: _____

Joel Rosenthal, Ph.D.
Professor in charge of thesis on behalf of the Advisory Committee

Approved: _____

Donald A. Watson, Ph.D.
Committee member from the Department of Chemistry and Biochemistry

Approved: _____

Salil Lachke, Ph.D.
Committee member from the Board of Senior Thesis Readers

Approved: _____

Michelle Provost-Craig, Ph.D.
Chair of the University Committee on Student and Faculty Honors

ACKNOWLEDGMENTS

I would like to thank Joel Rosenthal for his support and teaching me things that could never be taught within a classroom. I would also like to thank Dr. Glenn P. A. Yap for his work with the X-ray crystallogrphay, Allen Pistner for his help with the initial synthesis, John DiMeglio for his aid with gas chromatography, and Gabe Andrade for his help with crystallography.

Funding was provided by the Rosenthal Research La, Howard Hughes Medical Institute, Plastino Alumni Undergraduate Research Fellowship and the University of Delaware Undergraduate Research Program.

TABLE OF CONTENTS

LIST OF FIGURES

ABSTRACT

The reduction of carbon dioxide to chemical fuels is an important challenge in the field of renewable energy conversion chemistry. Given the thermodynamic stability of carbon dioxide, it is difficult to efficiently activate this molecule in a selective fashion. Several ruthenium and rhenium polypyridyl complexes have proven to be photocatalysts for this process but suffer from poor light absorption cross sections. To address this issue, BODIPY light harvesting moieties have been incorporated onto a 2,2'-(Bipyridine)tricarbonylrhenium(I) complex. The resulting compound has been studied using a combination of optical, electrochemical, and X-ray crystallographic experiments. The appended BODIPY chromophores influence the electronic structure of the rhenium complex and the ability of this system to electrochemically promote the reduction of CO_2.

Chapter 1

INTRODUCTION

1.1 The Detrimental Nature of Fossil Fuels

It is well known that the acquisition and use of fossil fuels have been the center of political and scientific debate. Burning fossil fuels is cost efficient compared to other methods; however the present issues associated with fossil fuels are the security of acquiring these fuels and environmental impact of burning these fuels. With the majority of the world's supply of oil residing primarily outside of the United States in areas of conflict, we have begun to rely more heavily on coal and natural gas. However, the impact that burning these fuels has on the environment has caused a major push to develop alternative methods of obtaining energy.

Over the past century, atmospheric concentrations of carbon dioxide have increased exponentially showing a strong correlation with the burning of hydrocarbons.[1] Due to the strong absorbing properties of carbon dioxide in the infrared region, it is a greenhouse gases that significantly contributes most to global warming and climate change.1 Data obtained from various regions of the globe have shown that there is an obvious connection between the atmospheric concentration of carbon dioxide and the global temperature (Figure 1.1).[2]

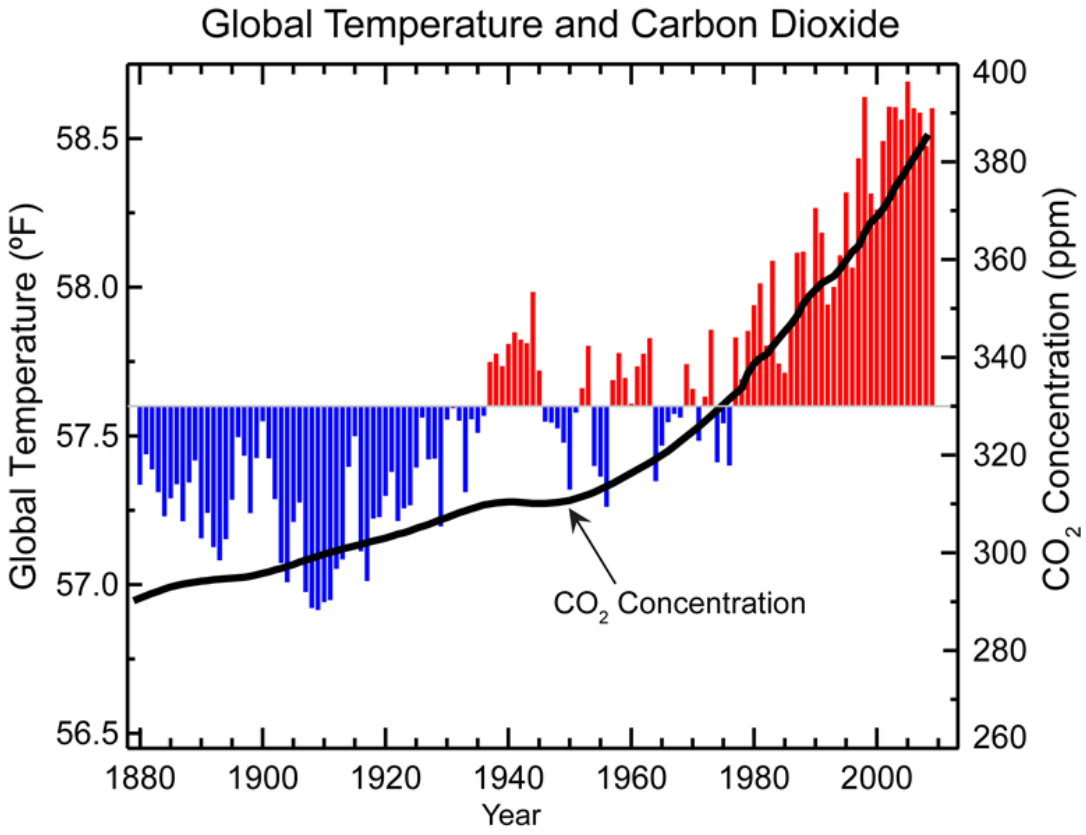

Figure 1.1: Historical Record of Atmospheric CO_2 Concentration and Global Temperature. Red bars indicate an increase from the average and blue bars indicate a decrease from the average.

Over the last 40 years, the concentration of carbon dioxide has increased by roughly 50 ppm, a 15% increase from the average over several hundred thousand years. Recent projections indicate that the concentration CO_2 in the atmosphere will surpass 400 ppm by 2013 and 500 ppm by 2050.[3]

1.2 The State of Our Energy Future

Currently global energy demand estimates exceed 14 TW[4,5] annually and is expected to increase by more than one third by 2035 as depicted in Figure 1.2.[6] With

these drastic increases in energy consumption, the world needs to decide from which source we acquire the needed energy to satisfy the projected demand.

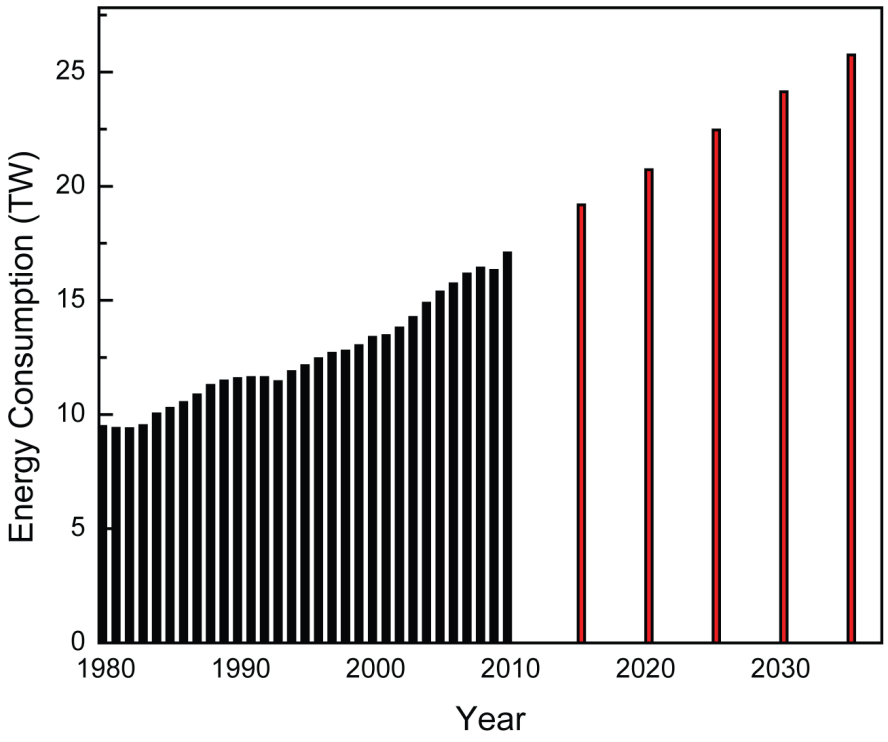

Figure 1.2: World Energy Consumption by year. Black bars are historical data and red bars are projected data. Data taken from the Annual Energy Review 2011 by the US Energy Information Administration.

Harnessing this energy from fossil fuels would be the easiest pathway as the system by which we acquire fossil fuels is already in place and the world's supply of fossil fuels is enough to last thousands of years.[7] However, the issue with fossil fuels is the impact that burning them has on the environment, as described in Section 1.1. Alternative sources such as wind, geothermal, biomass, hydroelectric, solar, etc. are promising

alternatives, yet each has their respective drawbacks. Despite the drawbacks of solar energy, the potential of this pathway as an alternative energy source far exceeds the potential of other pathways when considering the sheer amount of energy available for use.

1.3 Solar Energy as a Promising Alternative

As mentioned in Section 1.2, energy from the sun has been a focal point of scientific research for several decades. The sun produces approximately 120,000 TW of energy each year,[4] 800 TW of which fall onto Earth's landmass. Harnessing just a fraction of this energy reservoir at low to moderate efficiency would allow the world to be completely sustainable. As a result of this, much research is being done to design cost efficient systems that can harness and convert this energy for use as society's dominant power source.

Solar cells have been a topic of interest in research towards viable systems for mainstream use. Initial templates began with silicon-based cells that gave relatively low efficiencies.[8–14] Further research lead to the discovery of titanium dioxide nanoparticle scaffolds which are relatively cheap and yield respectable efficiencies.[15–25] Fine-tuning the photoexcitation cross-section via the addition of dye sensitizers continues to be a topic of interest in research today.

Being able to use this harnessed energy as a continuous power source also presents issues. Due to the intermittence of sunlight, an efficient and practical method of storage of the solar energy must be designed. Much research has been done in the area of designing efficient batteries for the storage of charge with some success;[26–34] however the most practical method, in terms of energy density, is the storage of energy in chemical bonds via transition metal catalysis.

1.4 Energy Storing via Organometallic Catalysis

The principles behind energy storing catalysis lie in the construction of the organometallic catalyst. A complex with redox properties capable of multiple electron storage is ideal for catalysis as well as selectivity for the substrate of interest. Typically, small, inert molecules such as carbon dioxide, dinitrogen, dioxygen, water, etc. are chosen as the substrate because they are cheap and abundant. Being able to generate products (liquids or gases) that are higher in energy allows for a simplistic scheme for the storage and transportation of electrons. In this work, we have chosen to focus on carbon dioxide as the substrate of interest due to its notoriety as a greenhouse gas and its ability to form a variety of products known to be precursors for the synthesis of fuels in the well studied Fisher-Tropsch methods.[35–37]

Much work has been done in the area of carbon dioxide reduction.[38,39] Researchers have reported various saturated and unsaturated macrocycle complexes containing nickel, iron, cobalt, and copper,[40–45] phosphine complexes containing nickel and palladium[46–50], and polypyrridyl complexes containing various metals.[51–64] The polypyrridyl system has yielded the most promising results, with the rhenium bipyridine system producing the highest turnover numbers, turnover frequencies, and selectivity for CO_2. This system, initially developed by Lehn[65], has been built upon by Kubiak[66–70] by changing the functionality of the bipyridine ligand (Figure 1.3) and studying how different functional groups change the electronic properties of the rhenium center.

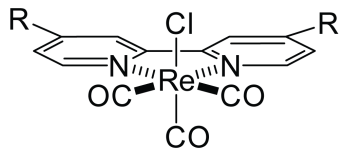

R = H, Me, OMe, tBu, COOH

Figure 1.3: Structure of the (2,2'-bipyridine)tricarbonylchlororhenium(I) catalyst. Substitution occurs at the 4 and 4' positions.

This catalytic system has has shown that CO_2 catalysis occurs upon reduction of the rhenium center to rhenium(0) after reduction of the bipyridine backbone occurs.(Figure 1.4) Through his studies, Kubiak has shown that by changing the electron donating ability of the substituents, the activity of the complex changes drastically. By incorporating more electron donating groups, CO_2 catalysis is significantly enhanced, with the 4,4'-*bis*(*tert*-Butyl) derivative producing the best results.

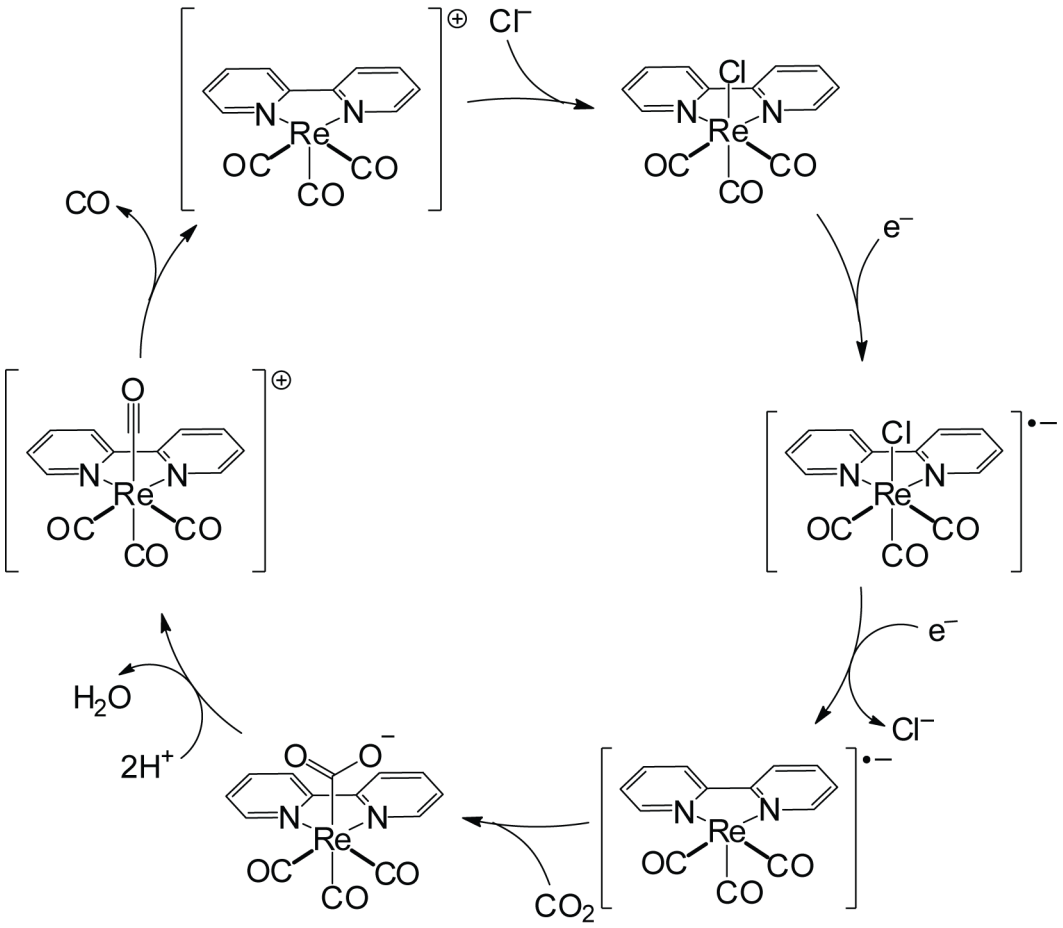

Figure 1.4: Mechanism by which CO_2 catalysis occurs with Lehn's catalyst. Reduction of the ligand backbone followed by reduction of the rhenium center allows for the binding of carbon dioxide.

The ^{t}Butyl derivative is also believed to stabilize the rhenium(0) radical that is active for CO_2 catalysis by preventing dimer formation. (Figure 1.5) It is proposed that the steric barrier for dimer formation is increased significantly when the bipyridine ligand is substituted with these bulky groups.

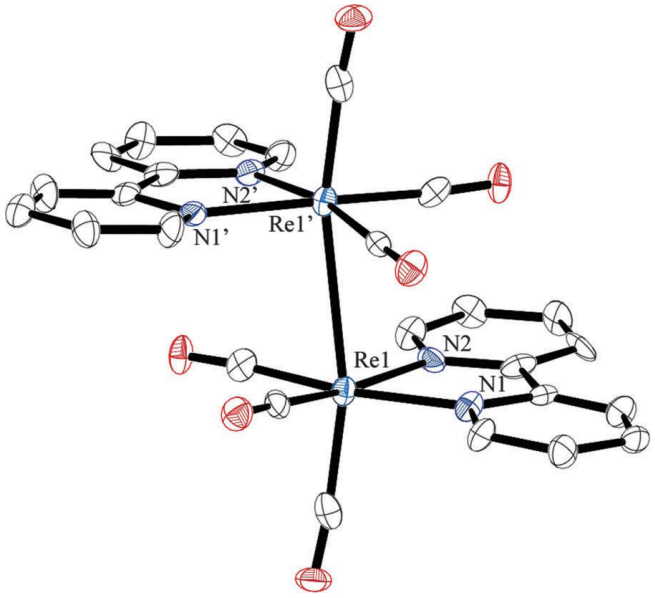

Figure 1.5: Solid-state structure of the rhenium(0) dimer.[67] Due to the small size of the bipyridine ligand, dimer formation occurs, however with the incorporation of sterically bulky groups, dimer formation can be inhibited.

Chapter 2

SYNTHESIS OF THREE NEW RHENIUM BIPYRIDINE COMPLEXES

2.1 Introduction

Inspired by the work done by Kubiak with these rhenium bipyridine complexes, our systems aim to address the two main issues that revolve around these catalysts: substituents that are sufficiently electron donating and that are bulky enough to prevent dimer formation. By incorporating borondipyromethene (BODIPY) function groups at the 4,4', 5,5', and 6,6' positions (Figure 2.1), we aim to increase the electron storage capacity of the ligand as well as to increase the photoexcitation profile of the ligand to allow for the potential of photochemical reduction of carbon dioxide.

2.2 Experimental

2.2.1 General Materials and Methods.

Reactions were performed in oven-dried round-bottomed flasks unless otherwise noted. Reactions that required an inert atmosphere were conducted under a positive pressure of N_2 using flasks fitted with Suba-Seal rubber septa or in nitrogen filled glove box. Air and moisture sensitive reagents were transferred using standard syringe or cannula techniques. Reagents and solvents were purchased from Sigma Aldrich, Acros, Fisher, Strem, or Cambridge Isotopes Laboratories. Solvents for synthesis were of reagent grade or better.

^{1}H NMR and ^{13}C NMR spectra were recorded at 25 °C on a Bruker 400 MHz spectrometer. Proton spectra are referenced to the residual proton resonance of the deuterated solvent ($CDCl_3$ = δ 7.26) and carbon spectra are referenced to the carbon resonances of the solvent ($CDCl_3$ = δ 77.23). All chemical shifts are reported using the standard δ notation in parts-per-million; positive chemical shifts are to higher frequency from the given reference. All NMR Spectra are shown in Appendix B. High-resolution mass spectrometry was performed at the University of Delaware Mass Spectromemtry Lab.

2.2.2 Synthetic Protocols.

2.2.2.1 [2,2'-bipyridine]-4,4'-dicarbonyl chloride.

This compound was prepared with slight modifications to a literature method.[71] [2,2'-bipyridine]-4,4'-dicarboxylic acid (0.5 g, 2.23 mmol) was suspended in 20 mL of thionyl chloride. The suspension was heated to reflux with stirring for 24 hours under nitrogen. After completion, the product was completely dissolved yielding a dark yellow solution. The solvent was removed under reduced pressure, dried for 30 minutes, and the resulting residue was used immediately in the following reaction. A quantitative yield was assumed.

2.2.2.2 4,4'-*bis*(BODIPY)-2,2'-bipyridine (BB2).

This compound was prepared with slight modifications to a literature method.[71] 100 mL of chloroform was sparged with nitrogen for 45 min. The [2,2'-bipyridine]-4,4'-dicarbonyl chloride synthesized in the previous step was dissolved in 100 mL of the degassed chloroform. 2,4-dimethyl-3-ethylpyrrole (2.11 mL, 15.6 mmol) was added to the solution. The reaction mixture was then heated to 50 °C and stirred for 90

min. under nitrogen. After approximately 25 minutes the solution became dark brown in color. After 90 min. the solvent was removed, and the residue was dissolved in 5% dichloromethane in toluene. Triethylammine (2.48 mL, 17.8 mmol) was added and the reaction was stirred for 30 minutes at room temperature under air. The solution was then heated to 50 °C and 3.85 mL (31.2 mmol) of BF_3•OEt_2 was added. The reaction was stirred for 90 minutes at 50°C. The solvent was removed under reduced pressure. The crude product was purified on silica, eluting CH_2Cl_2 first, and then increasing to 1% methanol in CH_2Cl_2 until the product fraction was collected. Further purification was required on silica by eluting 1% methanol in DCM to yield 0.780 g of a brick red powder (46%). ^{1}H NMR (400 MHz, $CDCl_3$) δ 8.79 (d, J = 4.9 Hz, 1H), 8.53 (s, 1H), 7.35 (dd, J = 4.8, 1.5 Hz, 1H), 2.55 (s, 6H), 2.30 (d, J = 7.6 Hz, 4H), 1.38 (s, 6H), 0.99 (t, J = 7.5 Hz, 6H). HR-MS: $[M]^+$ + H m/z: calculated for $C_{44}H_{51}B_2F_4N_6$, 761.4297; found 761.4302

2.2.2.3 Re[4,4'-*bis*(BODIPY)-2,2'-bipyridine](CO)$_3$Cl (Re(BB2)(CO)$_3$Cl).

This compound was prepared with slight modifications to a literature method.[70] chloropentacarbonylrhenium (I) (0.040 g, 0.11 mmol) and **BB2** (0.084 g, 0.11 mmol) were added to 50 mL of toluene and heated to reflux in open air overnight with stirring. Reaction was removed from heat yielding a dark red solution and the majority of the solvent was removed under reduced pressure (leaving approximately 2-3 mL of solvent). The resulting solution was then slowly added to 200 mL of hexane and stirred. The resulting solid was removed via filtration and dried to yield 0.106 g of a scarlet powder (90%). ^{1}H NMR (400 MHz, $CDCl_3$) δ 9.24 (d, J = 5.6 Hz, 1H), 8.19 (s, 1H), 7.60 (dd, J = 5.6, 1.5 Hz, 1H), 2.52 (d, J = 5.1 Hz, 6H), 2.29 (dq, J = 19.0, 7.5

Hz, 4H), 1.46 (s, 3H), 1.30 (s, 3H), 0.96 (dt, J = 19.4, 7.5 Hz, 6H). HR-MS: $[M]^+$ + H m/z: calculated for $C_{47}H_{51}B_2ClF_4N_6O_3Re$, 1067.3391; found 1067.3443.

2.2.2.4 [2,2'-bipyridine]-5,5'-dicarboxylic acid.

This compound was prepared according to a literature method.[72] 5,5'-dimethyl-2,2'-bipyridine (4.69 g, 0.025 mol) was added to 300 mL of water along with potassium permanganate (26.2 g, 0.17 mol). The reaction mixture was heated overnight at 90 °C with stirring under air. Upon completion, the brown precipitate was filtered off, and excess starting material was removed via extraction into diethyl ether (3 x 100 mL). The resulting aqueous solution was acidified to a pH of 2 with 1 M HCl. Upon acidification, a white precipitate was formed and filtered off. The residue was dried under reduced pressure yielding 4.27 g (70%) of the desired product. ^{1}H NMR (400 MHz, DMSO) δ/ppm: 9.22 (s, 2H), 8.60 (d, J = 8.3 Hz, 2H), 8.49 (s, 2H). HR-ESIMS $[M + H]^+$, m/z: Calculated for $C_{12}H_9N_2O_4$, 245.0562. Found 245.0558.

2.2.2.5 [2,2'-bipyridine]-5,5'-dicarbonyl chloride.

This compound was prepared with slight modifications to a literature method.[71] [2,2'-bipyridine]-4,4'-dicarboxylic acid (0.5 g, 2.23 mmol) was suspended in 20 mL of thionyl chloride. The suspension was heated to reflux with stirring for 24 hours under nitrogen. After this time, the product was completely dissolved yielding a dark yellow solution. The solvent was removed under reduced pressure and the resulting residue was used immediately in the following reaction. A quantitative yield was assumed.

2.2.2.6 5,5'-*bis*(BODIPY)-2,2'-bipyridine (BB3).

This compound was prepared according to the same method used for the preparation of 4,4'-*bis*(BODIPY)-2,2'-bipyridine, however [2,2'-bipyridine]-5,5'-dicarbonyl chloride was used in the place of [2,2'-bipyridine]-4,4'-dicarbonyl chloride. The crude product was purified on silica, eluting first with CH_2Cl_2, and then increasing to 1% methanol in CH_2Cl_2 until the product fraction was collected. Further purification was required on silica by eluting 1% methanol in DCM to yield 0.746 g of a brick red powder (44%). ^{1}H NMR (400 MHz, $CDCl_3$), δ/ppm: 8.66 (s, 2H), 8.64 (d, J = 4.0 Hz, 2H), 7.83 (d, 2H), 2.56 (s, 12H), 2.32 (q, 8H), 1.40 (s, 12H), 1.00 (t, 12H). HR-ESIMS $[M + H]^+$, m/z: Calculated for $C_{44}H_{52}B_2F_4N_6$, 761.4297. Found 761.4297.

2.2.2.7 Re[5,5'-*bis*(BODIPY)-2,2'-bipyridine](CO)$_3$Cl (Re(BB3)(CO)$_3$Cl).

5,5'-*bis*(BODIPY)-2,2'-bipyridine (**BB3**) (0.084 g, 0.11 mmol) and chloropentacarbonylrhenium (0.040 g, 0.11 mmol) were mixed together in 50 mL of 1,2-dichloroethane. The solution was heated to reflux, and stirred for 20 h under nitrogen. The solution color changed from orange to a dark red color. The solvent was removed under reduced pressure.The crude product was purified on silica, eluting DCM first, and then by eluting 1% methanol in DCM. The product band eluted just after the unreacted ligand. Further purification was required on silica to further remove unreacted ligand by eluting 1% methanol in DCM to yield 0.041 g of a dark red powder (35%). ^{1}H NMR (400 MHz, CDCl3) δ 9.05 (d, J = 1.7 Hz, 2H), 8.41 (d, J = 8.2 Hz, 2H), 8.11 (dd, J = 8.2, 1.9 Hz, 2H), 2.57 (s, 12H), 2.34 (dq, J = 15.2, 7.6 Hz, 8H), 1.46 (d, J = 7.0 Hz, 13H), 1.02 (dt, J = 10.7, 7.6 Hz, 13H). ^{13}C NMR (101 MHz, CDCl3) δ 196.02, 156.88, 155.35, 154.99, 152.40, 139.30, 138.18, 136.22, 134.44, 133.80, 130.64, 130.50, 129.89, 123.13, 29.50, 16.92, 16.89, 14.41, 14.29, 13.45,

13.01, 12.63, 12.51. HR-MS: $[M]^+$ + H m/z: calculated for $C_{47}H_{51}B_2ClF_4N_6O_3Re$, 1067.3391; found 1067.3428.

2.2.2.8 6,6'-dimethyl-2,2'-bipyridine.

This compound was prepared with modifications to a literature method.[73] Nickel (II) chloride (0.753 g, 5.81 mmol) and triphenylphosphine (6.09 g, 23.2 mmol) were dissolved in 50 mL of dry dimethylformamide. The solution was stirred until both reactants were dissolved. The mixture was heated to 50 °C under nitrogen, and the zinc powder (0.38 g, 5.81 mmol) was added in one portion. After the reaction was stirred for 1 h at 50 °C, the mixture became red orange in color. 2-bromo-6-methylpyridine (0.66 mL, 5.81 mmol) was added to the solution, and monitored by TLC. After 3 h, the starting material was completely consumed. The solution was poured into a dilute bicarbonate solution (200 mL) and the crude product was extracted into chloroform (3 x 100 mL). The organic layer was washed with water (3 x 100 mL), dried over sodium sulfate, and the solvent was removed under reduced pressure. The residue was washed with hexane and dried to remove excess dimethylformamide. The crude product was purified on silica by eluting with CH_2Cl_2 to remove byproducts containing triphenylphosphine and triphenylphosphine oxide. Then, the polarity of the mobile phase was slowly increased to 6% methanol in DCM until the product was collected. Further purification was required on basic alumina by eluting DCM until 0.310 g of the product was collected in the form of a white powder (31%). ^{1}H NMR (400 MHz, $CDCl_3$), δ/ppm: 8.16 (d, J = 8.0 Hz, 2H), 7.68 (t, J = 7.7 Hz, 2H), 7.15 (d, J = 7.6 Hz, 2H), 2.63 (s, 6H). HR-ESIMS $[M + H]^+$, m/z: Calculated for $C_{12}H_{13}N_2$, 185.1079. Found 185.1076.

2.2.2.9 [2,2'-bipyridine]-6,6'-dicarboxylic acid.

This compound was prepared according to the same method and scale used for the preparation of [2,2-bipyridine]-5,5'-dicarboxylic acid, however 6,6'-dimethyl-2,2'-bipyridine was used in place of the 5,5'-dimethyl-2,2'-bipyridine. Product was isolated with a 70% yield. ^{1}H NMR (400 MHz, DMSO), δ/ppm: 8.78 (d, J = 7.7 Hz, 2H), 8.22 (t, J = 8.0 Hz, 2H), 8.17 (d, J = 8.0 Hz, 4H). ^{13}C NMR (101 MHz, DMSO, 25C), δ/ppm: 165.92, 154.46, 148.10, 138.94, 125.24, 124.10. HR-ESIMS $[M + H]^{+}$, m/z: Calculated for $C_{12}H_9N_2O_4$, 245.0562. Found 245.0565.

2.2.2.10 [2,2'-bipyridine]-6,6'-dicarbonyl chloride.

This compound was prepared according to the same method and scale used for the preparation of [2,2-bipyridine]-4,4'-dicarbonyl chloride, however, [2,2'-bipyridine]-6,6'-dicarboxylic acid was used in place of the [2,2'-bipyridine]-4,4'-dicarboxylic acid. Product was not isolated, and used immediately in the following reaction. The yield was assumed to be quantitative.

2.2.2.11 6,6'-*bis*(BODIPY)-2,2'-bipyridine (BB4).

This compound was prepared according to the same method and scale used for the preparation of 4,4'-*bis*(BODIPY)-2,2'-bipyridine, however [2,2'-bipyridine]-6,6'-dicarbonyl chloride was used in the place of [2,2'-bipyridine]-4,4'-dicarbonyl chloride. The crude product was purified on silica by eluting DCM. Further purification was required on silica by eluting DCM. Product fraction was collected to yield 0.610 g (36%). ^{1}H NMR (400 MHz, $CDCl_3$) δ/ppm: 8.49 (d, J = 8.0 Hz, 2H), 7.92 (t, J = 7.8 Hz, 2H), 7.45 (d, J = 6.8 Hz, 2H), 2.56 (s, 12H), 2.31 (q, J = 7.5 Hz, 8H), 1.27 (s, 13H), 0.99 (t, J = 7.5 Hz, 12H). ^{13}C NMR (101 MHz, $CDCl_3$) δ 156.05, 154.67, 154.16, 138.04, 137.77, 137.26, 132.96, 130.74, 124.82, 121.43, 17.09, 14.68,

12.68, 11.49. HR-ESIMS $[M + H]^+$, m/z: Calculated for $C_{44}H_{52}B_2F_4N_6$, 761.4297. Found 761.4301.

2.2.2.12 Re[6,6'-*bis*(BODIPY)-2,2'-bipyridine](CO)$_3$Cl (Re(BB4)(CO)$_3$Cl).

6,6'-*bis*(BODIPY)-2,2'-bipyridine (**BB4**) (0.084 g, 0.11 mmol) and chloropentacarbonylrhenium (0.040 g, 0.11 mmol) were mixed together in 50 mL of 1,2-dichloroethane. The solution was heated to reflux, and stirred for 20 h under nitrogen. The solution color changed from orange to a dark red color. The solvent was removed under reduced pressure. The crude product was purified on silica, eluting DCM first, and then by eluting 1% methanol in DCM. The product band eluted just after the unreacted ligand. Further purification was required on silica to further remove unreacted ligand by eluting 1% methanol in DCM to yield 0.075 g of a dark red powder (64%). ^{1}H NMR (400 MHz, CDCl3) δ 8.47 (d, J = 7.3 Hz, 2H), 8.21 (t, J = 7.9 Hz, 2H), 7.73 (d, J = 6.7 Hz, 2H), 2.52 (s, 12H), 2.38 – 2.13 (m, 8H), 1.65 (s, 6H), 1.07 (s, 6H), 0.96 (t, J = 7.5 Hz, 6H), 0.87 (t, J = 7.5 Hz, 7H). HR-MS: $[M]^+$ + H m/z: calculated for $C_{47}H_{51}B_2ClF_4N_6O_3Re$, 1067.3391; found 1067.3435.

2.2.3 Single Crystal X-ray Diffraction

Re(BB2)(CO)$_3$Cl consistently deposited as red, multiple, crystal masses and the results herein represent the best of several trials. Crystals were selected, sectioned if required, and mounted on plastic mesh with viscous oil flash-cooled to 200 K. Data were collected on a Bruker-AXS Apex 2 Duo CCD diffractometer with Gobel mirror focused Cu-Kα radiation (λ=1.54178 Å) (for **Re(BB2)(CO)$_3$Cl**) or with graphite monochromated Mo-Kα radiation (λ=0.71073 Å) (for **Re(BB3)(CO)$_3$Cl** and **Re(BB4(CO)$_3$Cl**) from a sealed-beam X-ray tube. Unit cell parameters were obtained

from 60 data frames, 0.3º ω, from three different sections of the Ewald sphere. No symmetry higher than triclinic was observed for **Re(BB3)(CO)$_3$Cl** and **Re(BB2)(CO)$_3$Cl,** and solution in the centrosymmetric space group option yielded chemically reasonable and computationally stable results of refinement. The systematic absences in the diffraction data were consistent with *Pmn*2$_1$ and *Pmnm* [*Pmmn*]. Only the noncentrosymmetric space group option yielded chemically reasonable and computationally stable results of refinement.

The data-sets were treated with numerical absorption corrections. The structures were solved using direct methods and refined with full-matrix, least-squares procedures on F^2. All non-hydrogen atoms were refined with anisotropic displacement parameters. All hydrogen atoms were treated as idealized contributions. Atomic scattering factors and anomalous dispersion coefficients are contained in the SHELXTL 6.12 program library (Sheldrick, G.M. 2008. Acta Cryst. A64, 112-122).

A 1,2-dichloroethane solvent molecule was located in the asymmetric unit, one per compound molecule, for **Re(BB3)(CO)$_3$Cl** and **Re(BB4(CO)$_3$Cl**.

For **Re(BB3)(CO)$_3$Cl**, the carbonyl ligand C-O distances were constrained to be similar within a standard deviation of 0.02 Å.

For **Re(BB4(CO)$_3$Cl**, the compound molecule and the cocrystallized solvent molecule were each located on a mirror plane. The severely thermally active solvent molecule was modeled as a half-occupied albeit complete molecule with rigid bond constraints applied to the equivalent isotropic parameters and the anisotropic parameters.

For **Re(BB2)(CO)$_3$Cl**, two molecules of the compound and one disordered molecule of methylene chloride solvent were located in the asymmetric unit and rigid

bond displacement restraints were applied. One ethyl group was found disordered with a refined site occupancy of 72/28. The disordered solvent molecule was treated as a rigid body with idealized geometry and with a refined site occupancy ratio of 52/48.

2.3 Results and Discussion

The synthetic protocols used to construct 4,4'-*bis*(BODIPY)-2,2'-bipyridine (**BB2**), are shown in Figure 2.1. Preparation of **BB2** begins with the conversion of [2,2'-bipyridine]-4,4'-dicarboxylic acid to the acid chloride derivative via the reaction with excess thionyl chloride. After the excess thionyl chloride was removed under reduced pressure, subsequent reaction with 2,4-dimethyl-3-ethylpyrrole results in the condensation reaction, producing the 4,4'-dipyrromethane derivative. Upon addition of NEt_3 and $BF3{\bullet}OEt_2$, **BB2** is generated with a yield of 46%.

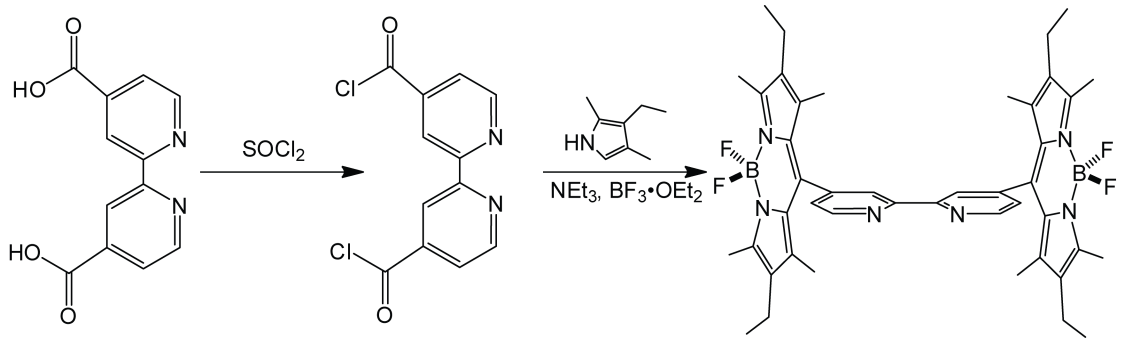

Figure 2.1 Synthesis of **BB2** as explained above.

Subsequent metallation of the **BB2** ligand required refluxing a solution of this compound in toluene with chloropentacarbonylrhenium (I) for 24 hours. After most of the solvent had been removed in vacuum, the remaining solution is added drop-wise to hexane. The product was then filtered off and isolated in a 90% yield. Product

formation was further confirmed by ^{1}H NMR spectroscopy as evidenced by the splitting of peaks in the aliphatic region.

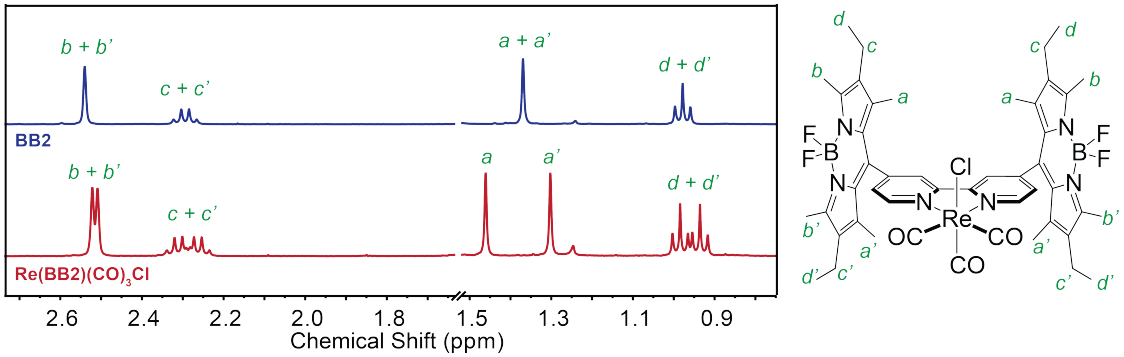

Figure 2.2 ^{1}H NMR overlay of **BB2** and **Re(BB2)(CO)$_3$Cl** showing the splitting of several signals in the aliphatic region. Residual solvent and water peaks were omitted for clarity.

More specifically, splitting of the alkyl groups attached to the pyrrole rings of the BODIPY is observed (Shown in Figure 2.2). The solid-state structure of the complex is shown in Figure 2.3 and is consistent with the NMR data reported above. For crystallographic data and key parameters, see Appendix C.

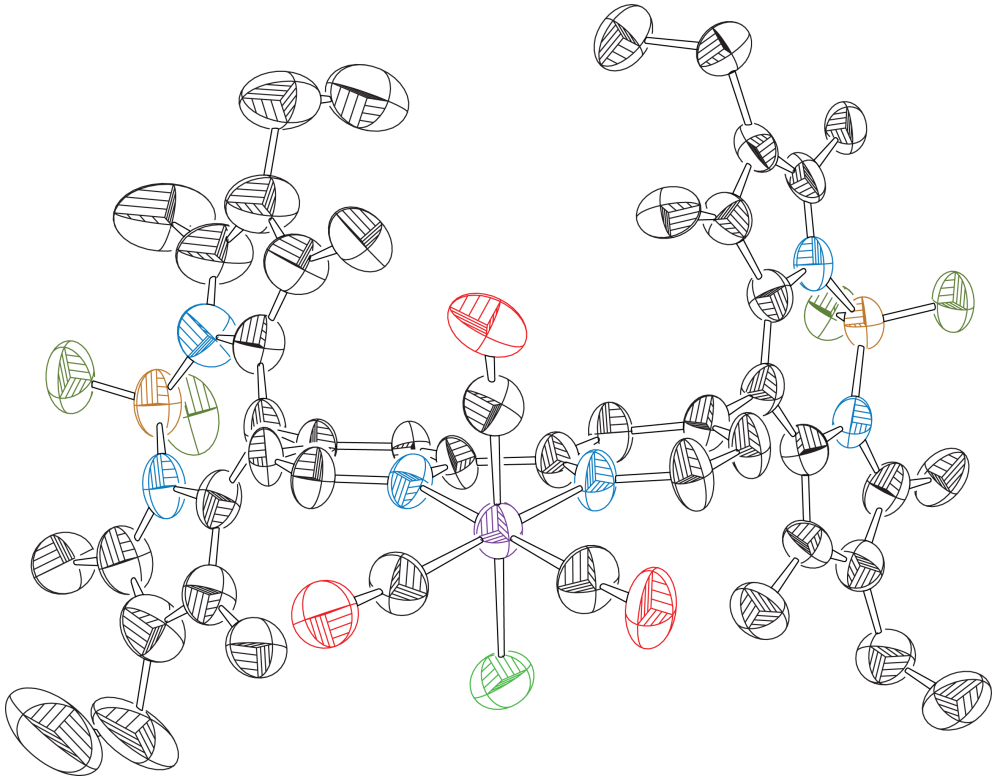

Figure 2.3 Molecular diagram of **Re(BB2)(CO)$_3$Cl** showing one of two symmetry unique molecules with 30% probability ellipsoids. H-atoms and solvent molecules omitted for clarity. (Color legend: purple = Re, lime = Cl, brown = B, olive = F, blue = N, red = O, gray = C.)

The synthetic protocols used to construct the BODIPY-bipyridine derivatives, 5,5'-*bis*(BODIPY)-2,2'-bipyridine (**BB3**) and 6,6'-*bis*(BODIPY)-2,2'-bipyridine (**BB4**), are shown in Figure 2.4 and Figure 2.5, respectively. Preparation of **BB3** began with the conversion of 5,5'-dimethyl-2,2'-bipyridine to the corresponding dicarboxylic acid (**1**) via reaction with $KMnO_4$ in water. After purification, the resulting dicarboxylic acid derivative was reacted with excess thionyl chloride to generate the acid chloride derivative (**2**). Subsequently, in a condensation reaction with 2,4-dimethyl-3-ethylpyrrole, the dicarbonyl chloride was converted to the 5,5'-

dipyrromethane derivative. Upon addition of NEt_3 and $BF3•OEt_2$, **BB3** was generated with a yield of 44%.

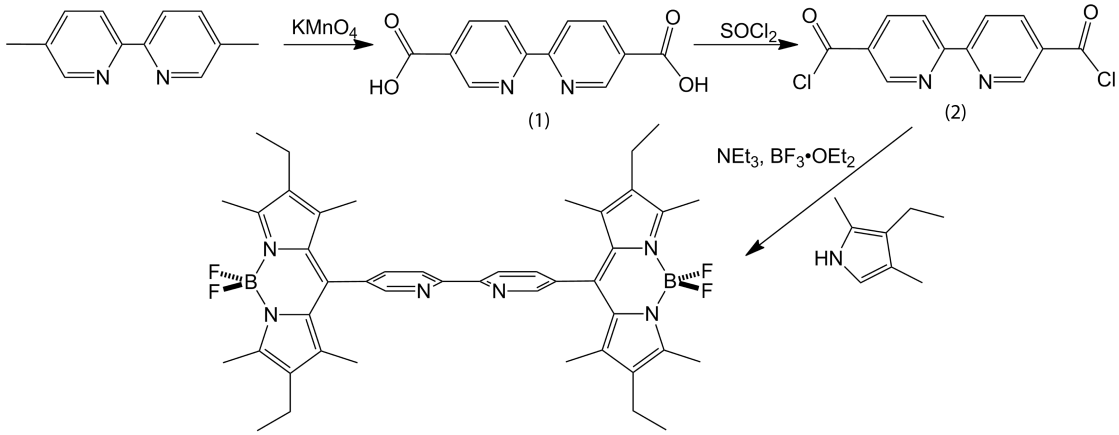

Figure 2.4 Synthesis of **BB3** from 5,5'-dimethylbipyridine.

Synthesis (shown in Figure 2.5) of **BB4** began with the coupling of 2-bromo-6-methylpyridine to form 6,6'-dimethyl-bipyridine (**3**), upon reaction with nickel(II) chloride, triphenylphosphine, and zinc dust. The next stages of the synthesis follow the same protocols as in the synthesis of **BB3**, starting from the dimethyl derivative. **BB4** was prepared in a 36% yield.

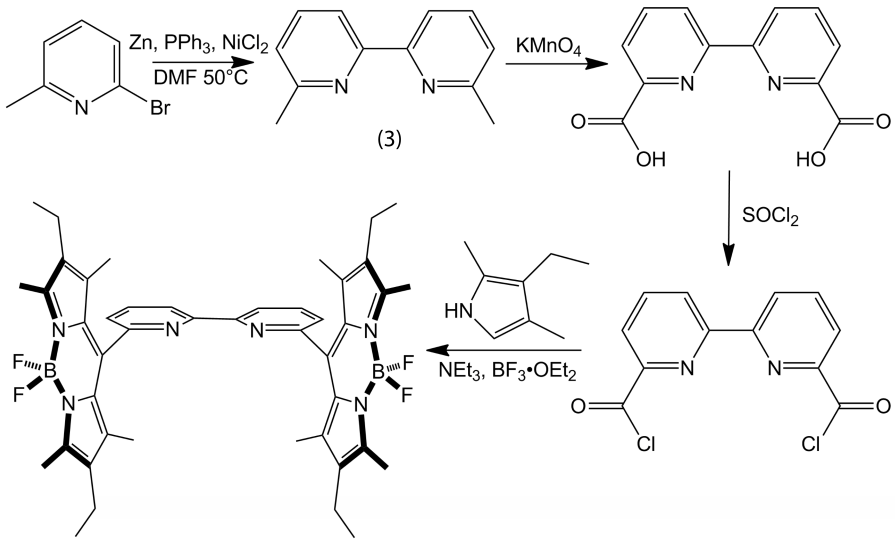

Figure 2.5 Synthesis of **BB4** from 6-methyl-2-bromopyridine.

Metallation of **BB3** and **BB4** was achieved via an overnight reflux in 1,2-dichloroethane with chloropentacarbonylrhenium(I). Following column chromatography on silica, **Re(BB3)(CO)$_3$Cl** and **Re(BB4)(CO)$_3$Cl** were isolated in 35% and 64% yields, respectively. Splitting of the aliphatic peaks in ^{1}H NMR occurs similarly to that of the 4,4' derivative. Overlays of the NMR spectra of the 5,5' and 6,6' derivatives are shown in Figures 2.6 and 2.7.

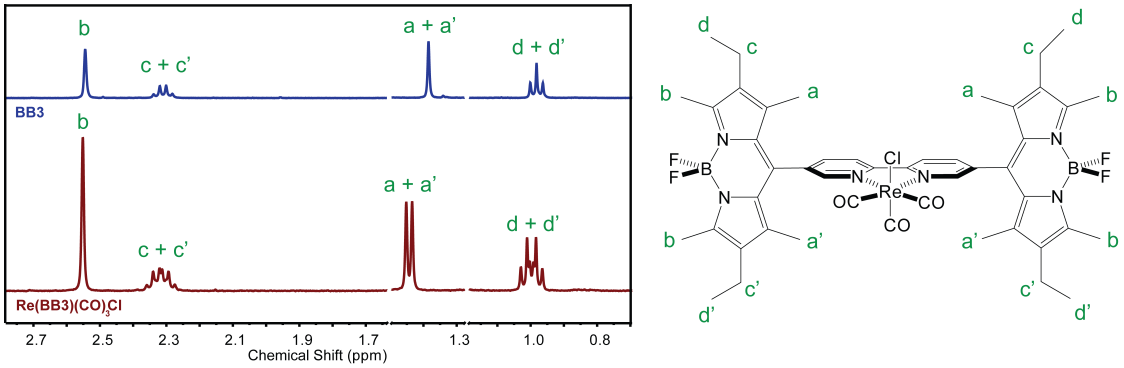

Figure 2.6 ^{1}H NMR overlay of **BB3** and **Re(BB3)(CO)$_3$Cl** showing the splitting of peaks in the aliphatic region. Residual solvent and water peaks are omitted for clarity.

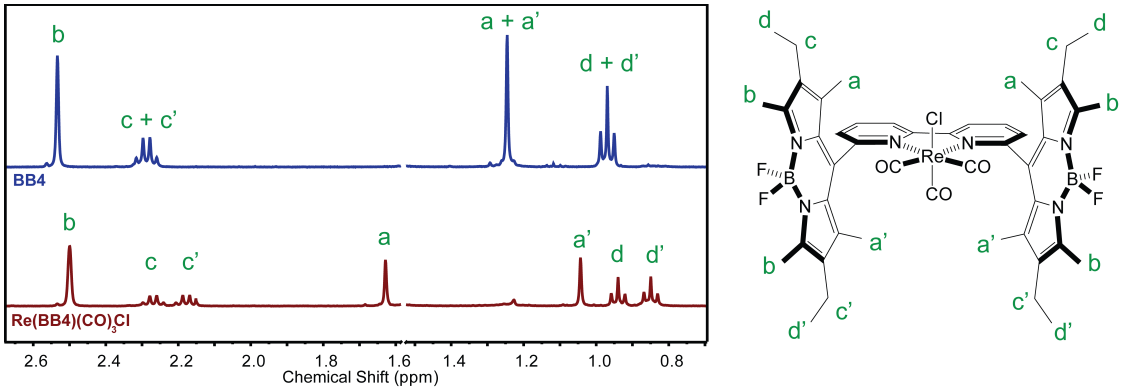

Figure 2.7 ^{1}H NMR overlay of **BB4** and **Re(BB4)(CO)$_3$Cl** showing the splitting of peaks in the aliphatic region. Residual solvent and water peaks are omitted for clarity. The signals at 1.05 ppm and 1.64 ppm for the rhenium complex are a result of the splitting of the singlet at 1.24 ppm for the free ligand.

Solid-state structures of the 5,5' and 6,6' derivative are shown in Figure 2.8 and Figure 2.9, respectively. For crystallographic data and key parameters, see Appendix C.

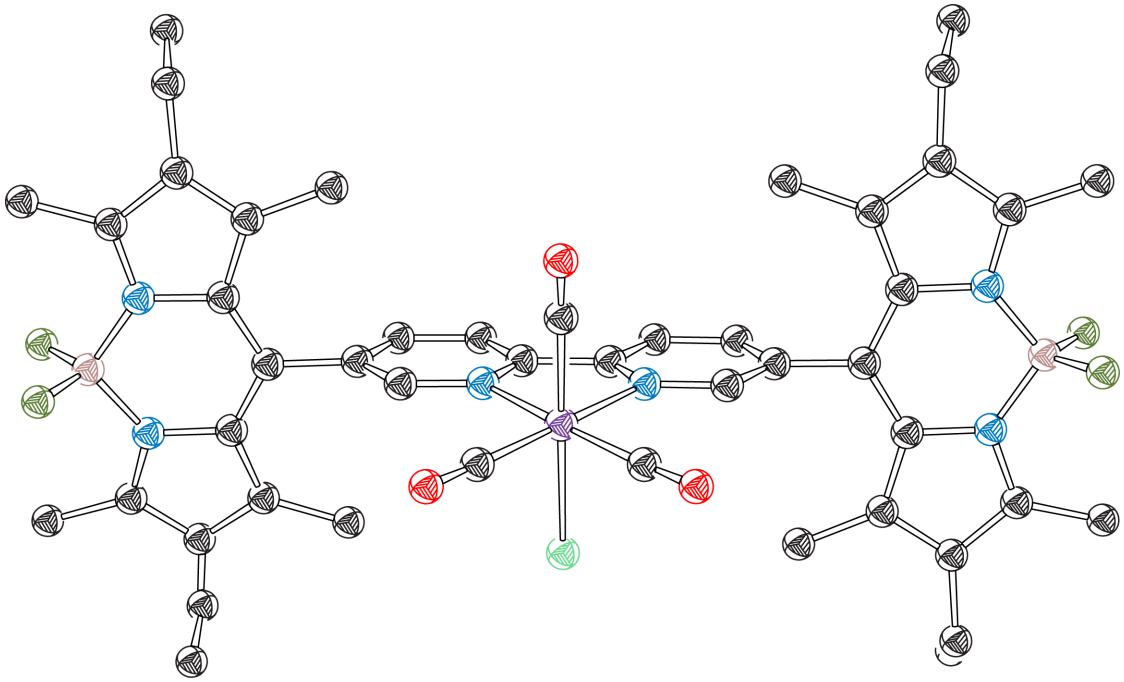

Figure 2.8 Crystal structure of **Re(BB3)(CO)$_3$Cl** with 30% probability ellipsoids. H-atoms and solvent molecules omitted for clarity. (Color legend: purple = Re, lime = Cl, brown = B, olive = F, blue = N, red = O, gray = C.)

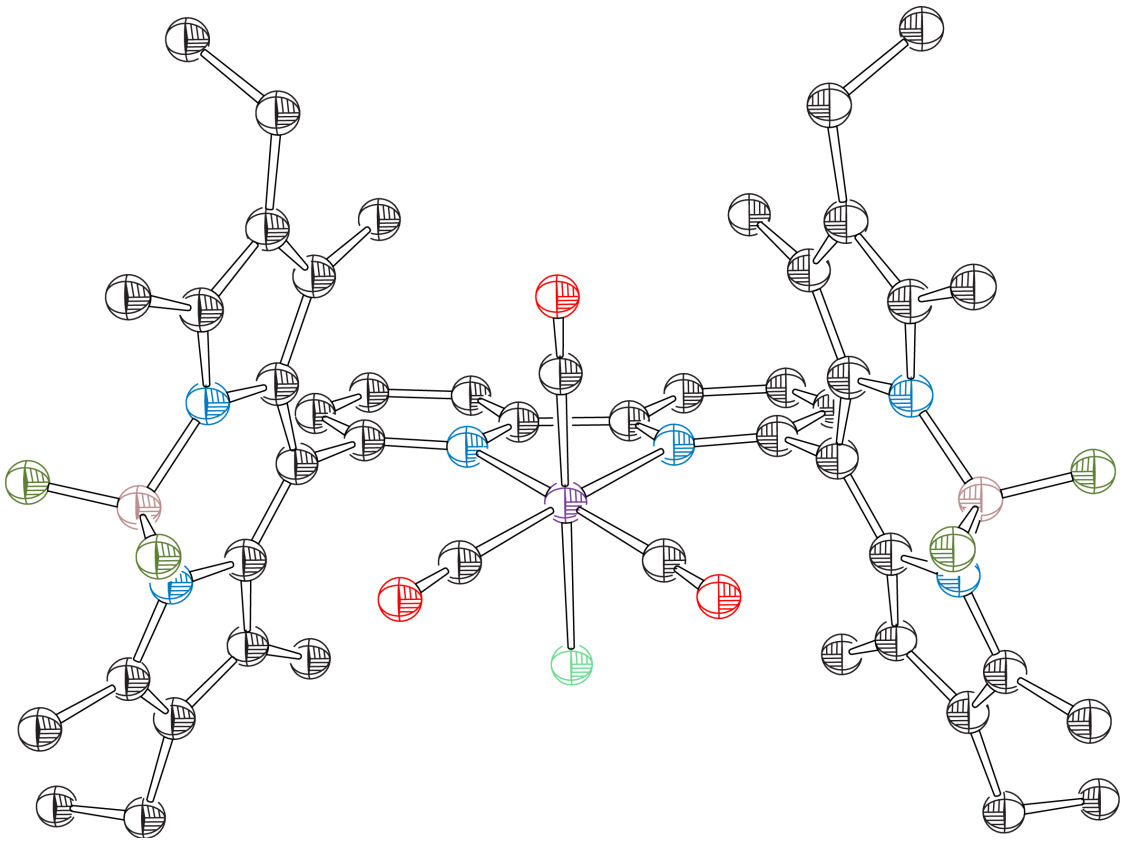

Figure 2.9 Crystal structure of **Re(BB4)(CO)$_3$Cl** with 30% probability ellipsoids. H-atoms and solvent molecules omitted for clarity. (Color legend: purple = Re, lime = Cl, brown = B, olive = F, blue = N, red = O, gray = C.)

Chapter 3

CHARACTERIZATION OF NOVEL RHENIUM COMPLEXES FOR CO_2 REDUCTION

3.1 Introduction

The sole purpose of synthesizing these catalysts was to improve the catalytic ability of the class of rhenium polypyridyl complexes. Typical methods of characterization of carbon dioxide reduction catalysts are via electrochemistry and photochemistry. In this work, electrochemical experiments, such as cyclic voltammetry and controlled potential electrolysis, were used to understand how well these target catalysts convert carbon dioxide to carbon monoxide.

3.2 Experimental

3.2.1 Theoretical Calculations

Geometry optimizations, frequency calculations, and molecular orbital calculations were performed using the Gaussian09 (G09) program package,[74] with the Becke three-parameter hybrid exchange and the Lee−Yang−Parr correlation functionals (B3LYP). The 6-31G* basis set was used for H, B, C, N, O, and F, along with the Stuttgart/Dresden (SDD) energy-consistent pseudopotentials for Re. Crystallographic coordinates were used as starting points for geometry optimizations. All geometry optimizations were performed in C_1 symmetry with subsequent vibrational frequency analysis to confirm that each stationary point was a minimum on the

potential energy surface. Molecular orbital were visualized using Visual Molecular Dynamics (VMD) software.

3.2.2 Electrochemistry

Electrochemistry was performed using either a CHI-620D potentiostat/galvanostat or a CHI-720D bipotentiostat. Cyclic voltammetry was performed using a standard three-electrode configuration. The working electrode was a polished glassy carbon electrode (GCE, 3.0 mm diameter CH Instruments). A piece of platinum wire was used as the counter electrode. All potentials were measured against a silver wire pseudo reference with a ferrocene internal standard and adjusted to saturate calomel electrode (SCE). Unless otherwise stated, the electrolyte was 0.1M $TBAPF_6$, the sample concentration was 1.0 mM, and all cyclic voltammetric experiments were carried out using a scan rate of 100 mV/s.

Controlled potential electrolysis was performed in a single-compartment cell. The same three-electrode setup was used with a polished glassy carbon disk electrode, a platinum mesh counter electrode, and a Ag/AgCl reference electrode (1.0 M KCl, CH Instruments) or a silver wire pseudo reference. Prior to electrolysis the solution was sparged with CO_2 gas for approximately 30 minutes. Once saturated with CO_2, the system was sealed and a potential was applied to the stirred solution. Headspace analysis during controlled potential electrolysis was performed using a gas chromatograph (GC, GC-2014 Shimadzu). The GC has two 10 port injection valves, each equipped with a HaySep-T 80/100 column. One injection line further contains a HaySep-D 80/100 column and a flame ionization detector (FID) with a methanizer to quantify CO and methane concentration. The second line leads to a packed MolSieve 5A 60/80 column with a thermal conductivity detector (TCD) to quantify hydrogen

concentration. The carrier gasses were helium (99.999%) and argon (99.999%), respectively.

3.3 Results and Discussion

3.3.1 Electrochemistry

Electrochemical studies of **Re(BB2)(CO)$_3$Cl**, **Re(BB3)(CO)$_3$Cl**, and **Re(BB4)(CO)$_3$Cl** have shown that all three complexes have shown catalytic ability for CO_2 reduction. A comparison of the initial turnover frequencies for each complex to those previously synthesized by Kubiak[70] and Lehn[65] was obtained via Foot-of-the-Wave Analysis.[75,76] Cyclic voltammetric studies were performed in acetonitrile (MeCN) to compare with the reference compounds, however only **Re(BB2)(CO)$_3$Cl** was soluble in MeCN. Consequently, the 4,4', 5,5', and 6,6' derivatives were studied in DMF as a comparison between the three complexes.

3.3.1.1 Electrochemistry in Acetonitrile

The rhenium (I) complex, **Re(BB2)(CO)$_3$Cl**, has shown interesting electrochemical properties. Cyclic voltammetry studies have been performed and the target catalyst has been compared to the Re(bpy)(CO)$_3$Cl catalyst originally synthesized by Lehn and Kubiak. Cyclic voltammograms of the 4,4' derivative and the reference compounds are shown in Figures 3.1 through 3.4.

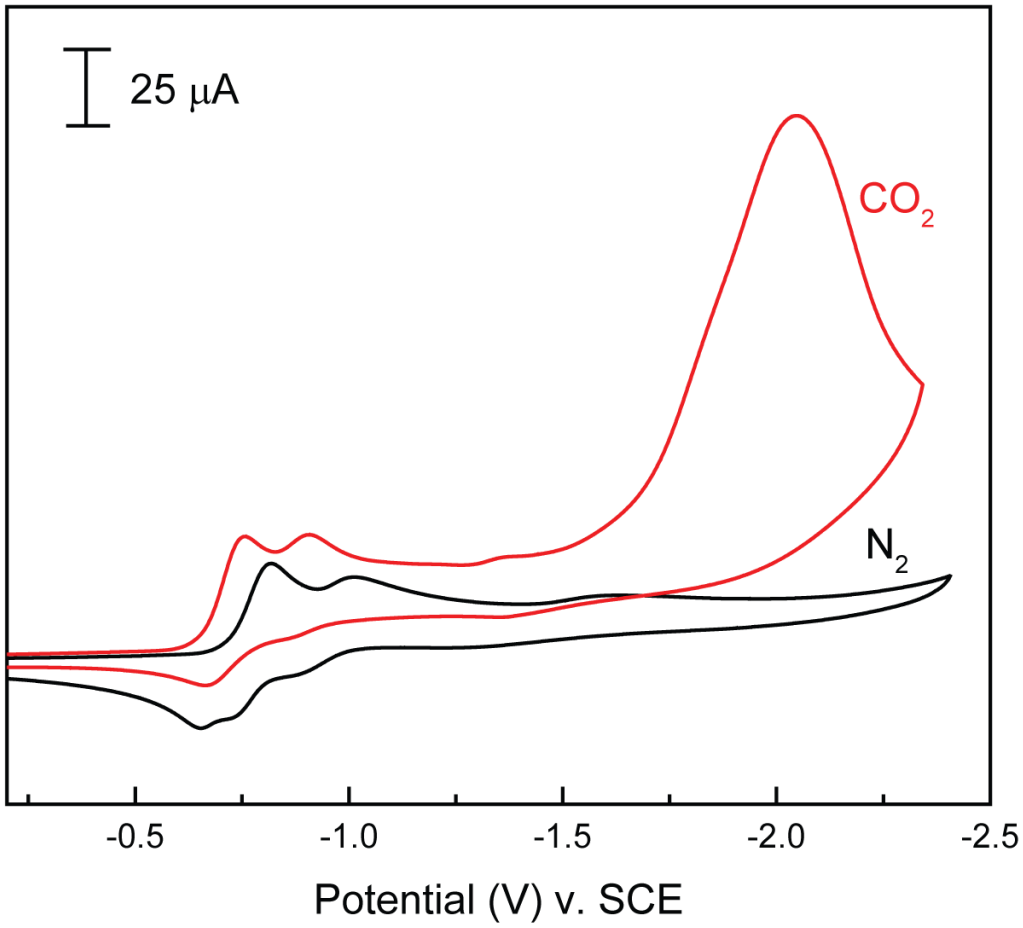

Figure 3.1 Cyclic voltammogram of **Re(BB2)(CO)$_3$Cl** (1 mM in MeCN). The black CV was taken while under an atmosphere of nitrogen and the red CV was taken while under an atmosphere of carbon dioxide. Experiment was performed in acetonitrile at a scan rate of 100 mV/s with a 0.1 M $TBAPF_6$ supporting electrolyte.

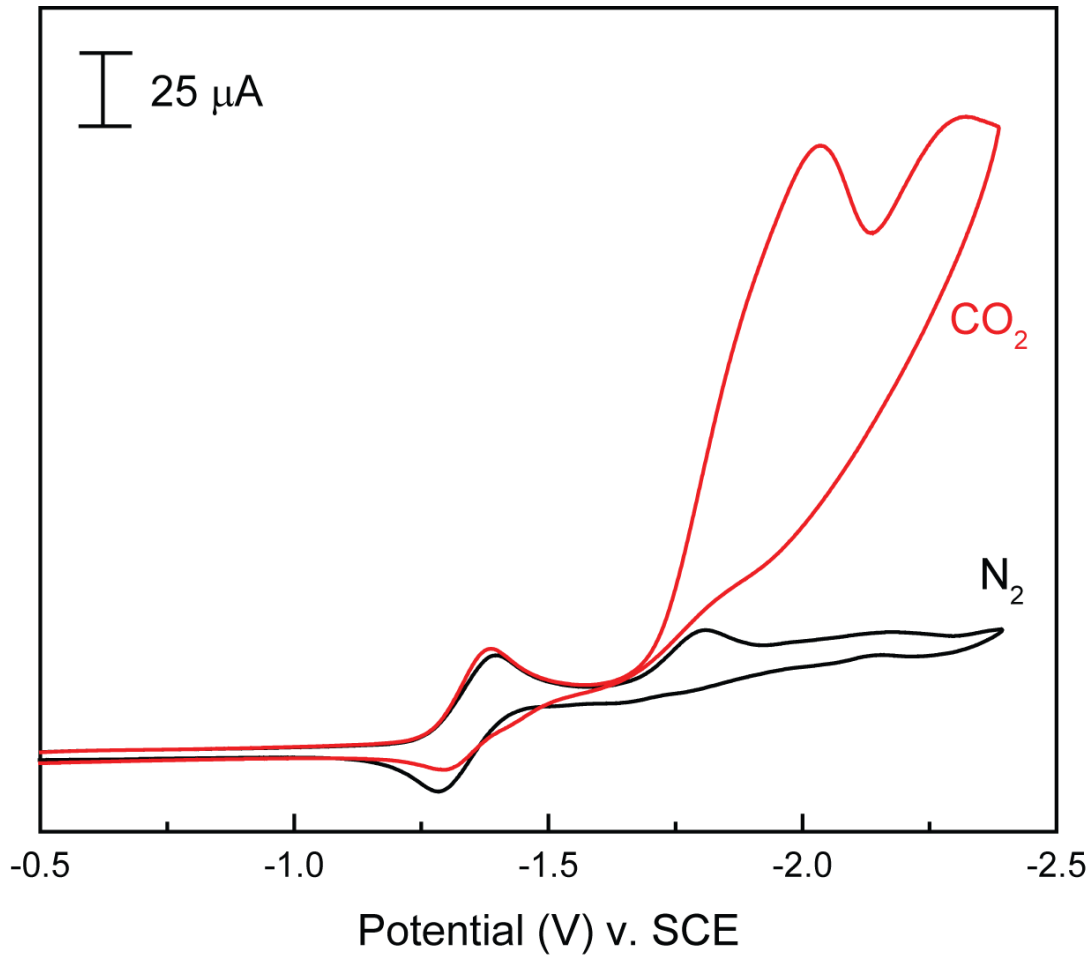

Figure 3.2 Cyclic voltammogram of $Re(bpy)(CO)_3Cl$ (1 mM in MeCN). The black CV was taken while under an atmosphere of nitrogen and the red CV was taken while under an atmosphere of carbon dioxide. Experiment was performed in acetonitrile at a scan rate of 100 mV/s with a 0.1 M $TBAPF_6$ supporting electrolyte.

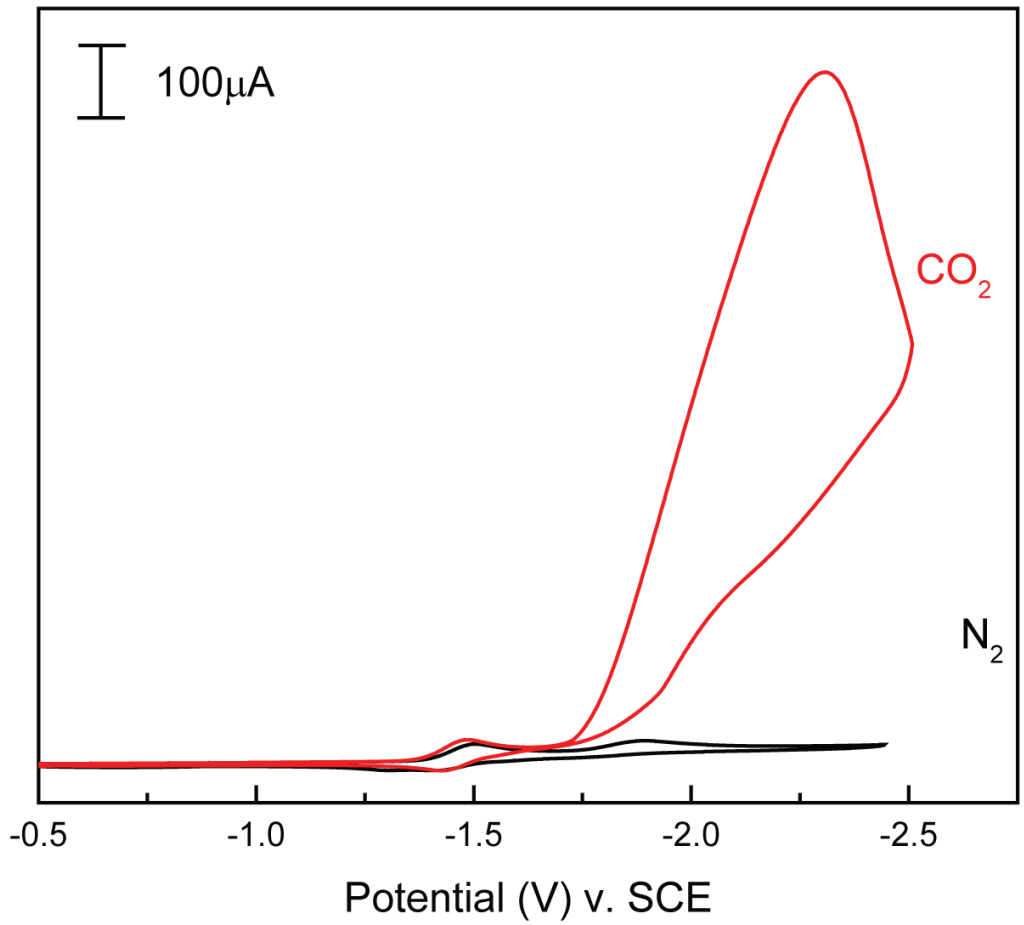

Figure 3.3 Cyclic voltammogram of Re(4,4'-t-Butyl-bpy)$(CO)_3Cl$ (1 mM in MeCN). The black CV was taken while under an atmosphere of nitrogen and the red CV was taken while under an atmosphere of carbon dioxide. Experiment was performed in acetonitrile at a scan rate of 100 mV/s with a 0.1 M $TBAPF_6$ supporting electrolyte.

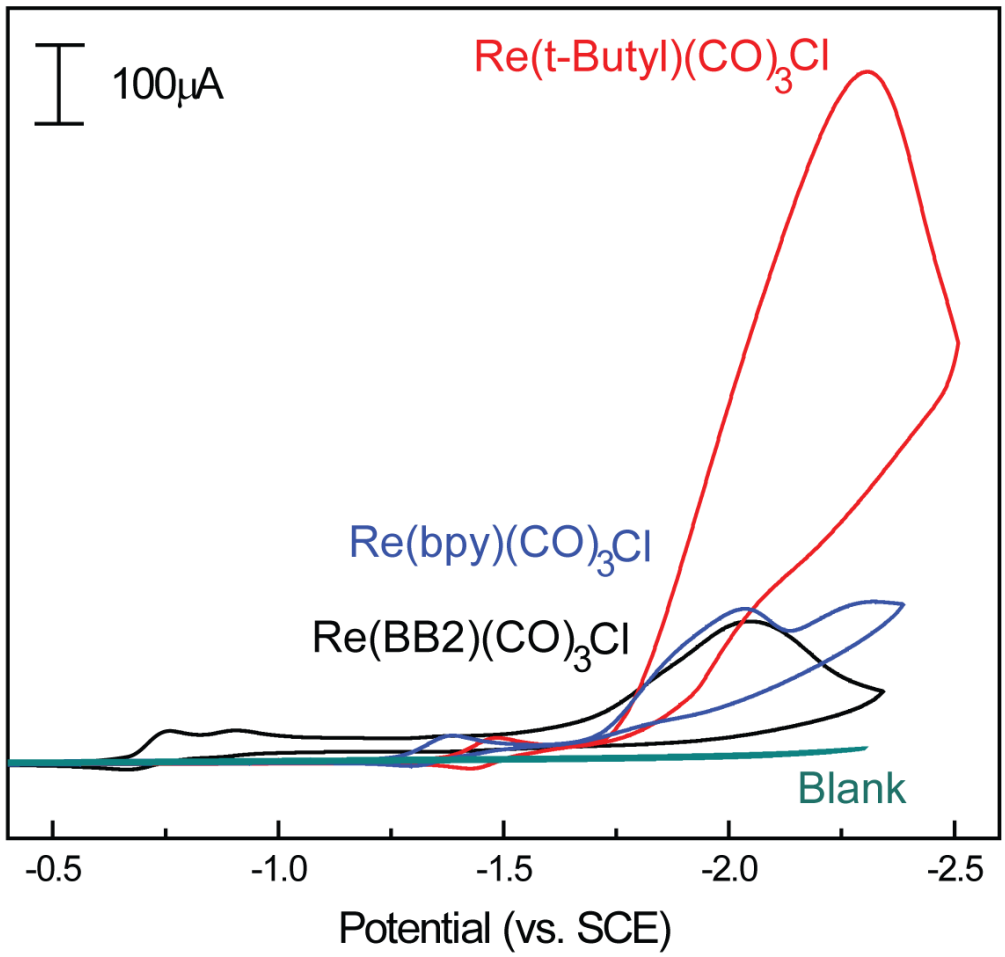

Figure 3.4 Overlay of CVs of **Re(BB2)(CO)$_3$Cl** (black), the 4,4'-t-butyl derivative (red), and unsubstituted derivative (blue), and a solution with no catalyst present (blank). Experiments were performed in acetonitrile (1 mM in catalyst) under an atmosphere of carbon dioxide at a scan rate of 100 mV/s with a 0.1 M $TBAPF_6$ supporting electrolyte.

Cyclic voltammetry performed by Kubiak[70] with a number of rhenium-bipyridine derivatives has shown that typical rhenium bipyridine complexes undergo two reductions. Reversible reduction of the bipyridine ligand occurs between –1.2 V

and –1.6 V and the broad $Re^{1/0}$ redox couple occurs between –1.7 V and –1.9 V. It is also important to note that both waves are identical in size due to the fact that both events are single-electron reductions. In Figure 3.2, cyclic voltammetry of Lehn's catalyst is comparable to those reported by the Kubiak group (Figure 3.3). Two reductions are observed at –1.4 V and –1.8 V, corresponding to the reduction of the ligand and metal center, respectively. In Figure 3.3, cyclic voltammetry of the 4,4'-^{t}Butyl-bipyridine derivative shows reductions at –1.5 V and –1.8 V, again corresponding to reduction of the ligand and the metal center, respectively. Under an atmosphere of carbon dioxide a significant catalytic increase for all systems is observed at –2.0 V, indicating CO_2 catalysis. Additionally, a third increase in current is observed for both the t-butyl derivative and the unsubstituted derivative that is not mentioned in the literature and is theorized to be the reduction of the complex in dimeric form. The cyclic voltammogram of **Re(BB2)(CO)$_3$Cl** shown in Figure 3.1 under an atmosphere of nitrogen shows three quasi-reversible reductions at –0.85 V, –1.0 V, and –1.6 V vs. SCE. Based on the work of the Kubiak group, the reduction of the bipyridine backbone for this system is assigned to the redox event at –1.0 V and reduction of the Re(I) center to Re(0) occurs at –1.6 V. The reduction couple at –0.85 V must therefore correspond to the simultaneous reduction of the BODIPY moieties. This 2-electron process is confirmed by the fact that the reduction wave is nearly twice as large as the subsequent 1-electron reductions that follow.

Theoretical calculations were performed for the **Re(BB2)(CO)$_3$Cl** catalyst and show that the first three reductions correspond to ligand-based reductions (Figure 3.5).

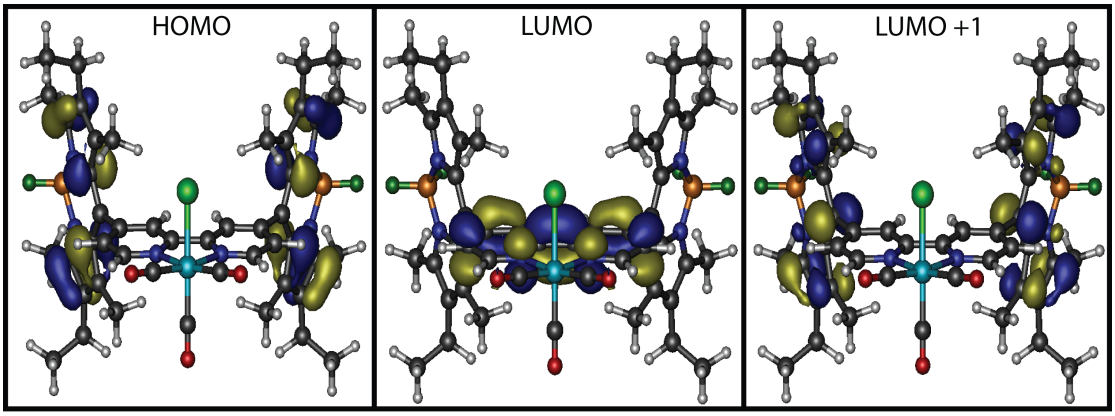

Figure 3.5 Theoretical calculations for the frontier molecular orbitals of **Re(BB2)(CO)$_3$Cl**. The LUMO+1 orbital is the next unoccupied orbital after the LUMO. However, these two are considered to be relatively close in energy. Calculations were performed by Daniel A. Lutterman at Oak Ridge National Laboratory.

Even though, based on the calculations, the LUMO is considered to be bipyridine-based indicating that the 2-electron reduction at –0.85 V is on the bipyridine backbone, the LUMO+1 orbital, which is heavily BODIPY-based, is relatively close in energy and may be reversed in order. Furthermore, four events occur on the return wave of the volatmmogram, which is mostly likely caused by the splitting of the oxidation of the BODIPY chromophores. When the acetonitrile solution was sparged with carbon dioxide, several changes in the cyclic voltammogram were observed. Reduction of the BODIPY moieties under CO_2 occurred at –0.75 V, followed by the reduction of the bipyridine base at –0.9 V, and finally, a large catalytic wave peaked at –2.0 V. This last peak is most logically assigned to that of the reduction of CO_2 by **Re(BB2)(CO)$_3$Cl**. There is also a small redox event that occurs at –1.4 V, which most likely corresponds to the reduction of the metal center prior to the activation of carbon dioxide.

Foot-of-the-Wave Analysis,[75,76,77] as described by Savéant, conducted for the cyclic voltammetry traces described above was carried out to determine and compare the kinetics of each system. The following equation was used in which the relationship between the current increase and the catalytic rate constant is determined.

$$\frac{i}{i_p^0} = \frac{2.24\sqrt{\frac{RT}{Fv}2kC_A^0}}{1 + \exp\left[\frac{F}{RT}\left(E - E_{PQ}^0\right)\right]} \qquad (1)$$

In the equation above, i is the current in the presence of substrate (which is carbon dioxide in this case), i_p^0 is the current in the absence of substrate, k is the second order rate constant, C_A^0 is the concentration of the substrate which is 0.270 M in MeCN.[78] E is the potential at which the current is measured, and E_{PQ}^0 is the peak potential of the redox couple in the absence of substrate. In other words, E_{PQ}^0 is the peak potential of the catalytic redox couple under nitrogen. Constructing a plot of $\frac{i}{i_p^0}$ $v.$ $\frac{1}{1 + \exp\left[\frac{F}{RT}\left(E - E_{PQ}^0\right)\right]}$ (See Appendix A) yields a linear line with a slope equal to $2.24\sqrt{\frac{RT}{Fv}2kC_A^0}$. Therefore, the second order constant, k, for the system can be calculated. Further implementation of the rate constant gives rise to the second order turnover frequency.

$$TOF = \frac{k}{1 + \exp\left[\frac{F}{RT}\left(E - E_{PQ}^0\right)\right]} \qquad (2)$$

Analysis of the **Re(BB2)(CO)$_3$Cl** produced a second order rate constant of 3400 M^{-1} s^{-1} and a subsequent TOF of 3400 M^{-1} s^{-1}. The system developed by Lehn gave a rate constant of 1100 M^{-1} s^{-1} and a TOF of 1100 M^{-1} s^{-1}, and the t-Butyl derivative showed an impressive rate constant and TOF of 9 x 10^5 M^{-1} s^{-1}. Based on these results, it is clear that the **BB2** framework engenders an enhanced catalysis, as the BODIPY appended catalyst is roughly three times more active than the analogous

unsubstituted complex. This enhancement is presumably due to the steric bulk imparted by the large indacene units, which impedes formation of reduced Re^{I}—Re^{I} dimers. Furthermore, recent work has shown that non-innocent ligand reservoirs can significantly alter metal-ligand bonding in fac-$Re^{I}(CO)_3$ complexes.[79] As such, the ability of the BODIPY appended ligand of **Re(BB2)(CO)$_3$Cl** to store multiple reducing equivalents during electrocatalysis may manifest in enhanced nucleophilic character at the metal center, while providing an electron reservoir that helps to drive the two electron reduction of CO_2 to CO.

Conrolled-Pontential Electrolysis experiments were performed in order to confirm and quantify the CO_2 catalysis that occurs. Experiments were performed in a single-compartment cell where both the anode (Pt mesh) and cathode (Glassy Carbon Disc Electrode) are present. The oxidation of products such as carbon monoxide at the anode were taken into account, and considered to be negligible compared to the quantity of CO produced. Analysis of the headspace verified that carbon dioxide undergoes a two-electron reduction to produce carbon monoxide in this system. However, the catalysis has shown to operate with relatively low faradaic efficiency. This result is due to catalyst deactivation most likely caused by the decomposition of the reduced species at the glassy carbon electrode surface. This phenomenon was analyzed by cyclic voltammetry (Figure 3.6) to confirm the reduced catalytic ability of the system.

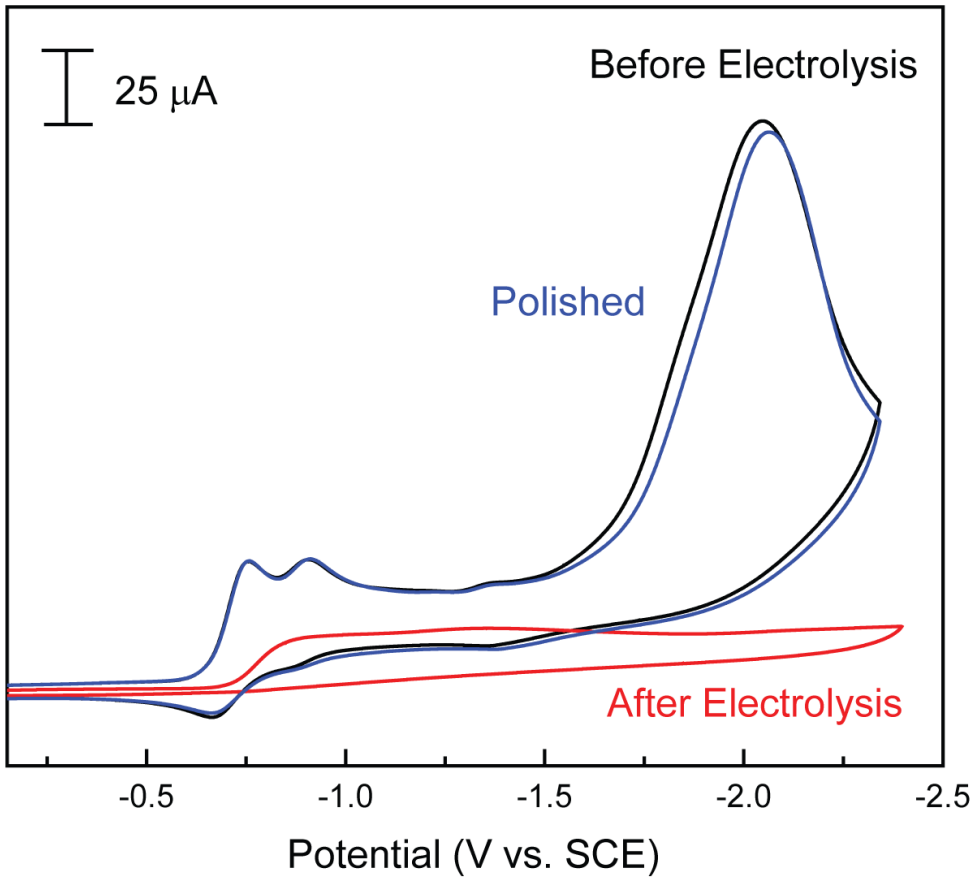

Figure 3.6: Cyclic voltammogram of **Re(BB2)(CO)$_3$Cl** (1 mM in MeCN) showing CO_2 activation before electrolysis (black), followed by suppression of the current enhancement (red) due to catalyst decomposition onto the electrode surface. The GCE electrode was then polished (blue) which revives the catalytic ability of the system. Experiments were performed in acetonitrile under an atmosphere of carbon dioxide at a scan rate of 100 mV/s with a 0.1 M $TBAPF_6$ supporting electrolyte.

3.3.1.2 Electrochemistry in DMF

In order to draw comparison between all three BODIPY derivatives, cyclic voltammetry was performed in DMF and turnover frequencies were determined via

Foot-of-the-Wave analysis. Voltammogram of each BODIPY derivative are shown in Figures 3.7, 3.8, and 3.9.

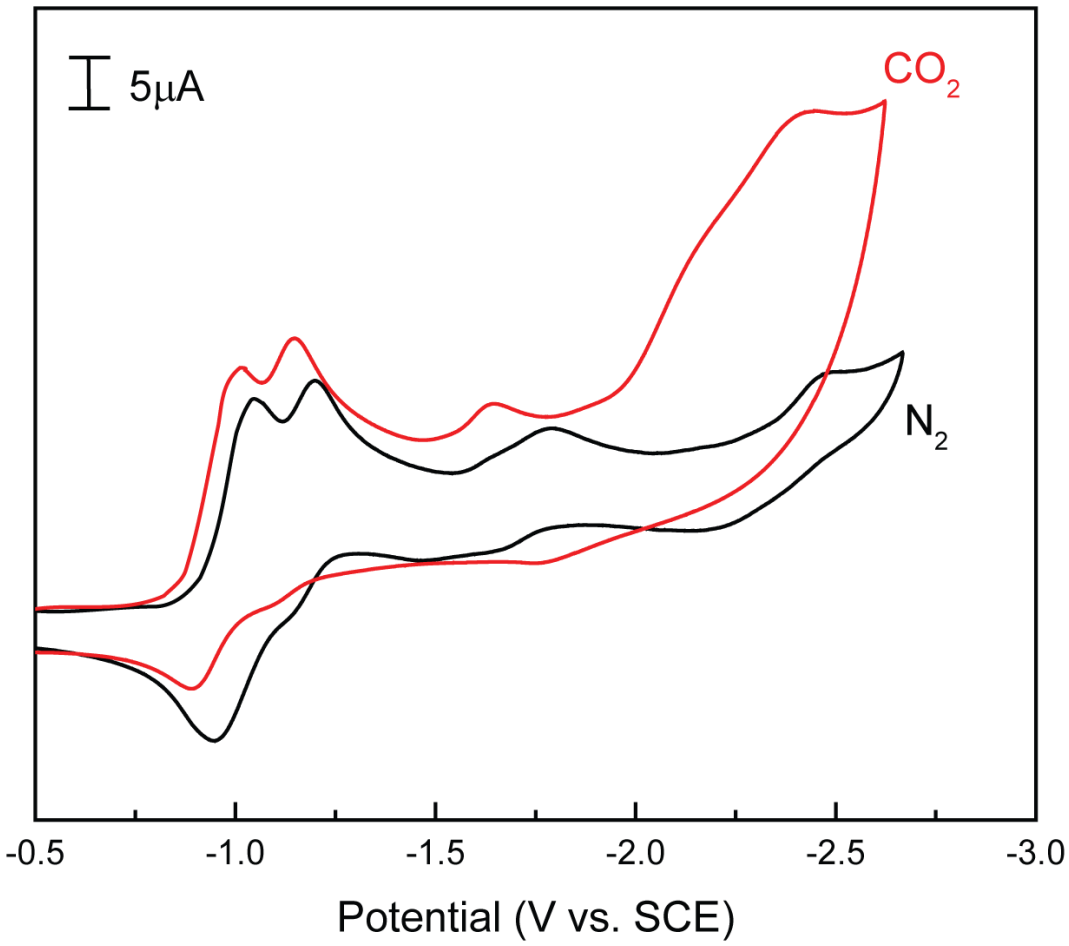

Figure 3.7 Cyclic voltammogram of **Re(BB2)(CO)$_3$Cl** (1 mM in DMF) under an atmosphere of nitrogen (black) and under an atmosphere of carbon dioxide (red). Experiment was performed in DMF at a scan rate of 100 mV/s with a 0.1 M TBAPF$_6$ supporting electrolyte.

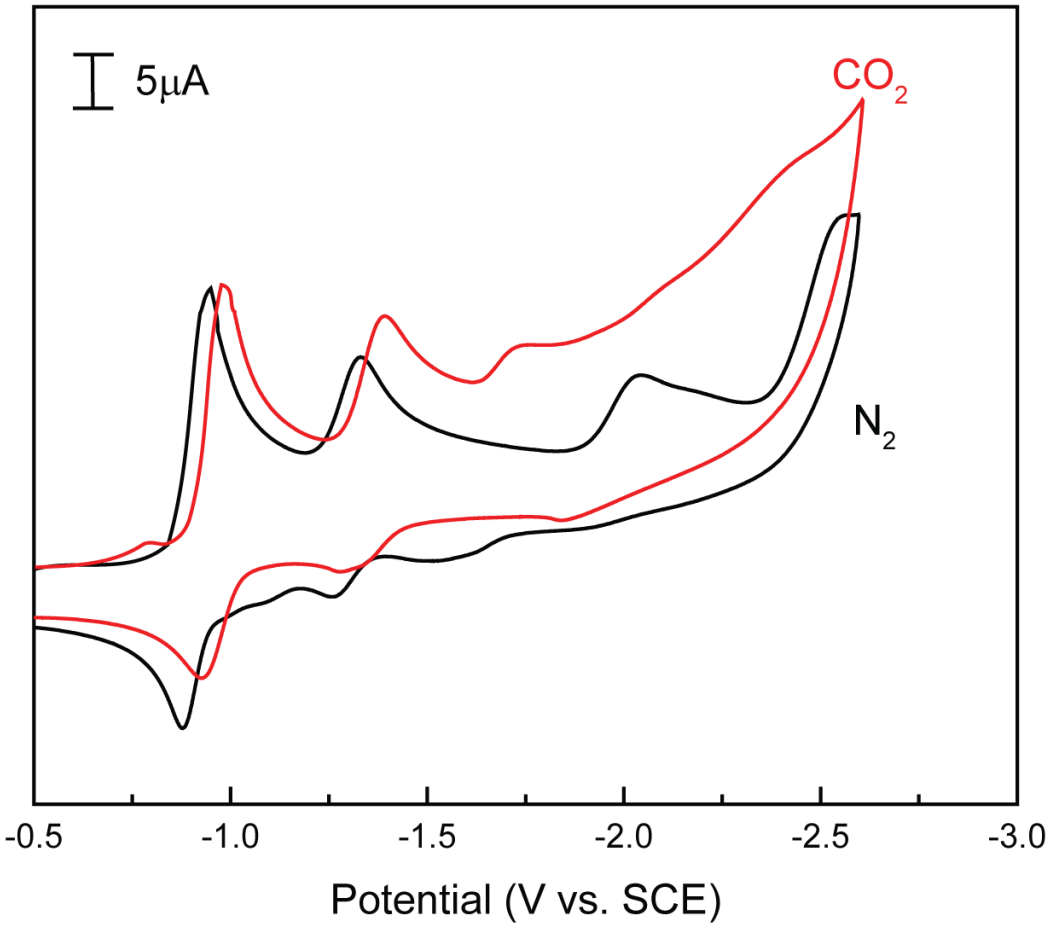

Figure 3.8 Cyclic voltammogram of **Re(BB3)(CO)$_3$Cl** (1 mM in DMF) under an atmosphere of nitrogen (black) and under an atmosphere of carbon dioxide (red). Experiment was performed in DMF at a scan rate of 100 mV/s with a 0.1 M $TBAPF_6$ supporting electrolyte.

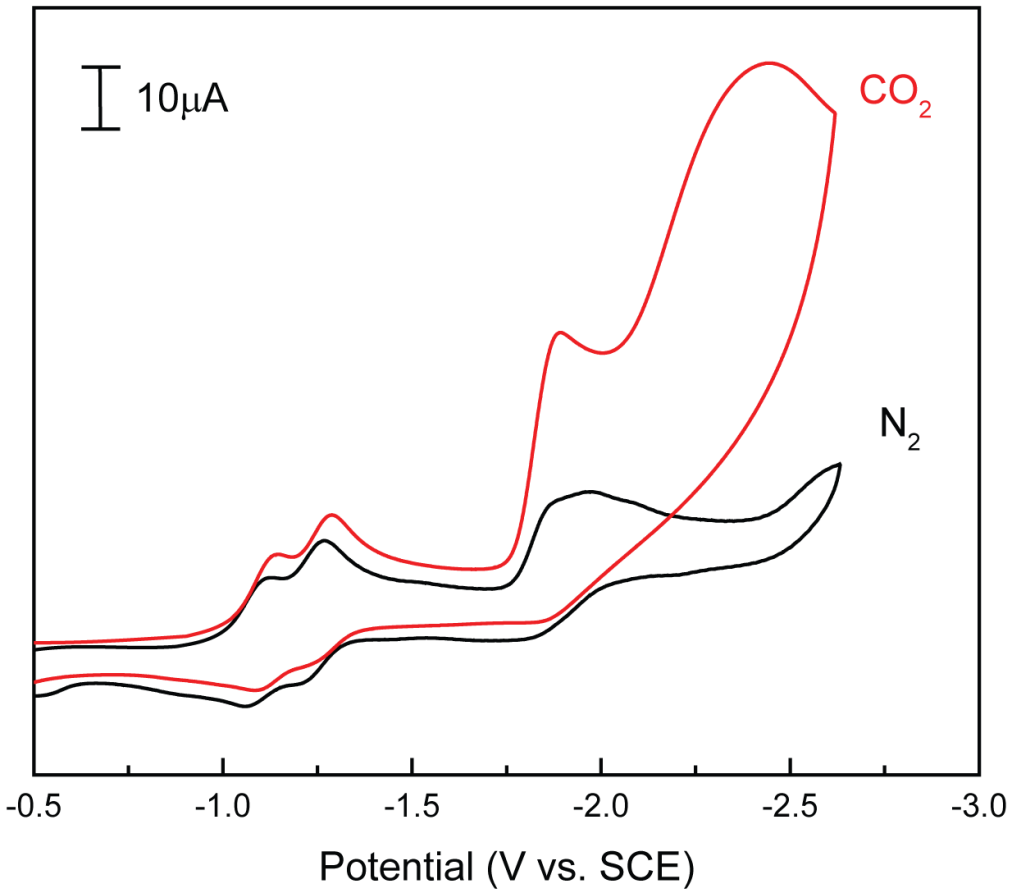

Figure 3.9 Cyclic voltammogram of **Re(BB3)(CO)$_3$Cl** (1 mM in DMF) under an atmosphere of nitrogen (black) and under an atmosphere of carbon dioxide (red). Experiment was performed in DMF at a scan rate of 100 mV/s with a 0.1 M TBAPF$_6$ supporting electrolyte.

The CVs recorded in DMF provide more information to help further understand the catalytic processes of these complexes. All three complexes follow the electronic profile laid out in the previous section for **Re(BB2)(CO)$_3$Cl**: simultaneous reduction of the BODIPY chromophores, followed by reduction of the bipyridine backbone, and the $Re^{I/0}$ couple. However, a new feature becomes apparent under

nitrogen around –2.5V for each complex. An interesting feature occurs for the 6,6' derivative (Figure 3.9) where two current enhancements are observed at –1.8V and –2.35V. The first current enhancement occurs on top of the Re^{I}/Re^{0} couple, and therefore must be the reduction of carbon dioxide by the rhenium(0) radical. The second current enhancement appears to be associated with the redox event at –2.5V under nitrogen; however no data has been collected to determine the identity of this couple.

The electrochemistry data recorded in DMF was also analyzed using Foot-of-the-Wave. Constructing the same plots for all three derivatives (See Appendix A) allowed for calculation of the rate constants and TOFs associated with catalysis. Analysis of the 4,4' derivative (Figure 3.7) yielded a second order rate constant of 0.015 M^{-1} s^{-1} and an initial turnover frequency of 0.015 M^{-1} s^{-1}. The significant decrease in catalytic activity is most likely due to solvent affects or the reduced solubility of carbon dioxide in DMF. Analysis of the 5,5' derivative (Figure 3.8) produced a second order rate constant of 0.44 M^{-1} s^{-1} and an initial turnover frequency of 0.4 M^{-1} s^{-1}. Foot-of-the-wave was applied to both current enhancements for the 6,6' derivative (Figure 3.9) with respect to the same E_{PQ} of –1.8V. The first current enhancement produced a second order rate constant of 2.4 x 10^5 M^{-1} s^{-1} and an initial turnover frequency of 9600 M^{-1} s^{-1}. The second current enhancement yielded a second order rate constant and initial turnover frequency of 59 M^{-1} s^{-1}.

As a result of this interesting chemistry, the mechanism of catalysis is more complex than previously anticipated. Due to multiple catalytic enhancements under an atmosphere of carbon dioxide for **Re(BB4)(CO)$_3$Cl**, it is now apparent that the mechanism of catalysis does not occur in the pathway described in Figure 1.4.

Consequently, it would appear that two distinct pathways are taking place simultaneously during catalysis. The most logical explanation for a second enhancement under an atmosphere of carbon dioxide would be as a result of further reduction of the bipyridine backbone. The question that follows this logic is at what point in the catalytic cycle is the ligand reduced again. Figure 3.10 depicts reduction of the rhenium(I) carboxylate complex.

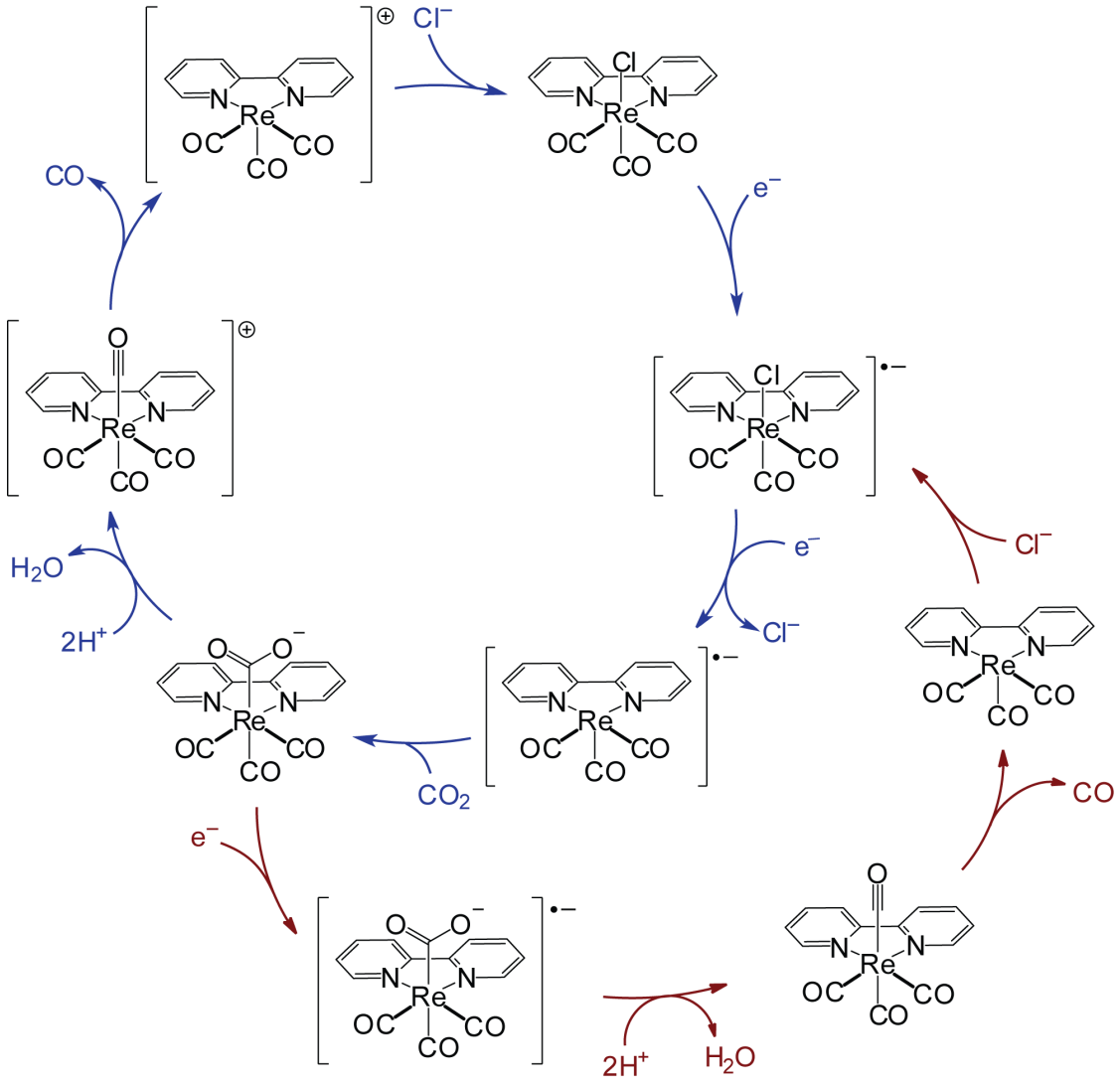

Figure 3.10: Proposed catalytic cycle for the rhenium(I) BODIPY complexes based upon the cyclic voltammetry in DMF. BODIPY substituents are excluded for clarity. Pathway highlighted in blue indicated catalysis based upon the mechanism described in Figure 1.4. The red pathways indicates further reduction of the ligand after formation of the rhenium(I) carboxylate complex.

The pathway highlighted in blue shows the cycle described in Figure 1.4 which is still a possible mechanism. The pathway highlighted in red indicates the reduction

of the bipyridine backbone of the rhenium(I) carboxylate complex to generate the dianionic species. Carbon-oxygen bond cleavage occurs to generate the neutral rhenium(I) tetracarbonyl complex in which the ligand is still reduced. Dissociation of one of the axial carbonyls forms the neutral rhenium(I) tricarbonyl complex which can then re-enter into the catalytic cycle. It is worth noting that a solvent molecule could associate to the complex instead of the chloride ligand, however this ligand dissociates in the next step which means that the identity of the ligand is not important to catalysis. The difference between these two pathways involves the basicity of the anionic carboxylate ligand. A more electron donating metal center would allow for the carboxylate group to be basic enough to proceed with catalysis (blue pathway). Therefore the electron donating ability of the ligand is a pivotal factor of the mechanism. If the ligand is not sufficiently electron donating, further reduction of the ligand is required to increase the basicity of the carboxylate complex.

This mechanism not only explains why we see two enhancements, but also explains the trends we see for the various rhenium(I) complexes described in this discussion. The fact that Kubiak's catalyst (4,4'-di-*tert*-butyl-bpy) has a ligand reduction that occurs the most negative potential of the set indicates that this ligand is the most electron rich. This implies that less back-bonding occurs with the metal center, allowing for sufficient electron density build up on the carboxylate anion. Following this line of thought explains why we see a large enhancement of the $Re^{I/0}$ couple, and a small secondary enhancement for this complex (Appendix A). The large first enhancement implies that Kubiak's catalyst proceeds primarily through the pathway highlighted in blue in Figure 3.10. Moving to Lehn's catalyst, the same trend is apparent, with the complex readily proceeding via either pathway due to the fact

that the ligand is less electron rich compared to Kubiak's catalyst. (Figure 3.2) When electron withdrawing groups are appended to the bipyridine backbone, such as the BODIPY moieties described in this work, catalysis proceeds primarily through the red pathway of Figure 3.10. This would explain the delayed onset of catalysis for **Re(BB2)(CO)$_3$Cl**. Moving to **Re(BB4)(CO)$_3$Cl**, the explanation of both current increases can be accounted for. Due to the reduction potentials of the ligand occurring at a more negative potential than for **Re(BB2)(CO)$_3$Cl** (about 100 mV), **Re(BB4)(CO)$_3$Cl** can proceed through the blue pathway, which explains the enhancement at –1.8 V. However, this enhancement is much smaller compared to Kubiak's and Lehn's catalyst due to the electron withdrawing ability of the BODIPY substituents, even when reduced. The second enhancement, which has a similar shape and occurs at a similar potential as for **Re(BB2)(CO)$_3$Cl**, is catalysis via the red pathway in Figure 3.10.

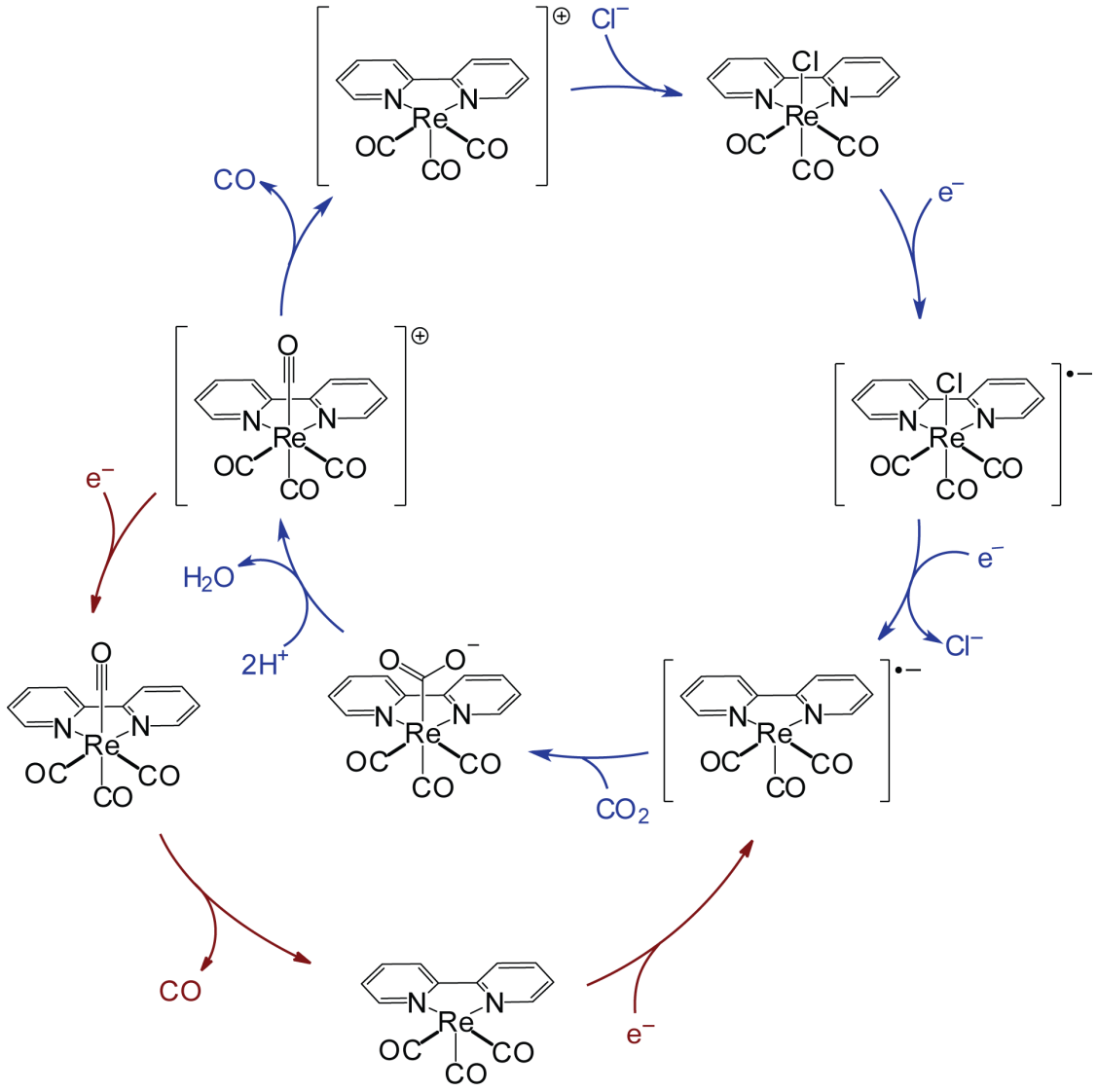

Figure 3.11: Mechanism by which further reduction of the ligand occurs upon formation of the rhenium(I) tetracarbonyl complex. The pathway in blue indicates the mechanism put forth in Figure 1.4, whereas as the pathway in red depicts further reduction of the ligand to drive the catalysis. BODIPY substituents are omitted for clarity.

Another possible mechanism was recently proposed by Kubiak,[80] in which further reduction of the ligand occurs upon generation of the rhenium(I) tetracarbonyl

complex. (Figure 3.11) The original mechanism of carbon dioxide reduction by rhenium bipyridine catalyst raises the question of the driving force behind carbon monoxide dissociation to regenerate the starting catalyst. The fact that the tetracarbonyl complex is a 19-electron complex affords some destabilization to allow for the labilization of one of the carbonyl ligands to generate the 17-electron tricarbonyl complex. However, having an electron deficient ligand can cause stabilization of this intermediate and shut down catalysis via this pathway (blue). If electron deficient ligand are coordinated to the rhenium center, further reduction of the ligand to yield a 20 electron molecule is required to cause enough destabilization to drive the reaction forward to produce the 18-electron tricarbonyl complex. This explains the different catalytic abilities of the rhenium bipyridine derivatives based upon the electron donating ability of the ligand framework (4,4'-di-*tert*-butyl-bpy >> bpy > **BB4** > **BB2**) and how that affects the catalytic properties of the rhenium(I) complex.

3.4 Conclusions

The conversion of CO_2 to CO is a process of potential importance for the storage and distribution of renewable energy resources. In this work, we have developed a set of new electrocatalysts for this reaction. This system is comprised of a *fac*-$Re^{I}(CO)_3$ center supported by a non-innocent bipyridine ligand with appended BODIPY moieties. Electrochemical experiments reveal that **Re(BB2)(CO)$_3$Cl** in acetonitrile and **Re(BB4)(CO)$_3$Cl** in DMF support rich redox chemistry and can be reduced by up to four electrons at modest potentials, with each BODIPY unit serving as a redox reservoir. The ability of the ligand set to store multiple electron equivalents is manifest in enhanced activity for electrocatalytic CO_2 reduction relative to Lehn's

unsubstituted Re-bipyridine homologue (**Re(bpy)(CO)$_3$Cl**). Foot-of-the-wave analysis shows that the rate constant for activation of CO_2 by **Re(BB2)(CO)$_3$Cl** in acetonitrile is approximately three times greater than for **Re(bpy)(CO)$_3$Cl** at –2.0 V. Foot-of-the-wave analysis also shows that the second order rate constant for reduction of carbon dioxide by **Re(BB4)(CO)$_3$Cl** is over one hundred times greater than that of **Re(bpy)(CO)$_3$Cl** in DMF[77] at –2.0 V as well as a 10-fold increase in initial turnover frequency It is notable that this enhancement is realized despite the fact that the BODIPY appended complex is reduced at potentials that are roughly 350 mV more positive than the corresponding unsubstituted variant. Additionally, the electron donating ability of the ligand framework to the rhenium center is essential to the mechanism of carbon dioxide reduction catalysis.

In addition to the voltammetric analyses, CPE experiments confirm that **Re(BB2)(CO)$_3$Cl** and is an electrocatalyst for conversion of CO_2 to CO. These CPE experiments also reveal that while this system is stable in MeCN solution under electrolysis conditions, the extended π-systems that comprise the **BB2** ligand lead to decomposition of **Re(BB2)(CO)$_3$Cl** onto and passivation of the working electrode surface. When taken together, these findings suggest that this platform might be especially effective as a homogeneous catalyst for CO_2 reduction. Moreover, the notable ability of BODIPY[81,,,85] and other polypyrrole derivatives[86,,,89] to absorb light throughout the visible region may distinguish **Re(BB2)(CO)$_3$Cl** and similar complexes for the direct photochemical reduction of CO_2. It is with this goal in mind that the photophysics and photocatalytic activity of **Re(BB2)(CO)$_3$Cl** and related platforms are currently being evaluated in our laboratory.

REFERENCES

[1] Hoffert, M. I.; Caldeira, K.; Jain, A. K.; Haites, E. F.; Harvey, L. D. D.; Potter, S. D.; Schlesinger, M. E.; Schneider, S. H.; Watts, R. G.; Wigley, T. M. L.; Wuebbles, D. J., Energy implications of future stabilization of atmospheric CO2 content. *Nature* **1998,** *395* (6705), 881-884.

[2] National Climate Data Center. http://www.ncdc.noaa.gov/indicators/ (Accessed Apr. 11, 2013).

[3] Data Distribution Centre. http://www.ipcc-data.org/ddc_co2.html (Accesssed on Apr. 1, 2013).

[4] *Annual Energy Review 2011*. US Energy Information Administration, September 2012.

[5] Lewis, N. S., Powering the Planet. *MRS Bulletin* **2007,** *32* (10), 808-820.

[6] *World Energy Outlook 2012 Executive Summary*. International Energy Agency, March 2013.

[7] International Energy Agency. http://www.iea.org/ (Accessed on Mar. 21, 2013).

[8] Carlson, D. E.; Wronski, C. R. *Appl. Phys. Lett.* **1976**, *28*, 671.

[9] Chapin, D. M.; Fuller, C. S.; Pearson, G. L. *J. Appl. Phys.* **1954**, *25*, 676.

[10] Staebler, D. L.; Wronski, C. R. *Appl. Phys. Lett.* **1977**, *31*, 292.

[11] Gregg, B. A. *J. Phys. Chem. B* **2003**, *107*, 4688.

[12] Wang, P.; Zakeeruddin, S. M.; Moser, J. E.; Nazeeruddin, M. K.; Sekiguchi, T.; Graetzel, M. *Nat. Mater.* **2003**, *2*, 402.

13 Tian, B.; Zheng, X.; Kempa, T. J.; Fang, Y.; Yu, N.; Yu, G.; Huang, J.; Lieber, C. M. *Nature (London, U. K.)* **2007**, *449*, 885.

14 Garnett, E.; Yang, P. *Nano Lett.* **2010**, *10*, 1082.

15 Anpo, M.; Takeuchi, M. *J. Catal.* **2003**, *216*, 505.

16 Barbe, C. J.; Arendse, F.; Comte, P.; Jirousek, M.; Lenzmann, F.; Shklover, V.; Gratzel, M. *J. Am. Ceram. Soc.* **1997**, *80*, 3157.

17 Carp, O.; Huisman, C. L.; Reller, A. *Prog. Solid State Chem.* **2004**, *32*, 33.

18 Horiuchi, T.; Miura, H.; Sumioka, K.; Uchida, S. *J. Am. Chem. Soc.* **2004**, *126*, 12218.

19 Kim, J. Y.; Kim, S. H.; Lee, H.-H.; Lee, K.; Ma, W.; Gong, X.; Heeger, A. J. *Adv. Mater. (Weinheim, Ger.)* **2006**, *18*, 572.

20 Mor, G. K.; Shankar, K.; Paulose, M.; Varghese, O. K.; Grimes, C. A. *Nano Lett.* **2006**, *6*, 215.

21 Mor, G. K.; Varghese, O. K.; Paulose, M.; Shankar, K.; Grimes, C. A. *Sol. Energy Mater. Sol. Cells* **2006**, *90*, 2011.

22 Nazeeruddin, M. K.; Kay, A.; Rodicio, I.; Humphry-Baker, R.; Mueller, E.; Liska, P.; Vlachopoulos, N.; Graetzel, M. *J. Am. Chem. Soc.* **1993**, *115*, 6382.

23 O'Regan, B.; Graetzel, M. *Nature (London)* **1991**, *353*, 737.

24 Robel, I.; Subramanian, V.; Kuno, M.; Kamat, P. V. *J. Am. Chem. Soc.* **2006**, *128*, 2385.

25 Yella, A.; Lee, H.-W.; Tsao, H. N.; Yi, C.; Chandiran, A. K.; Nazeeruddin, M. K.; Diau, E. W.-G.; Yeh, C.-Y.; Zakeeruddin, S. M.; Graetzel, M. *Science (Washington, DC, U. S.)* **2011**, *334*, 629.

26 Padhi, A. K.; Nanjundaswamy, K. S.; Goodenough, J. B. *J. Electrochem. Soc.* **1997**, *144*, 1188.

[27] Mizushima, K.; Jones, P. C.; Wiseman, P. J.; Goodenough, J. B. *Mater. Res. Bull.* **1980**, *15*, 783.

[28] Kang, B.; Ceder, G. *Nature (London, U. K.)* **2009**, *458*, 190.

[29] Goodenough, J. B.; Kim, Y. *Chem. Mater.* **2010**, *22*, 587.

[30] Conway, B. E. *J. Electrochem. Soc.* **1991**, *138*, 1539.

[31] Che, G.; Lakshmi, B. B.; Fisher, E. R.; Martin, C. R. *Nature (London)* **1998**, *393*, 346.

[32] Chan, C. K.; Peng, H.; Liu, G.; McIlwrath, K.; Zhang, X. F.; Huggins, R. A.; Cui, Y. *Nat. Nanotechnol.* **2008**, *3*, 31.

[33] Bruce, P. G.; Scrosati, B.; Tarascon, J.-M. *Angew. Chem., Int. Ed.* **2008**, *47*, 2930.

[34] Arico, A. S.; Bruce, P.; Scrosati, B.; Tarascon, J.-M.; van, S. W. *Nat. Mater.* **2005**, *4*, 366.

35. Rofer-DePoorter, C. K. *Chem. Rev.* **2012**, *81*, 447–474.

36. Vennestrøm, P. N. R.; Osmundsen, C. M.; Christensen, C. H.; Taarning, E. *Angew. Chem. Int. Ed.* **2011***, 50*, 10502–10509.

37. T. Takeshita, K. Yamaji *Energy Policy* **2008**, *36*, 2773–2784.

[38] Takeda, H.; Ishitani, O. *Coord. Chem. Rev.* **2010**, *254*, 346.

[39] Sutin, N.; Creutz, C.; Fujita, E. *Comments Inorg. Chem.* **1997**, *19*, 67.

[40] Bazzicalupi, C.; Bencini, A.; Bencini, A.; Bianchi, A.; Corana, F.; Fusi, V.; Giorgi, C.; Paoli, P.; Paoletti, P.; et, a. *Inorg. Chem.* **1996**, *35*, 5540.

[41] Costamagna, J.; Ferraudi, G.; Canales, J.; Vargas, J. *Coord. Chem. Rev.* **1996**, *148*, 221.

[42] Fisher, B. J.; Eisenberg, R. *J. Am. Chem. Soc.* **1980**, *102*, 7361.

[43] Matsuoka, S.; Yamamoto, K.; Ogata, T.; Kusaba, M.; Nakashima, N.; Fujita, E.; Yanagida, S. *J. Am. Chem. Soc.* **1993**, *115*, 601.

[44] Ogata, T.; Yanagida, S.; Brunschwig, B. S.; Fujita, E. *J. Am. Chem. Soc.* **1995**, *117*, 6708.

[45] Vigato, P. A.; Tamburini, S.; Fenton, D. E. *Coord. Chem. Rev.* **1990**, *106*, 25.

[46] DuBois, D. L.; Miedaner, A.; Haltiwanger, R. C. *J. Am. Chem. Soc.* **1991**, *113*, 8753.

[47] Elek, J.; Nadasdi, L.; Papp, G.; Laurenczy, G.; Joo, F. *Appl. Catal., A* **2003**, *255*, 59.

[48] Gassner, F.; Leitner, W. *J. Chem. Soc., Chem. Commun.* **1993**, 1465.

[49] Laurenczy, G.; Joo, F.; Nadasdi, L. *Inorg. Chem.* **2000**, *39*, 5083.

[50] Miedaner, A.; Curtis, C. J.; Barkley, R. M.; DuBois, D. L. *Inorg. Chem.* **1994**, *33*, 5482.

51. Ishida, H.; Tanaka, K.; Tanaka, T. *Organometallics*, **1987**, *6*, 181–186.

52. Nagao, H.; Mizukawa, T.; Tanaka, K. *Inorg. Chem.* **1994**, *33*, 3415–3420.

53. Takeuchi, K. J.; Thompson, M. S.; Pipes, D. W.; Meyer, T. J. *Inorg. Chem.* **1984**, *23*, 1845–1851.

54. Concepcion, J. J.; Jurss, J. W.; Norris, M. R.; Chen, Z.; Templeton, J. L.; Meyer, T. J. *Inorg. Chem.* **2010**, *49*, 1277–1279.

55. Chen, Z.; Chen, C.; Weinberg, D. R.; Kang, P.; Concepcion, J. J.; Harrison, D. P.; Brookhart, M. S.; Meyer, T. J. *Chem. Commun.* **2011,** *47*, 12607–12609.

56. Chen, Z.; Concepcion, J. J.; Brennaman, M. K.; Kang, P.; Norris, M. R.; Hoertz, P. G.; Meyer, T. J. *Proc. Natl. Acad. Sci. USA* **2012,** *109*, 15606–15611.

57. Sullivan, B. P.; Meyer, T. J., *Organometallics* **1986,** *5*, 1500–1502.

58. O'Toole, T. R.; Sullivan, B. P.; Bruce, M. R. M.; Margerum, L. D.; Murray, R. W.; Meyer, T. J. *J. Electroanal. Chem. Interfacial Electrochem.* **1989,** *259*, 217–39.

59. O'Toole, T. R.; Margerum, L. D.; Westmoreland, T. D.; Vining, W. J.; Murray, R. W.; Meyer, T. J. *Chem. Commun.* **1985**, 1416–1417.

60. Agarwal, J.; Sanders, B. C.; Fujita, E.; Schaefer, I. I. I. H. F.; Harrop, T. C.; Muckerman, J. T. *Chem. Commun.* **2012,** *48*, 6797–6799.

61. Agarwal, J.; Johnson, R. P.; Li, G. *J. Phys. Chem. A* **2011,** *115*, 2877–2881.

62. Agarwal, J.; Fujita, E.; Schaefer, H. F.; Muckerman, J. T. *J. Am. Chem. Soc.* **2012,** *134,* 5180–5186.

63. Sullivan, B. P.; Meyer, T. J. *Organometallics* **1986**, *5*, 1500–1502.

64. Sullivan, B. P.; Meyer, T. J., *Chem. Commun* **1984**, 1244–1245.

65 Hawecker, J.; Lehn, J.-M.; Ziessel, R. *Journal of the Chemical Society, Chemical Communications* **1984**, *0*, 328.

66 Kumar, B.; Smieja, J. M.; Kubiak, C. P. *J. Phys. Chem. C* **2010**, *114*, 14220.

67 Benson, E. E.; Kubiak, C. P. *Chem. Commun. (Cambridge, U. K.)* **2012**, *48*, 7374.

68 Kumar, B.; Smieja, J. M.; Sasayama, A. F.; Kubiak, C. P. *Chem. Commun. (Cambridge, U. K.)* **2012**, *48*, 272.

69 Smieja, J. M.; Benson, E. E.; Kumar, B.; Grice, K. A.; Seu, C. S.; Miller, A. J. M.; Mayer, J. M.; Kubiak, C. P. *Proc. Natl. Acad. Sci. U. S. A.* **2012**, *109*, 15646.

70 Smieja, J. M.; Kubiak, C. P. *Inorg. Chem.* **2010**, *49*, 9283.

71. Rosenthal, J.; Nepomnyashchii, A. B.; Kozhukh, J.; Bard, A. J.; Lippard, S. J., *J. Phys. Chem. C* **2011,** *115*, 17993–18001.

72 Uhlich, N. A.; Sommer, P.; Buhr, C.; Schurch, S.; Reymond, J.-L.; Darbre, T. *Chem Commun (Camb)* **2009**, 6237.

[73] Tiecco, M.; Testaferri, L.; Tingoli, M.; Chianelli, D.; Montanucci, M. *Synthesis* **1984**, 736.

[74].Frisch, M. J.; Trucks, G. W.; Schlegel, H. B.; Scuseria, G. E.; Robb, M. A.; Cheeseman, J. R.; Scalmani, G.; Barone, V.; Mennucci, B.; Petersson, G. A.; Nakatsuji, H.; Caricato, M.; Li, X.; Hratchian, H. P.; Izmaylov, A. F.; Bloino, J.; Zheng, G.; Sonnenberg, J. L.; Hada, M.; Ehara, M.; Toyota, K.; Fukuda, R.; Hasegawa, J.; Ishida, M.; Nakajima, T.; Honda, Y.; Kitao, O.; Nakai, H.; Vreven, T.; Montgomery, Jr., J. A.; Peralta, J. E.; Ogliaro, F.; Bearpark, M.; Heyd, J. J.; Brothers, E.; Kudin, K. N.; Staroverov, V. N.; Kobayashi, R.; Normand, J.; Raghavachari, K.; Rendell, A.; Burant, J. C.; Iyengar, S. S.; Tomasi, J.; Cossi, M.; Rega, N.; Millam, J. M.; Klene, M.; Knox, J. E.; Cross, J. B.; Bakken, V.; Adamo, C.; Jaramillo, J.; Gomperts, R.; Stratmann, R. E.; Yazyev, O.; Austin, A. J.; Cammi, R.; Pomelli, C.; Ochterski, J. W.; Martin, R. L.; Morokuma, K.; Zakrzewski, V. G.; Voth, G. A.; Salvador, P.; Dannenberg, J. J.; Dapprich, S.; Daniels, A. D.; Farkas, Ö.; Foresman, J. B.; Ortiz, J. V.; Cioslowski, J.; Fox, D. J. Gaussian 09, Revision **A.1;** Gaussian, Inc., Wallingford CT, 2009.

[75] Costentin, C.; Drouet, S.; Robert, M.; Saveant, J.-M., Turnover Numbers, Turnover Frequencies, and Overpotential in Molecular Catalysis of Electrochemical Reactions. Cyclic Voltammetry and Preparative-Scale Electrolysis. *J. Am. Chem. Soc.* **2012,** *134* (Copyright (C) 2013 American Chemical Society (ACS). All Rights Reserved.), 11235-11242.

[76] Costentin, C.; Drouet, S.; Robert, M.; Saveant, J.-M., Turnover Numbers, Turnover Frequencies, and Overpotential in Molecular Catalysis of Electrochemical Reactions. Cyclic Voltammetry and Preparative-Scale Electrolysis [Erratum to document cited in CA157:116043]. *J. Am. Chem. Soc.* **2012,** *134* (Copyright (C) 2013 American Chemical Society (ACS). All Rights Reserved.), 19949-19950.

[77] Costentin, C.; Drouet, S.; Robert, M.; Saveant, J.-M., A Local Proton Source Enhances CO2 Electroreduction to CO by a Molecular Fe Catalyst. *Science (Washington, DC, U. S.)* **2012,** *338* (Copyright (C) 2013 American Chemical Society (ACS). All Rights Reserved.), 90-94.

[78] Y. Tomita, S. T., O. Koga, and Y. Hori, Electrochemical Reduction of Carbon Dioxide at a Platinum Electrode in Acetonitrile-Water Mixtures. *Journal of The Electrochemical Society* **200,** *147* (11), 4164-4167.

[79] Roy, S.; Blane, T.; Lilio, A.; Kubiak, C. P. *Inorg. Chim. Acta*, **2011**, *374*, 134–139.

[80] Grice, K. A.; Gu, N. X.; Sampson, M. D.; Kubiak, C. P. *Dalton Trans.*, **2013**. In press.

[81] Loudet, A.; Burgess, K. *Chem. Rev*. **2007**, *107*, 4891−4932.

[82] Ziessel, R.; Ulrich, G.; Harriman, A. *New J. Chem*. **2007**, *31*, 496− 501.

[83] Lazarides, T.; McCormick, T. M.; Wilson, K. C.; Lee, S.; McCamant, D. W.; Eisenberg, R. J. *Am. Chem. Soc*. **2011**, *133*, 350–364.

[84] B. Turfan and E. U. Akkaya, *Org. Lett*. **2002**, *4*, 2857–2859.

[85] Nepomnyashchii, A. B.; Pistner, A. J.; Bard, A. J.; Rosenthal, J. *J. Phys. Chem. C*, **2013**, 117, 5599–5609.

[86] Lee, C. Y.; Hupp, J. T. *Langmuir* **2010**, *26*, 3760−3765.

[87] Leonardi, M. J.; Topka, M. R.; Dinolfo, P. H. *Inorg. Chem.* **2012**, *51*, 13114–13122.

[88] Pistner, A. J.; Yap, G. P. A.; Rosenthal, J. *J. Phys. Chem. C* **2012**, *116*, 16918–16924.

[89] Pistner, A. J.; Lutterman, D. A.; Ghidiu, M. J.; Ma, Y. –Z.; Rosenthal, J. *J. Am. Chem. Soc.* **2013**, *135*, In press.

Appendix A

ELECTROCHEMISTRY

Additional Cyclic Voltammetry.

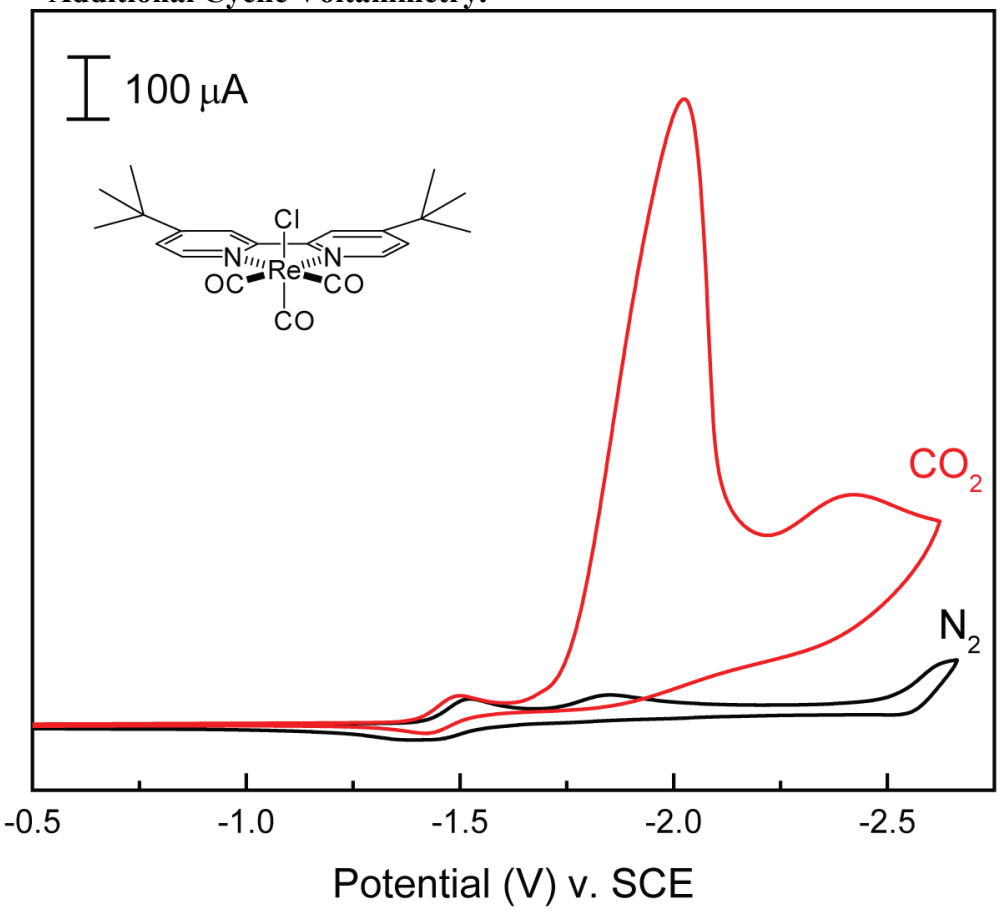

Foot-of-the-Wave Analysis in Acetonitrile.

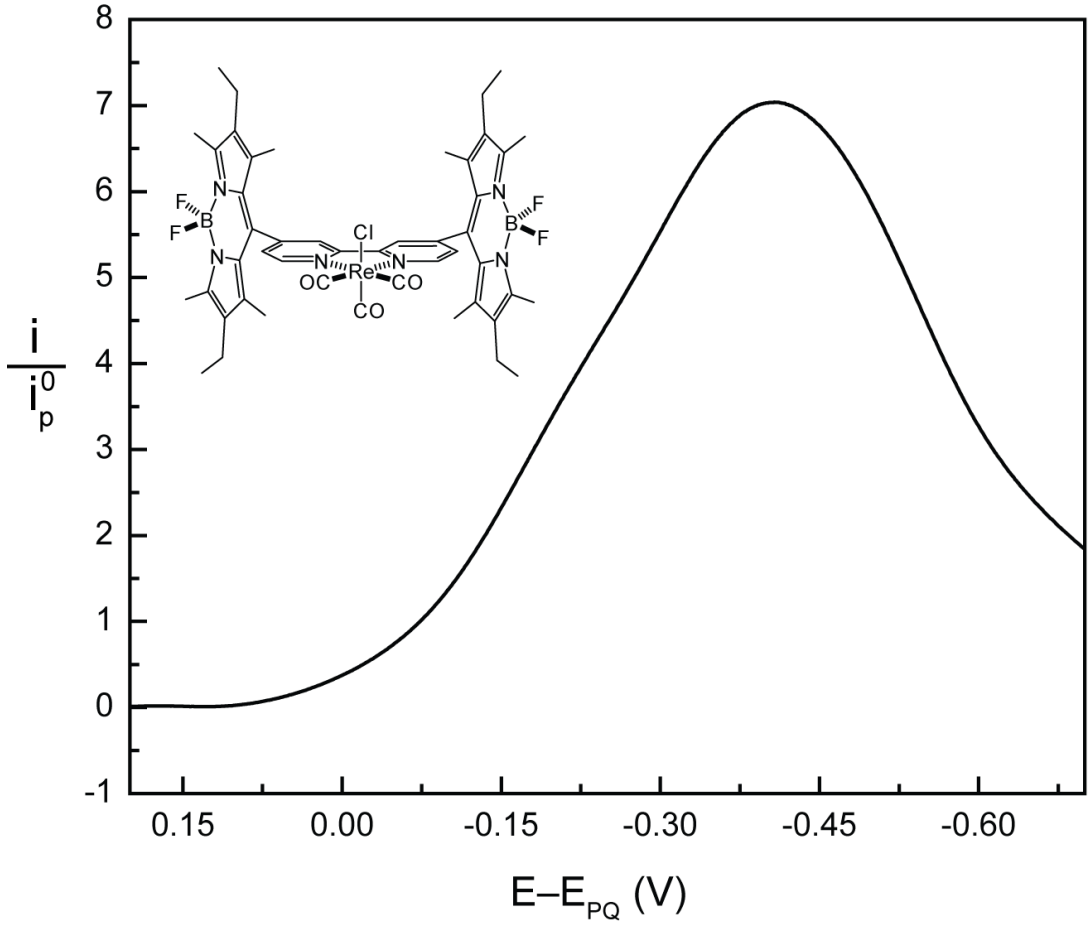
8
7
6
5
4
3
2
1
0
-1
0.15
0.00
-0.15
-0.30
-0.45
-0.60
i / i_p^0
E–E_PQ (V)
F
B
F
N
N
Cl
N
Re
N
OC
CO
CO
N
B
F
F
N

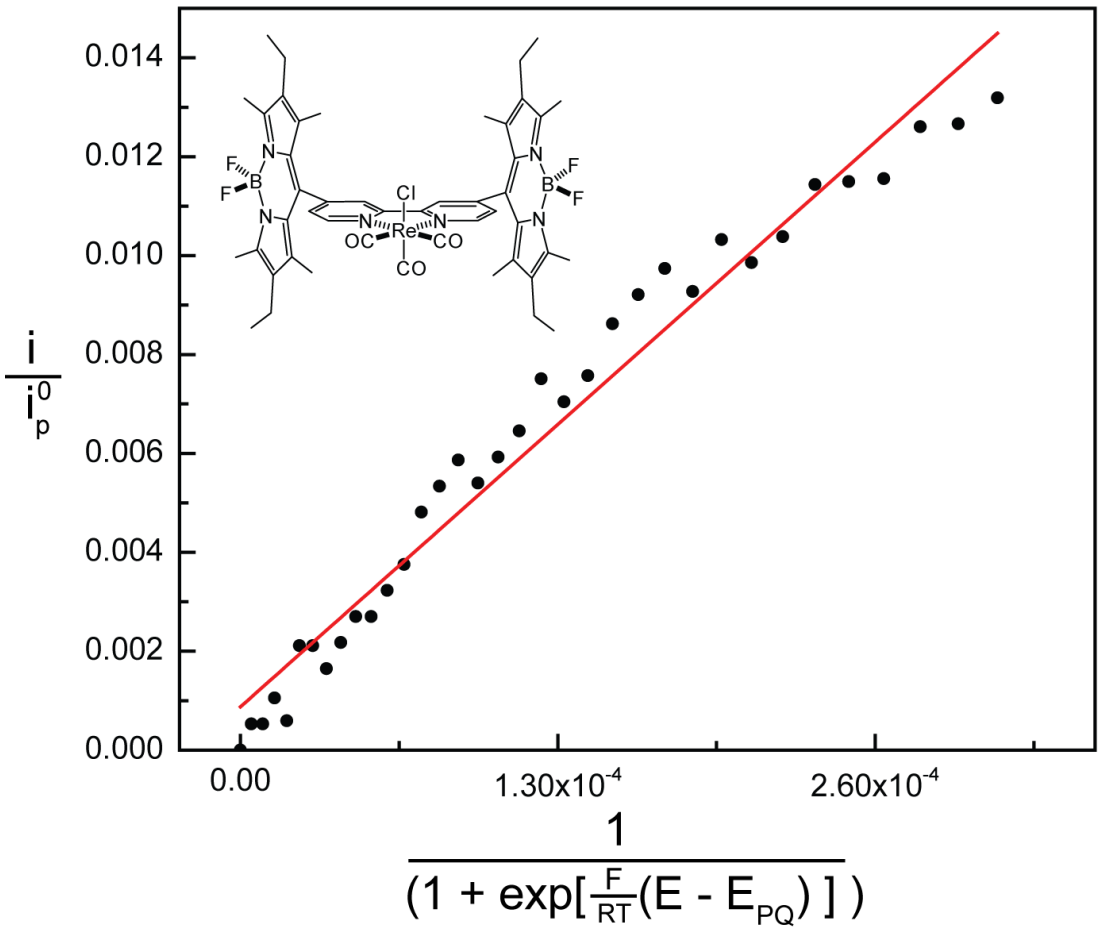
0.014
0.012
0.010
0.008
0.006
0.004
0.002
0.000
i / i_p^0
0.00
1.30x10^-4
2.60x10^-4
1 / (1 + exp[F/RT(E - E_PQ)])
F
B
N
Cl
Re
OC
CO

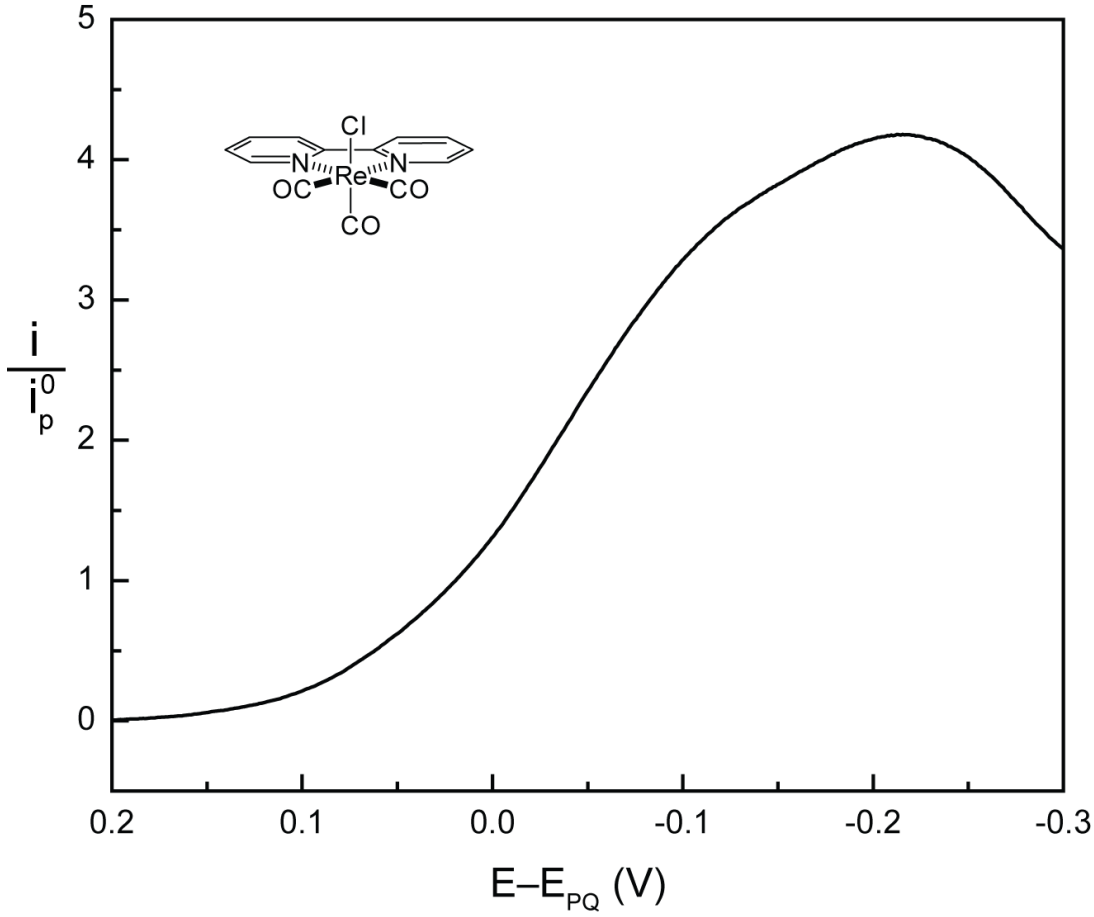
5
4
3
2
1
0
i / i_p^0
0.2
0.1
0.0
-0.1
-0.2
-0.3
E–E_PQ (V)
Cl
N
Re
N
OC
CO
CO

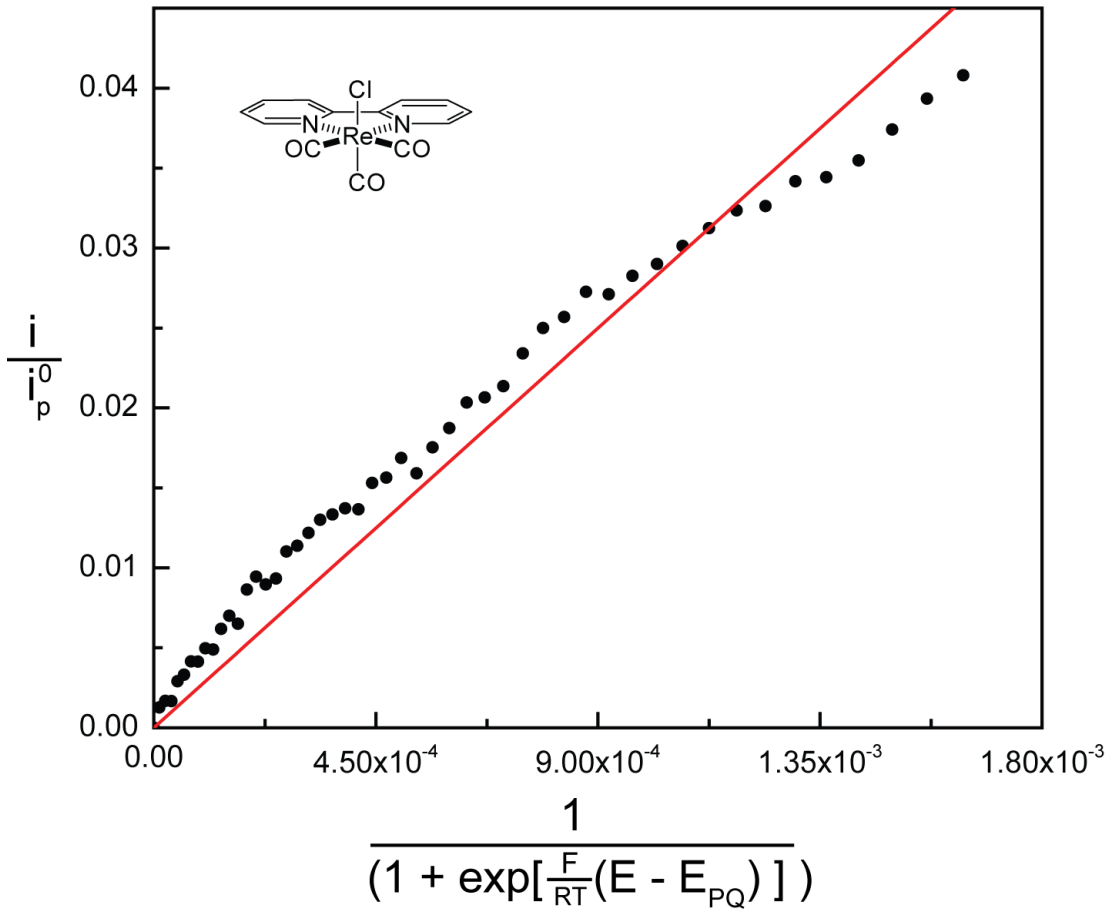
Cl
N
N
OC
Re
CO
CO
0.04
0.03
0.02
0.01
0.00
i / i_p^0
0.00
4.50x10^-4
9.00x10^-4
1.35x10^-3
1.80x10^-3
1 / (1 + exp[F/RT (E - E_PQ)])

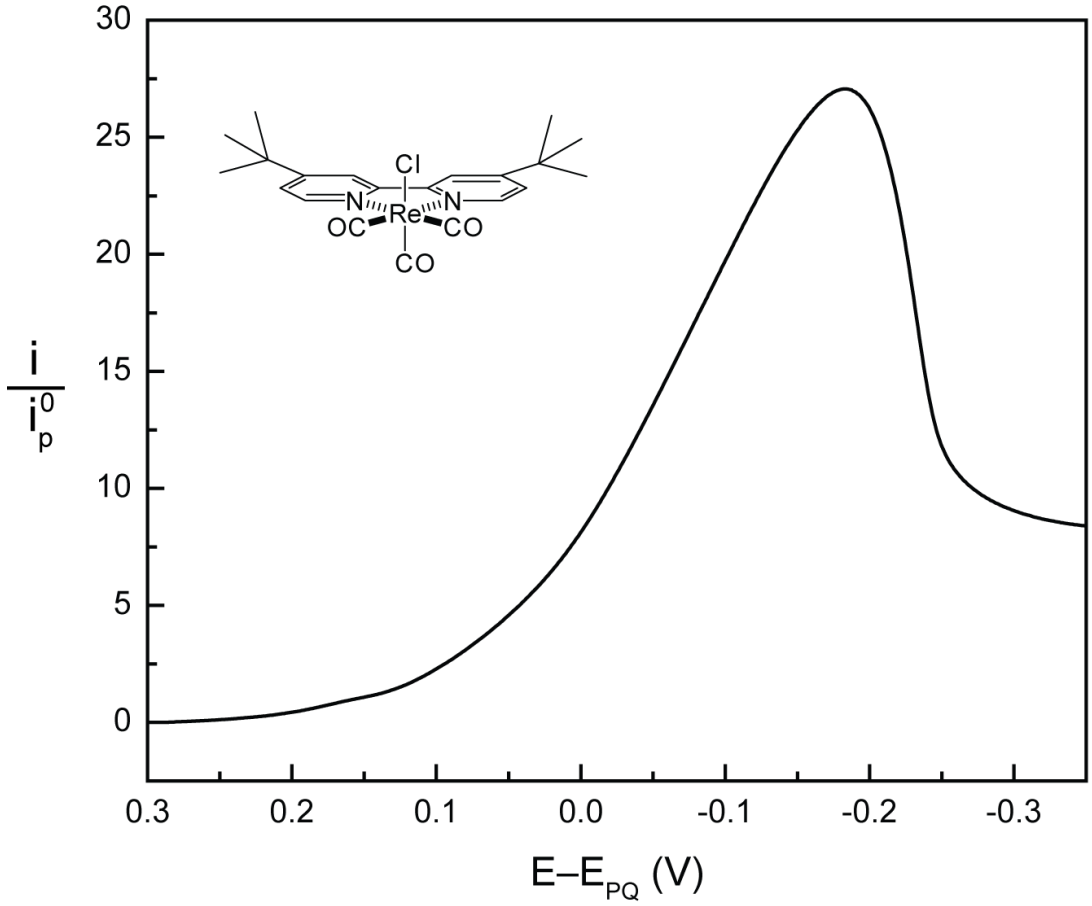
30
25
20
15
10
5
0
i
i_p^0
0.3
0.2
0.1
0.0
-0.1
-0.2
-0.3
E–E_PQ (V)
Cl
N
Re
N
OC
CO
CO

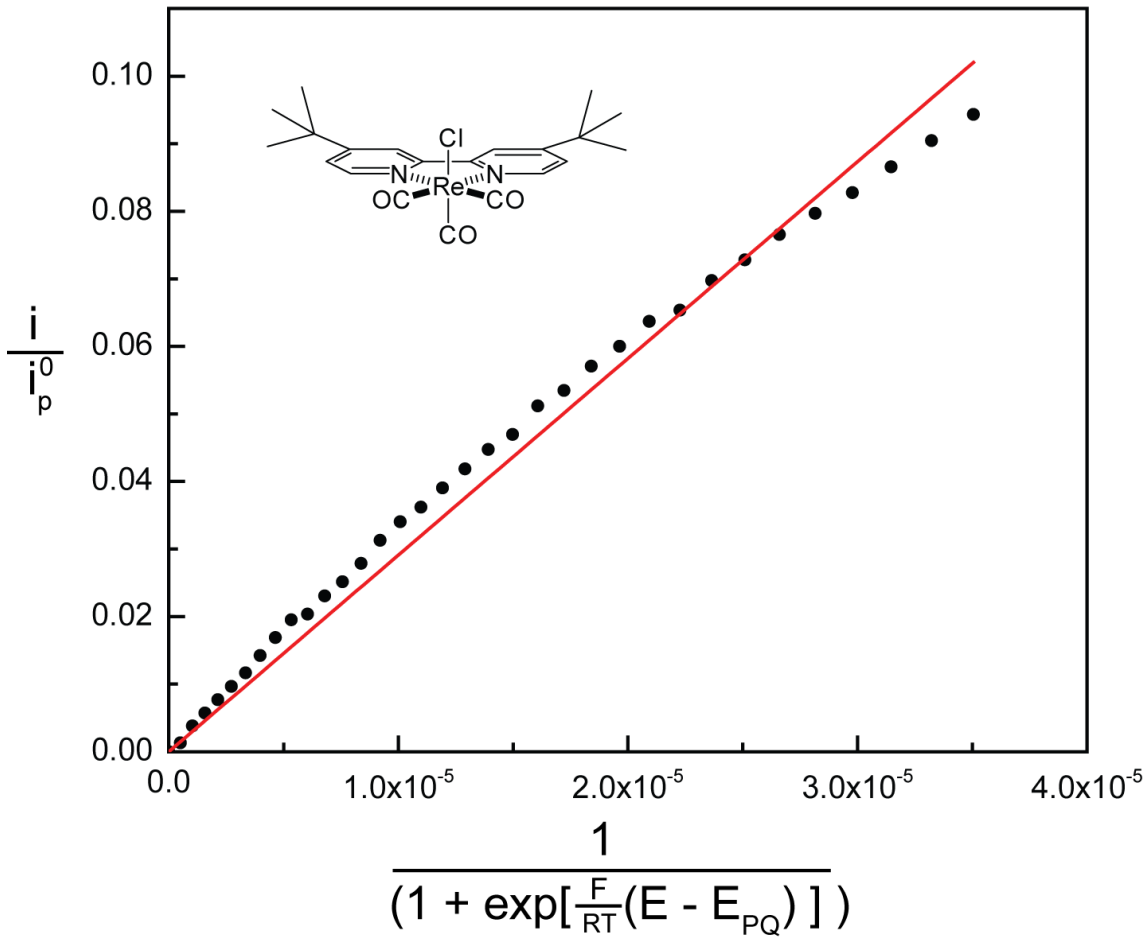

Foot-of-the-Wave Analysis in DMF

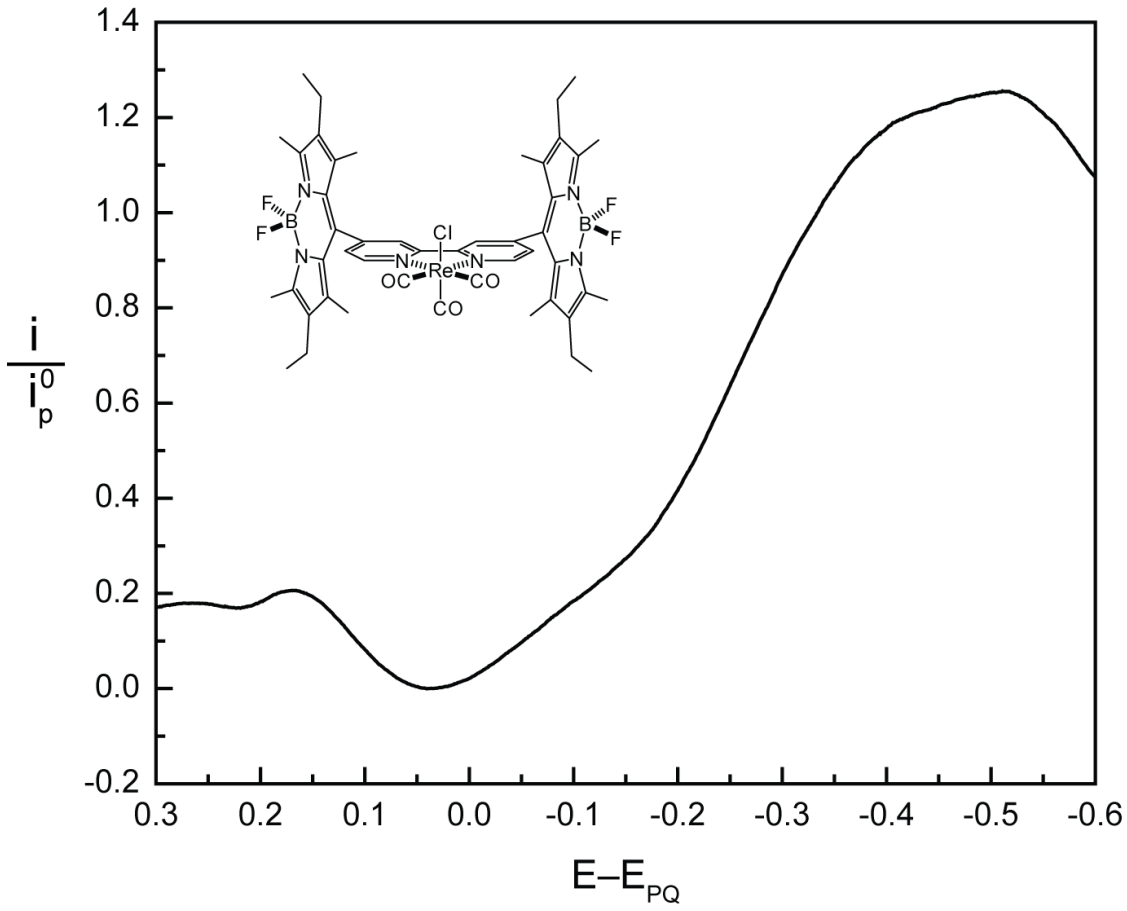
1.4
1.2
1.0
0.8
0.6
0.4
0.2
0.0
-0.2
i / i_p^0
0.3
0.2
0.1
0.0
-0.1
-0.2
-0.3
-0.4
-0.5
-0.6
E–E_PQ
F
B
F
N
Cl
N
Re
N
OC
CO
CO

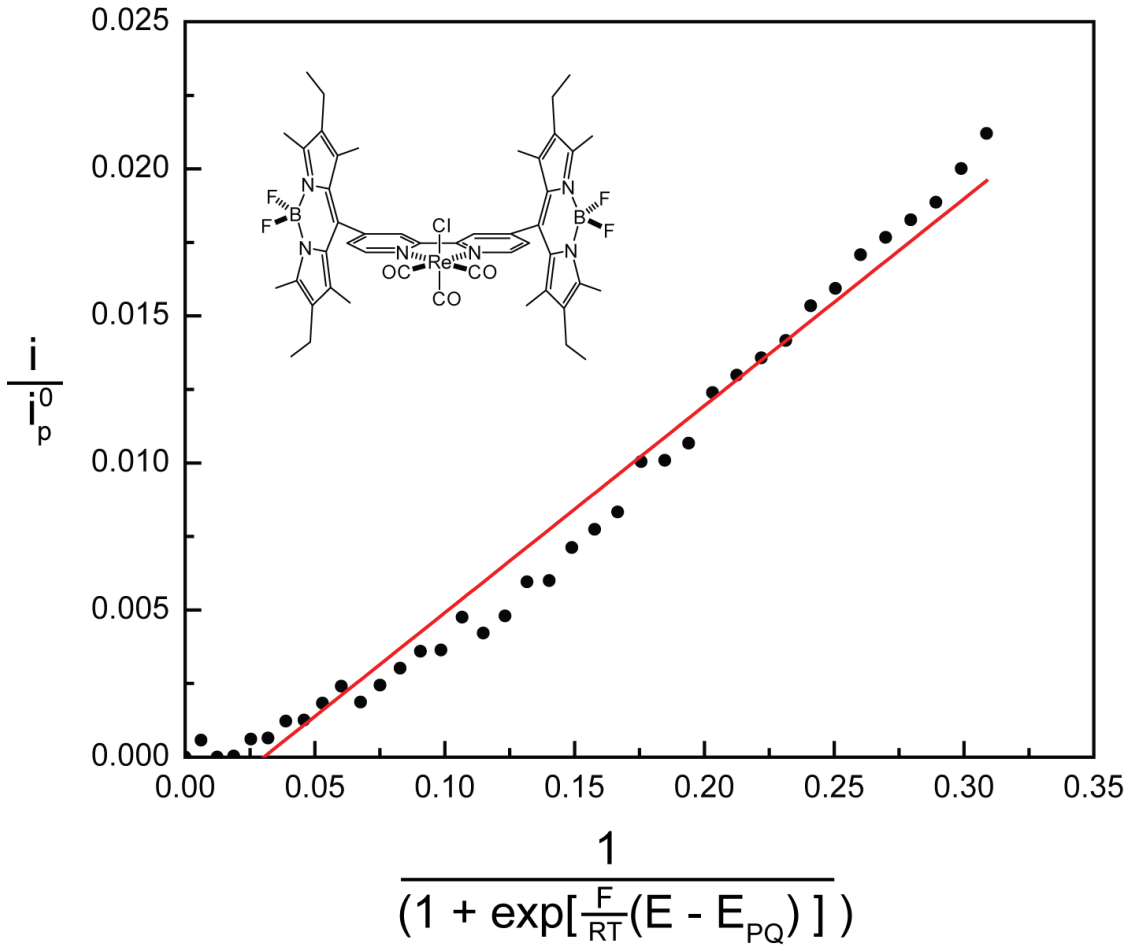
0.025
0.020
0.015
0.010
0.005
0.000
0.00
0.05
0.10
0.15
0.20
0.25
0.30
0.35
i / i_p^0
1 / (1 + exp[F/RT (E - E_PQ)])
F
B
F
N
Cl
N
Re
N
OC
CO
CO

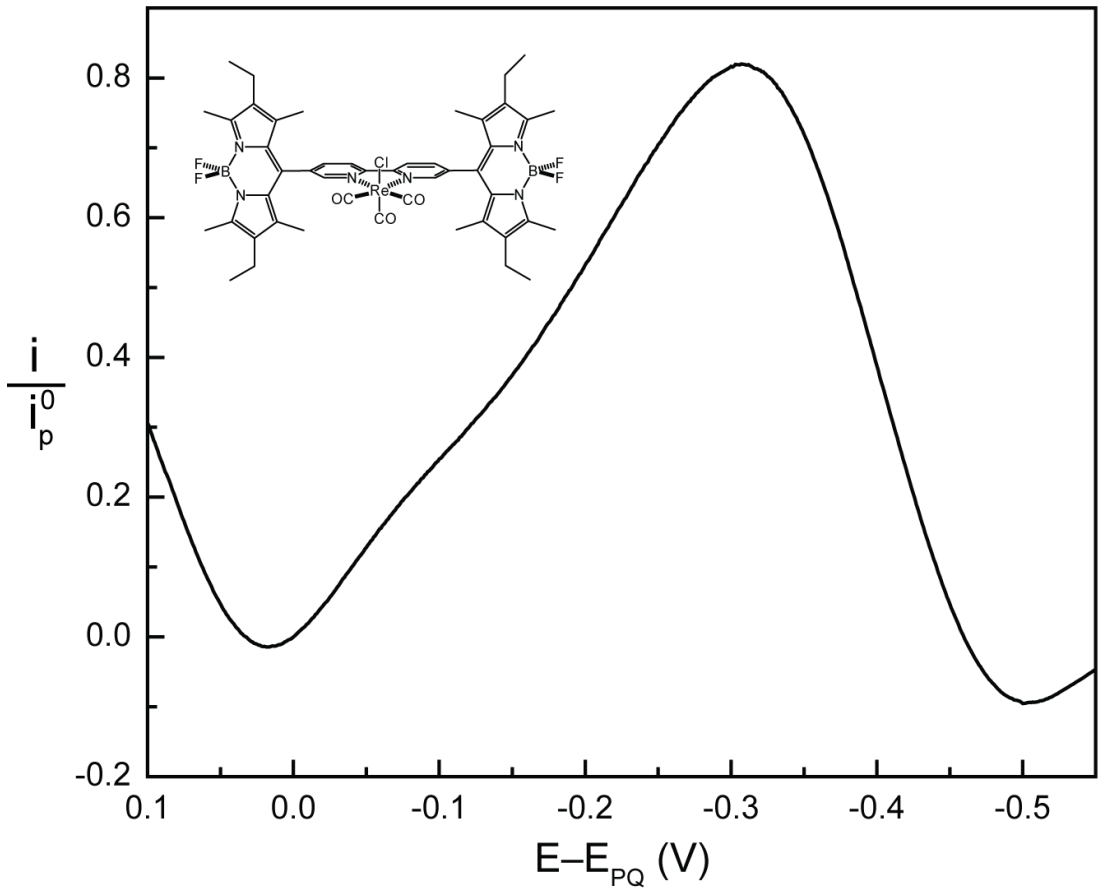
0.8
0.6
0.4
0.2
0.0
-0.2
i / i_p^0
0.1
0.0
-0.1
-0.2
-0.3
-0.4
-0.5
E–E_PQ (V)
F
F
B
N
Cl
Re
OC
CO
CO

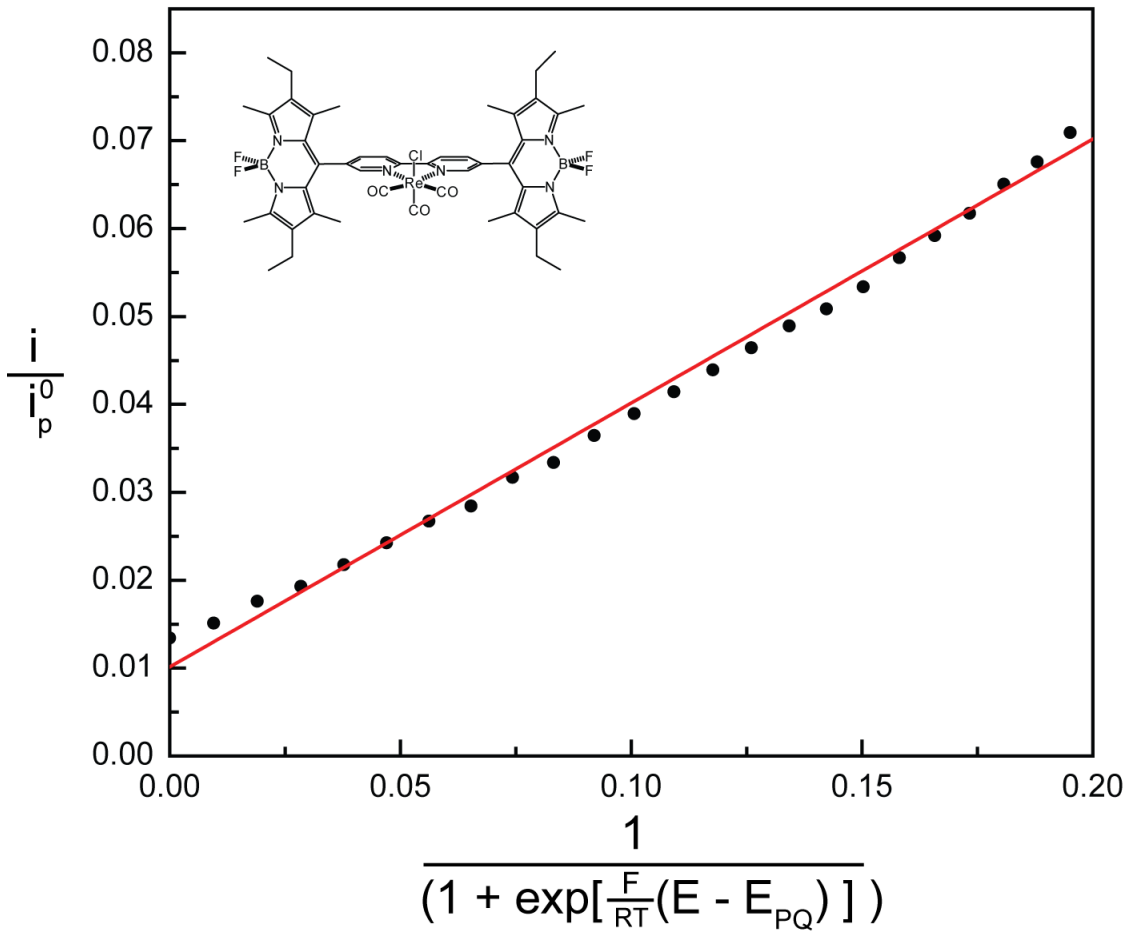
0.08
0.07
0.06
0.05
0.04
0.03
0.02
0.01
0.00
0.00
0.05
0.10
0.15
0.20
i / i_p^0
1 / (1 + exp[F/RT(E - E_PQ)])

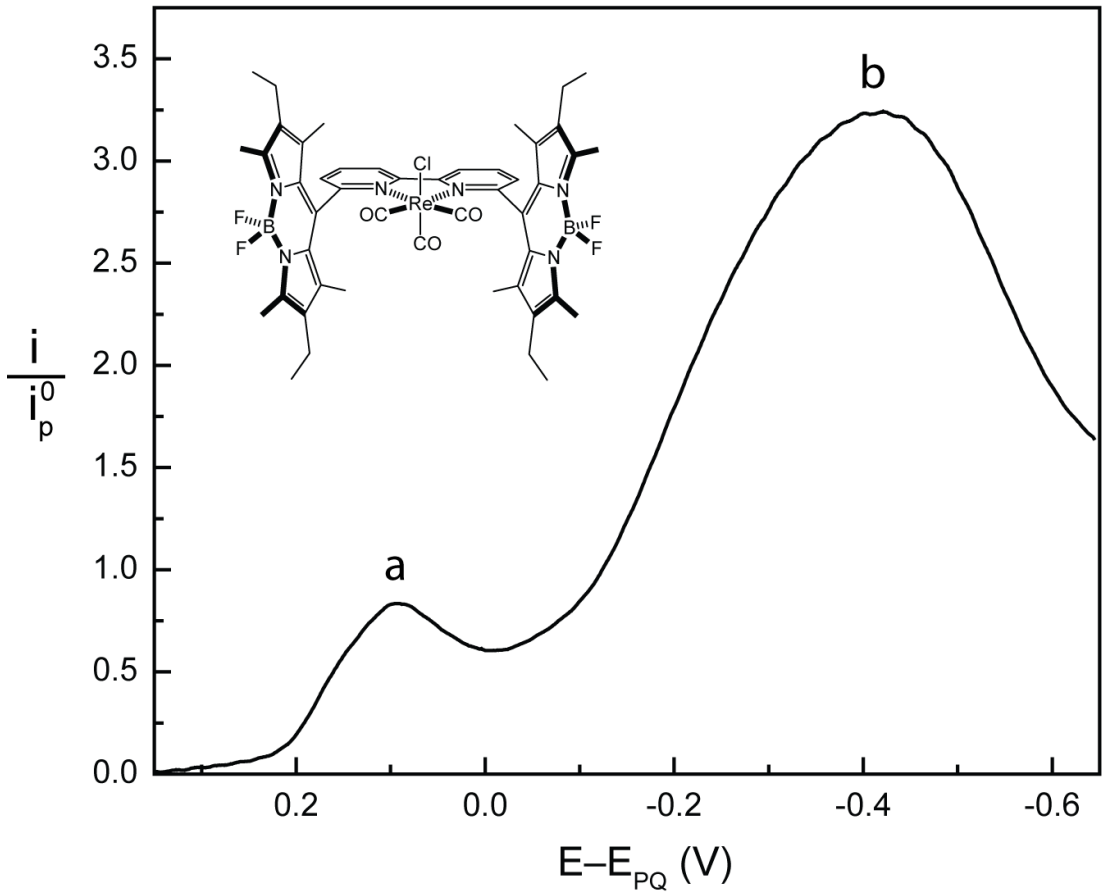
3.5
3.0
2.5
2.0
1.5
1.0
0.5
0.0
i / i_p^0
0.2
0.0
-0.2
-0.4
-0.6
E–E_PQ (V)
a
b
Cl
N
Re
OC
CO
CO
F
B
F
N
N
N
B
F
F
N

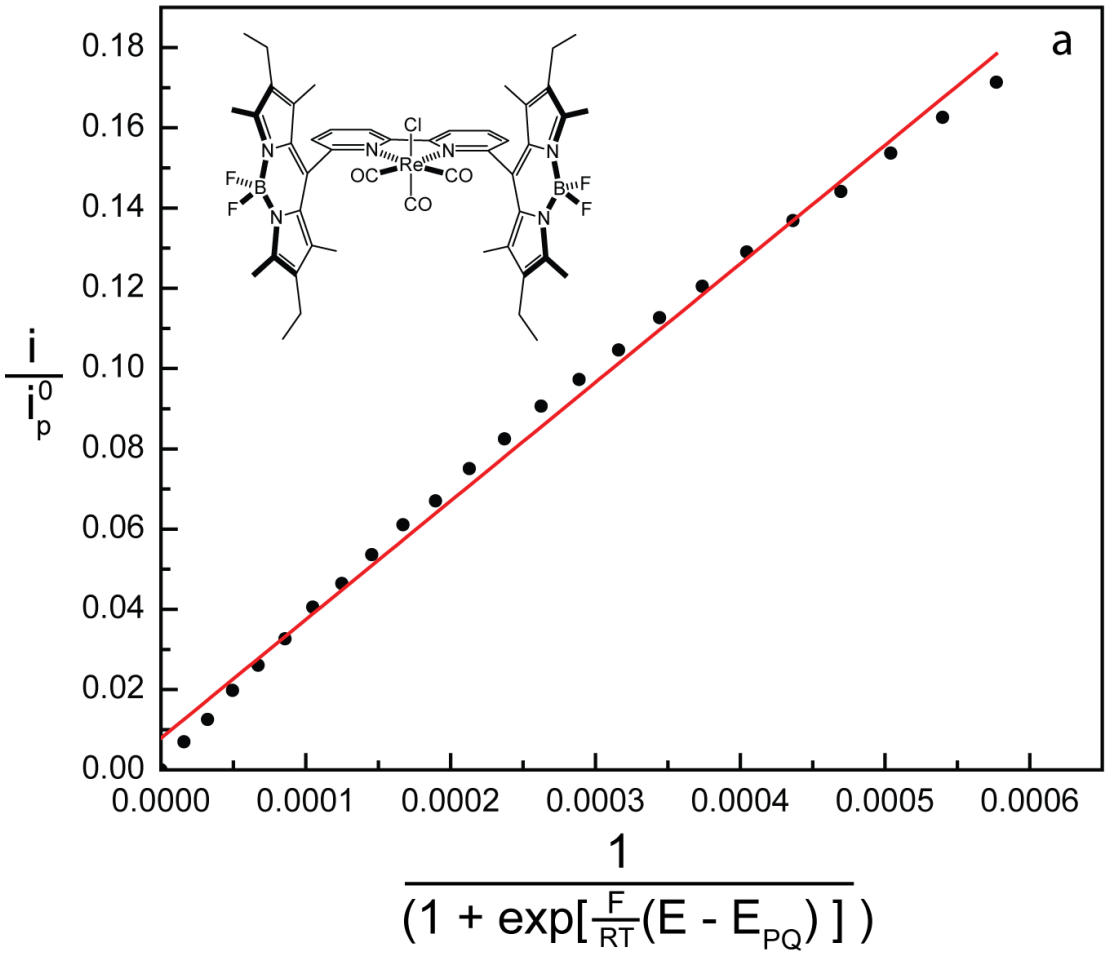
a
0.18
0.16
0.14
0.12
0.10
0.08
0.06
0.04
0.02
0.00
0.0000
0.0001
0.0002
0.0003
0.0004
0.0005
0.0006
i / i_p^0
1 / (1 + exp[F/RT (E - E_PQ)])
Cl
Re
OC
CO
CO
N
B
F
F

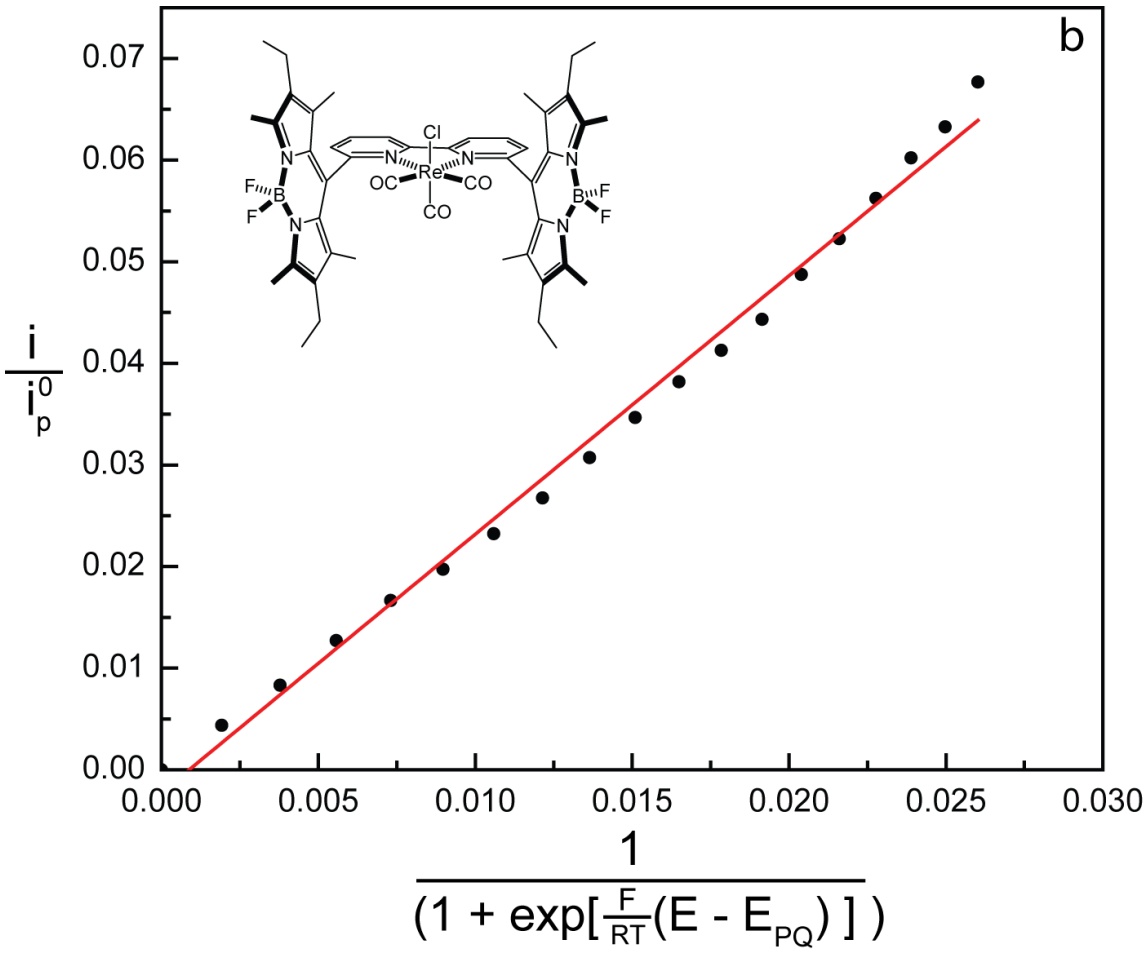

Appendix B

NMR SPECTROSCOPY

NMR Methods. All compounds were analyzed is CD_3Cl for ^{1}H and ^{13}C NMR except for the 5,5'and 6,6' dicarboxylic acid derivatives, which were analyzed in DMSO-d^6. All integrated peaks in ^{1}H NMR belong to the target compound, and remaining peaks belong to residual water or solvent.

^{1}H NMR Spectra

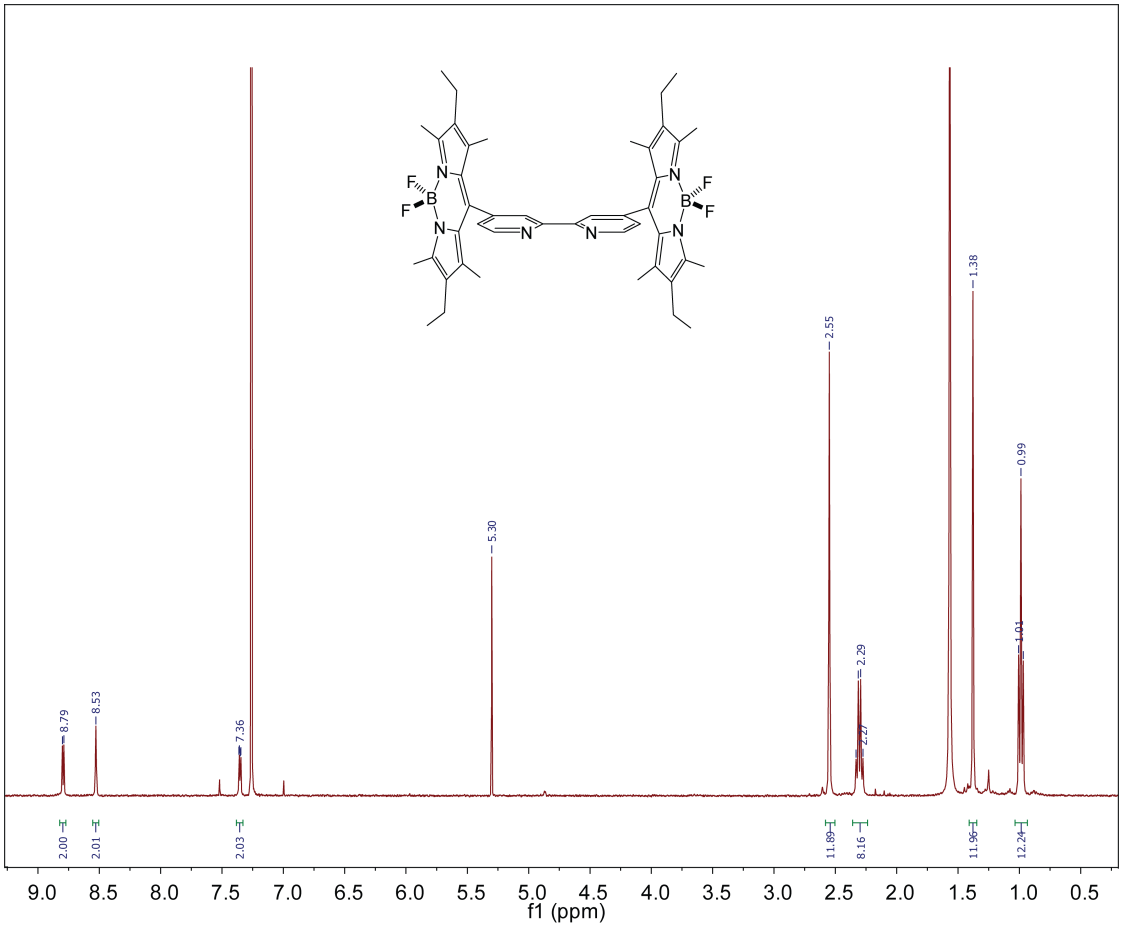

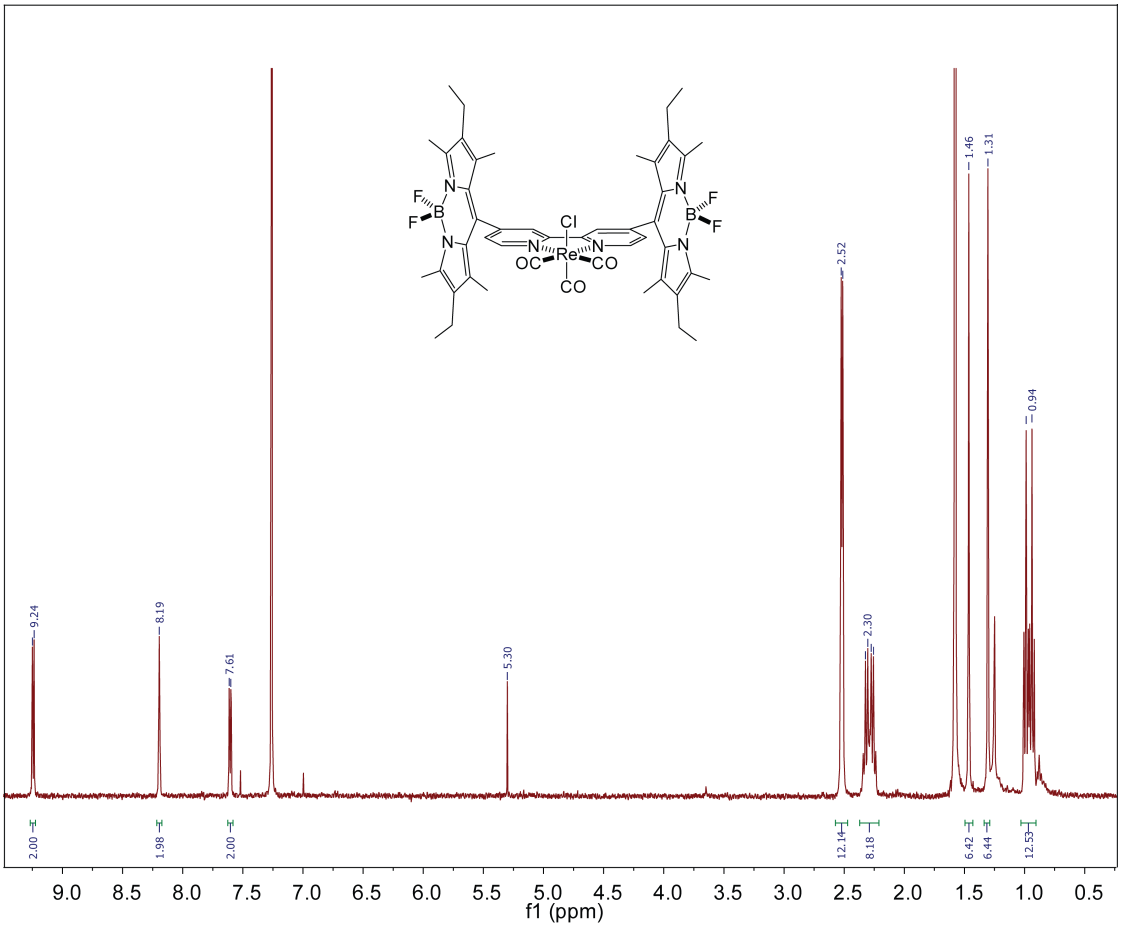
9.24
8.19
7.61
5.30
2.52
2.30
1.46
1.31
0.94
2.00
1.98
2.00
12.14
8.18
6.42
6.44
12.53
9.0 8.5 8.0 7.5 7.0 6.5 6.0 5.5 5.0 4.5 4.0 3.5 3.0 2.5 2.0 1.5 1.0 0.5
f1 (ppm)

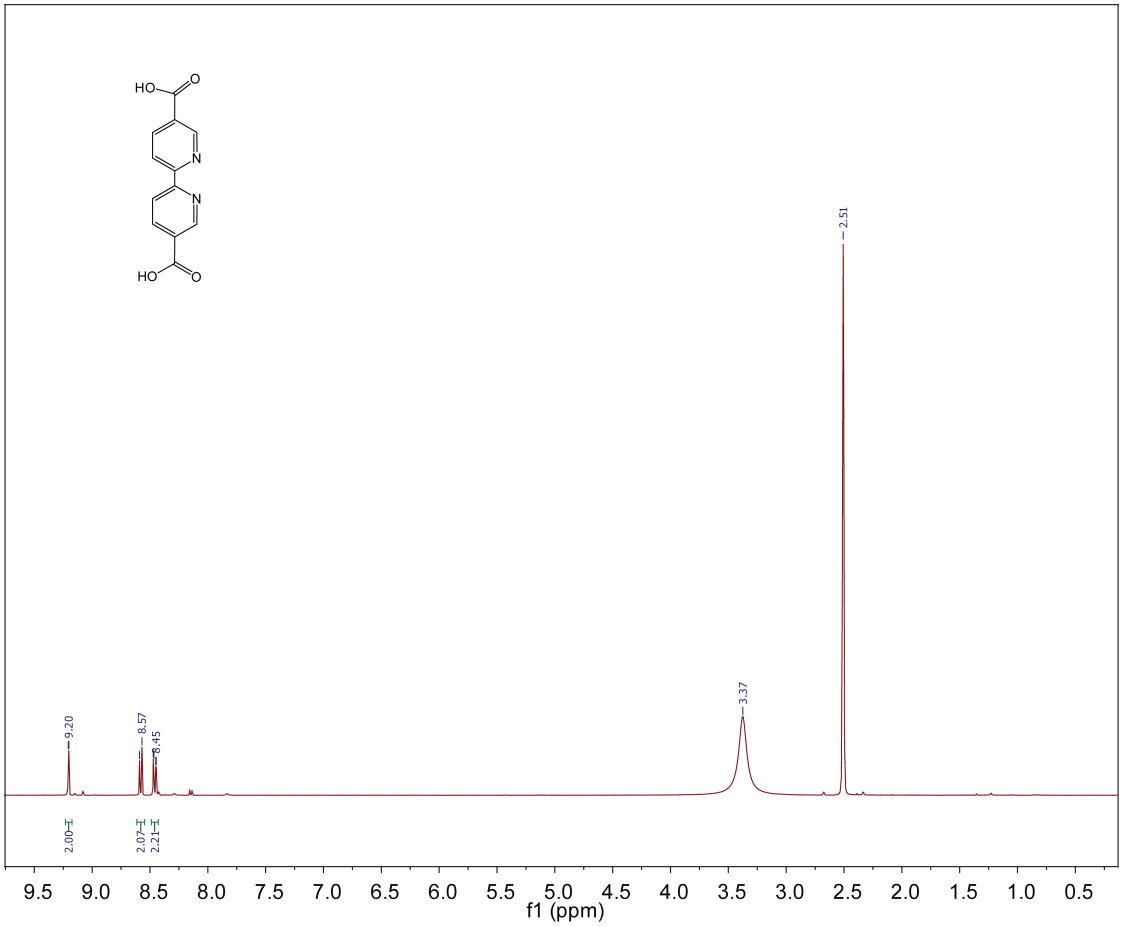
HO
O
N
N
HO
O
9.20
8.57
8.45
3.37
2.51
2.00
2.07
2.21
9.5 9.0 8.5 8.0 7.5 7.0 6.5 6.0 5.5 5.0 4.5 4.0 3.5 3.0 2.5 2.0 1.5 1.0 0.5
f1 (ppm)

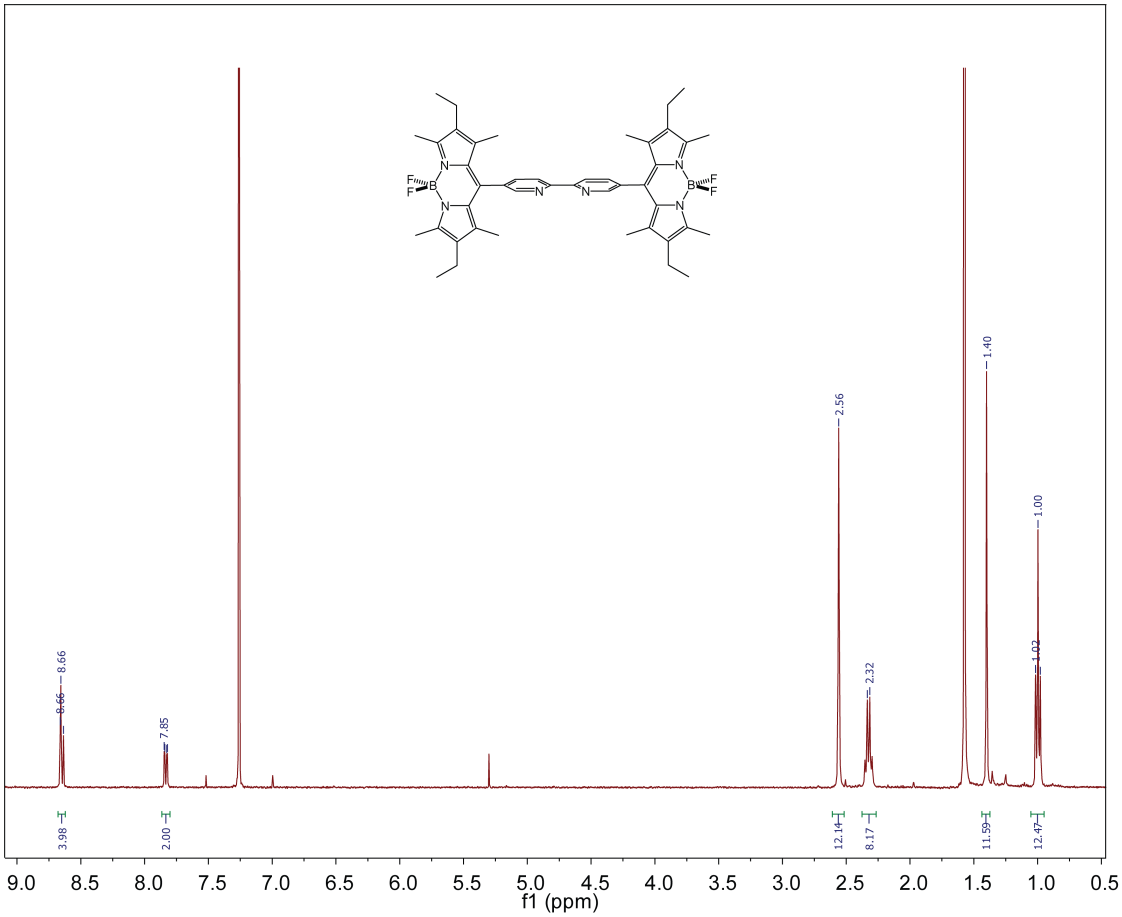
8.66
8.66
7.85
2.56
2.32
1.40
1.00
1.02
3.98
2.00
12.14
8.17
11.59
12.47
9.0 8.5 8.0 7.5 7.0 6.5 6.0 5.5 5.0 4.5 4.0 3.5 3.0 2.5 2.0 1.5 1.0 0.5
f1 (ppm)

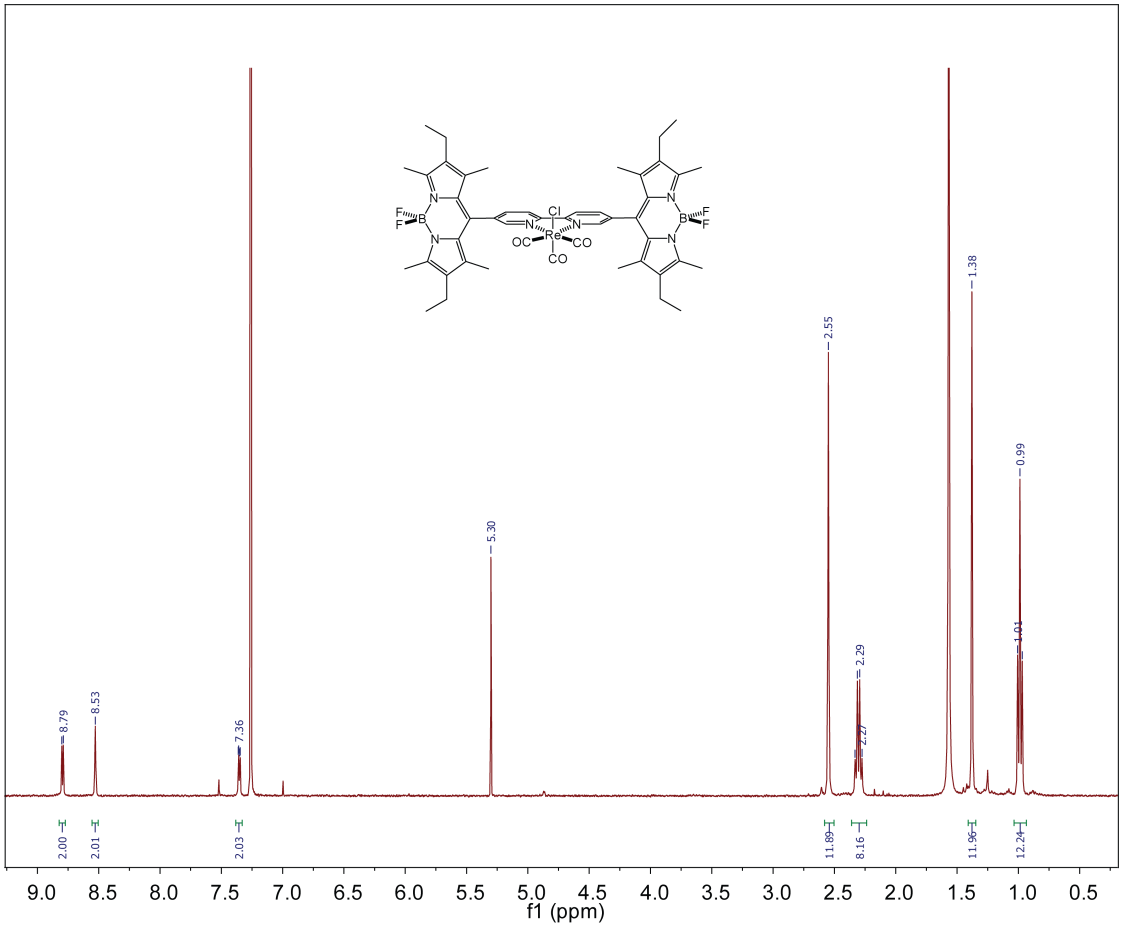
8.79
8.53
7.36
5.30
2.55
2.29
2.27
1.38
0.99
1.01
2.00
2.01
2.03
11.89
8.16
11.96
12.24
9.0 8.5 8.0 7.5 7.0 6.5 6.0 5.5 5.0 4.5 4.0 3.5 3.0 2.5 2.0 1.5 1.0 0.5
f1 (ppm)

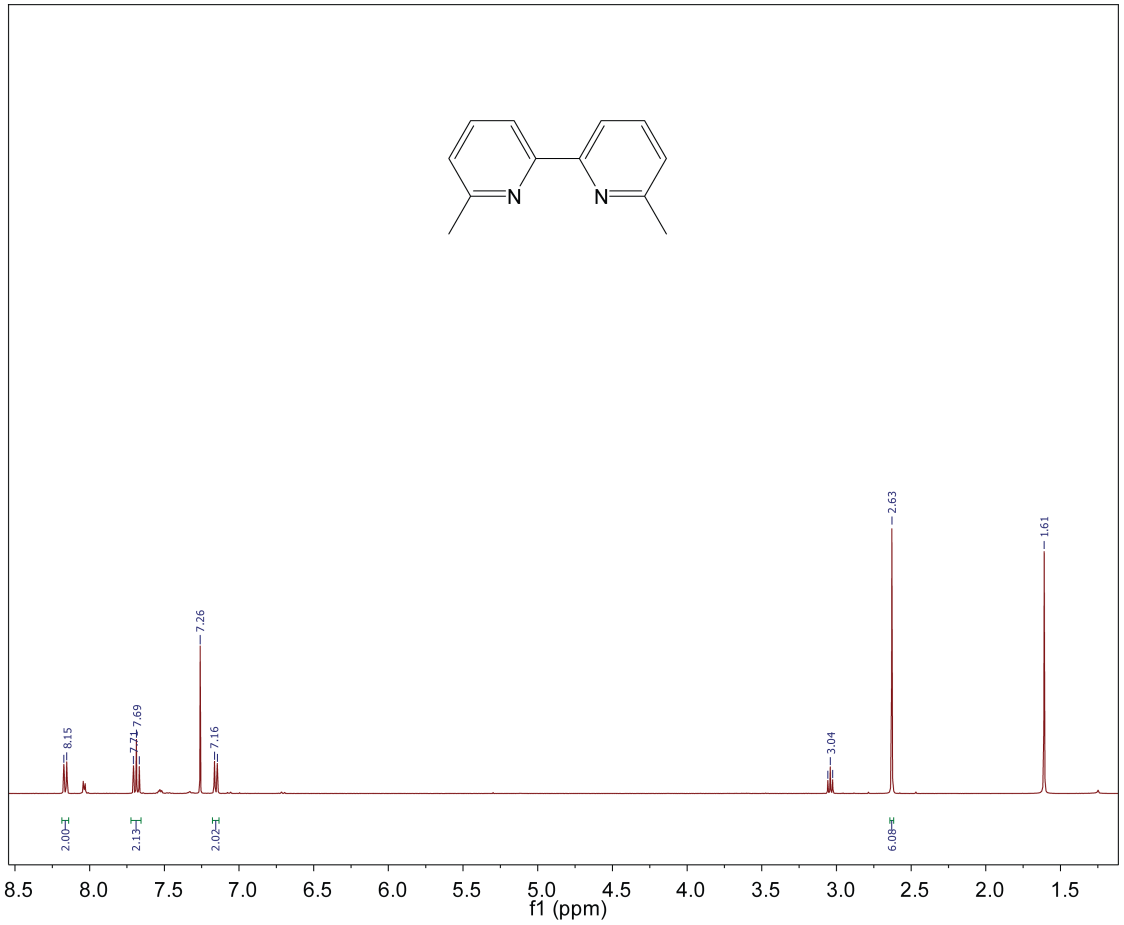
N
N
8.15
7.71
7.69
7.26
7.16
3.04
2.63
1.61
2.00
2.13
2.02
6.08
8.5
8.0
7.5
7.0
6.5
6.0
5.5
5.0
4.5
4.0
3.5
3.0
2.5
2.0
1.5
f1 (ppm)

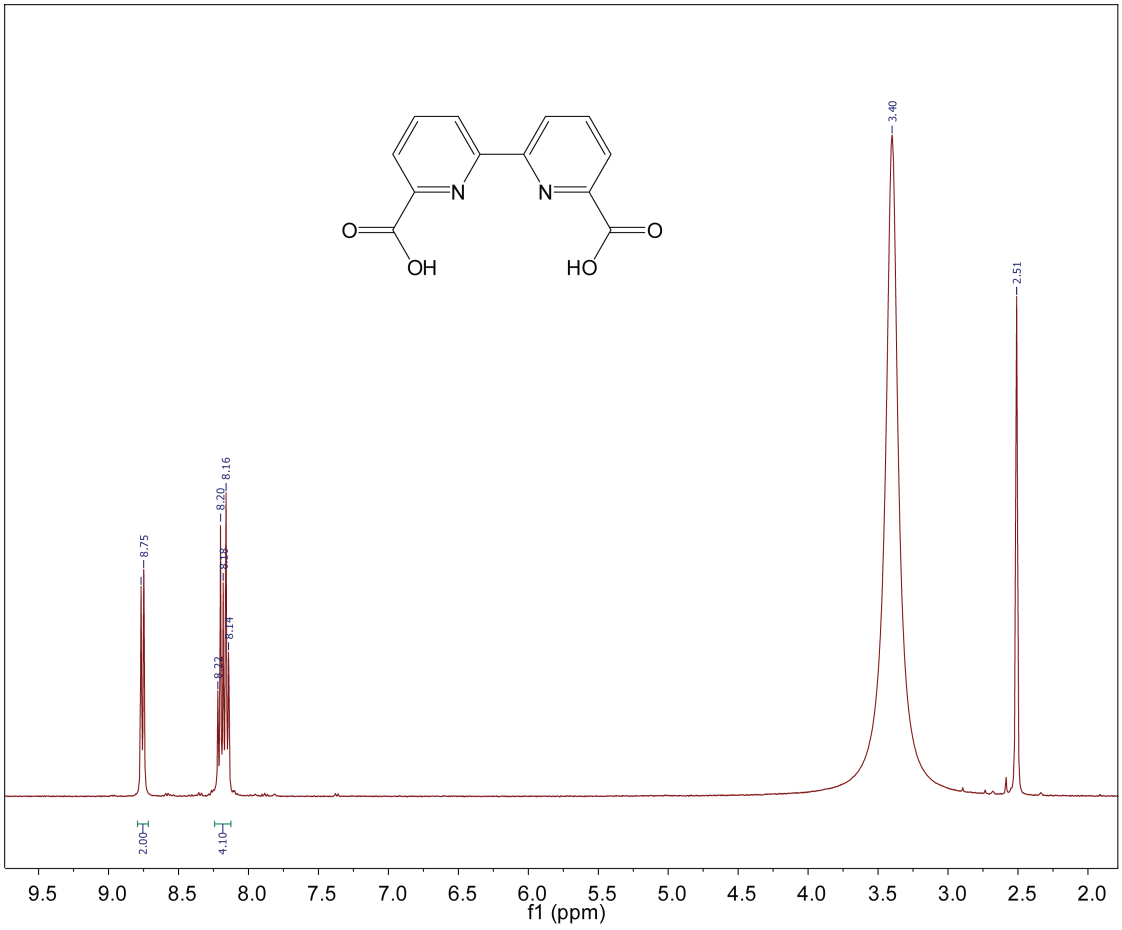
N
N
O
OH
HO
O
3.40
2.51
8.75
8.20
8.16
8.18
8.14
8.22
2.00
4.10
9.5
9.0
8.5
8.0
7.5
7.0
6.5
6.0
5.5
5.0
4.5
4.0
3.5
3.0
2.5
2.0
f1 (ppm)

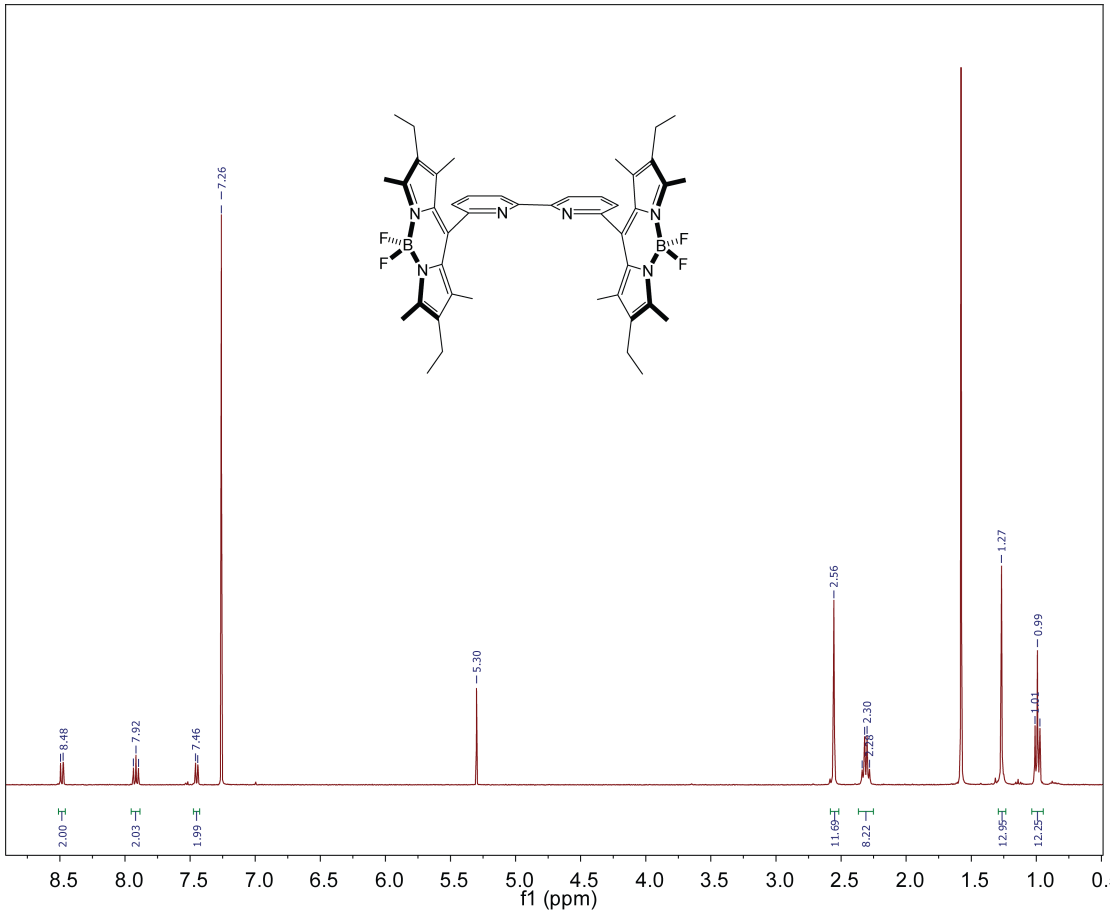
7.26
8.48
7.92
7.46
5.30
2.56
2.30
1.27
1.01
0.99
2.00
2.03
1.99
11.69
8.22
12.95
12.25
8.5 8.0 7.5 7.0 6.5 6.0 5.5 5.0 4.5 4.0 3.5 3.0 2.5 2.0 1.5 1.0 0.5
f1 (ppm)

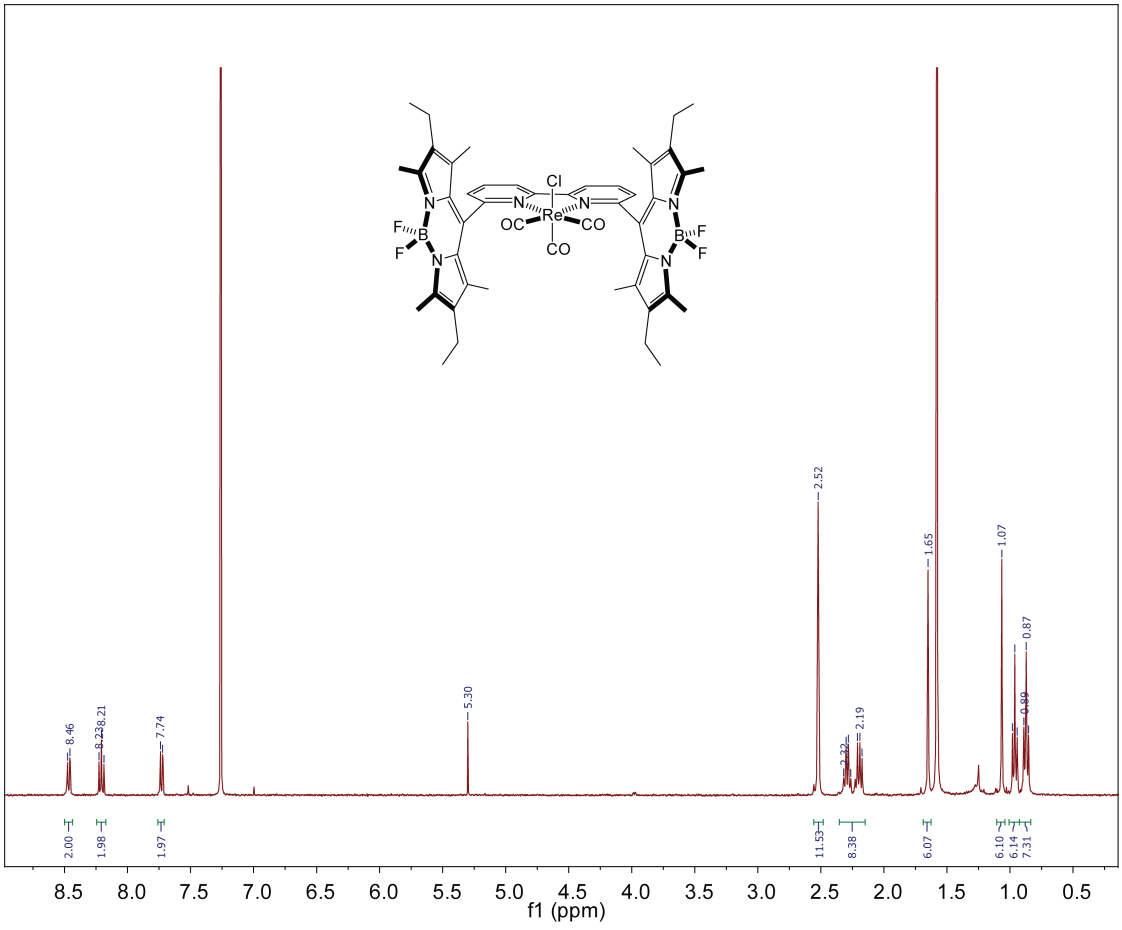

^{13}C NMR Spectra

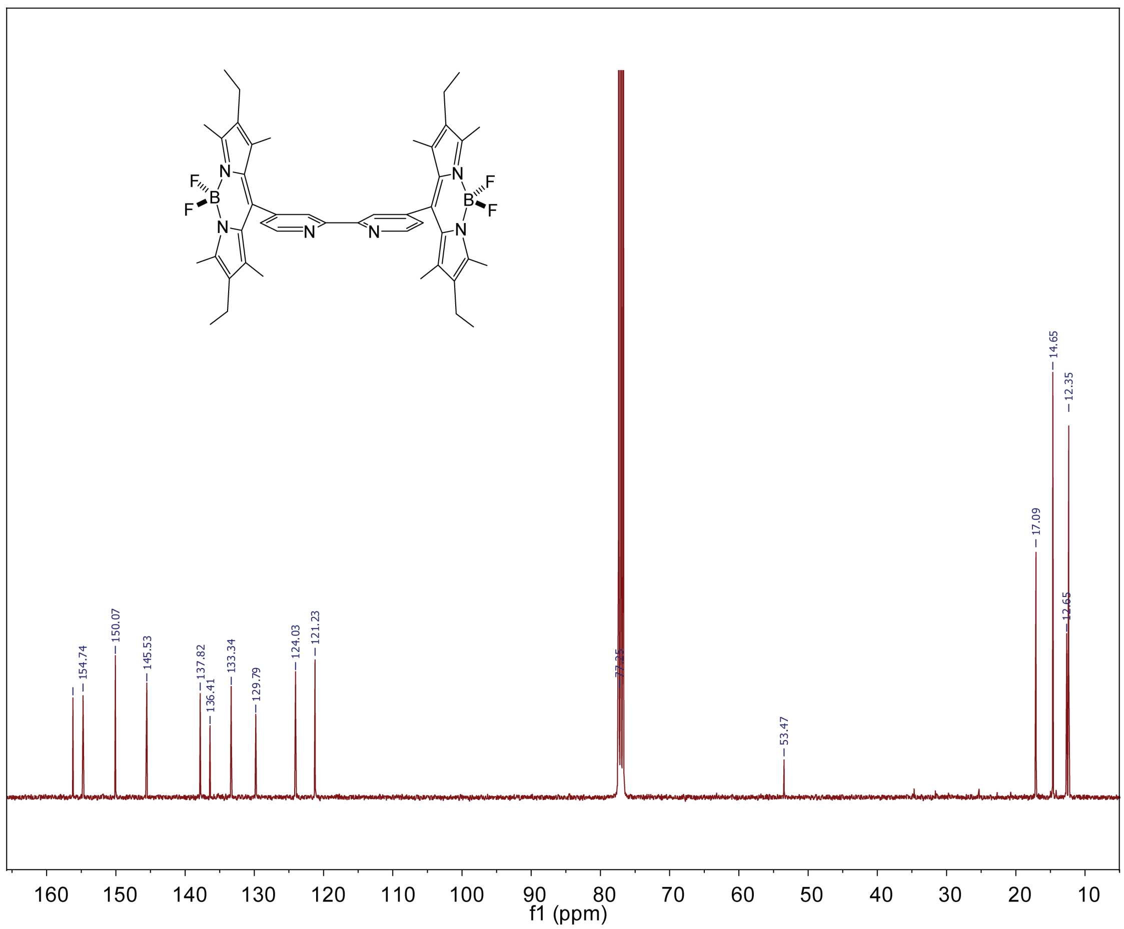
F
F
B
N
N
N
N
B
F
F
N
N
154.74
150.07
145.53
137.82
136.41
133.34
129.79
124.03
121.23
53.47
17.09
14.65
12.35
12.65
160 150 140 130 120 110 100 90 80 70 60 50 40 30 20 10
f1 (ppm)

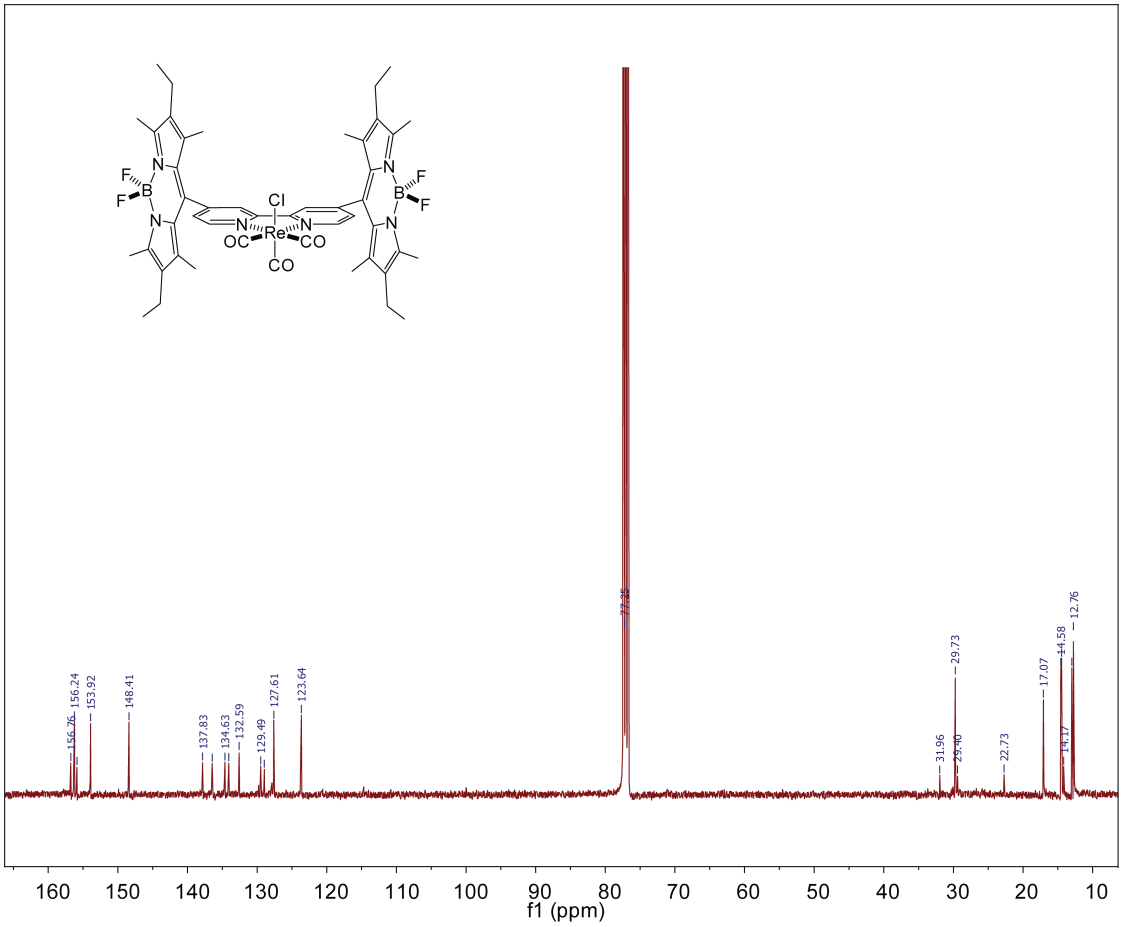
F
F
B
N
N
Cl
N
Re
N
OC
CO
CO
F
F
B
N
N
156.76
156.24
153.92
148.41
137.83
134.63
132.59
129.49
127.61
123.64
77.25
31.96
29.73
29.40
22.73
17.07
14.58
14.17
12.76
160
150
140
130
120
110
100
90
80
70
60
50
40
30
20
10
f1 (ppm)

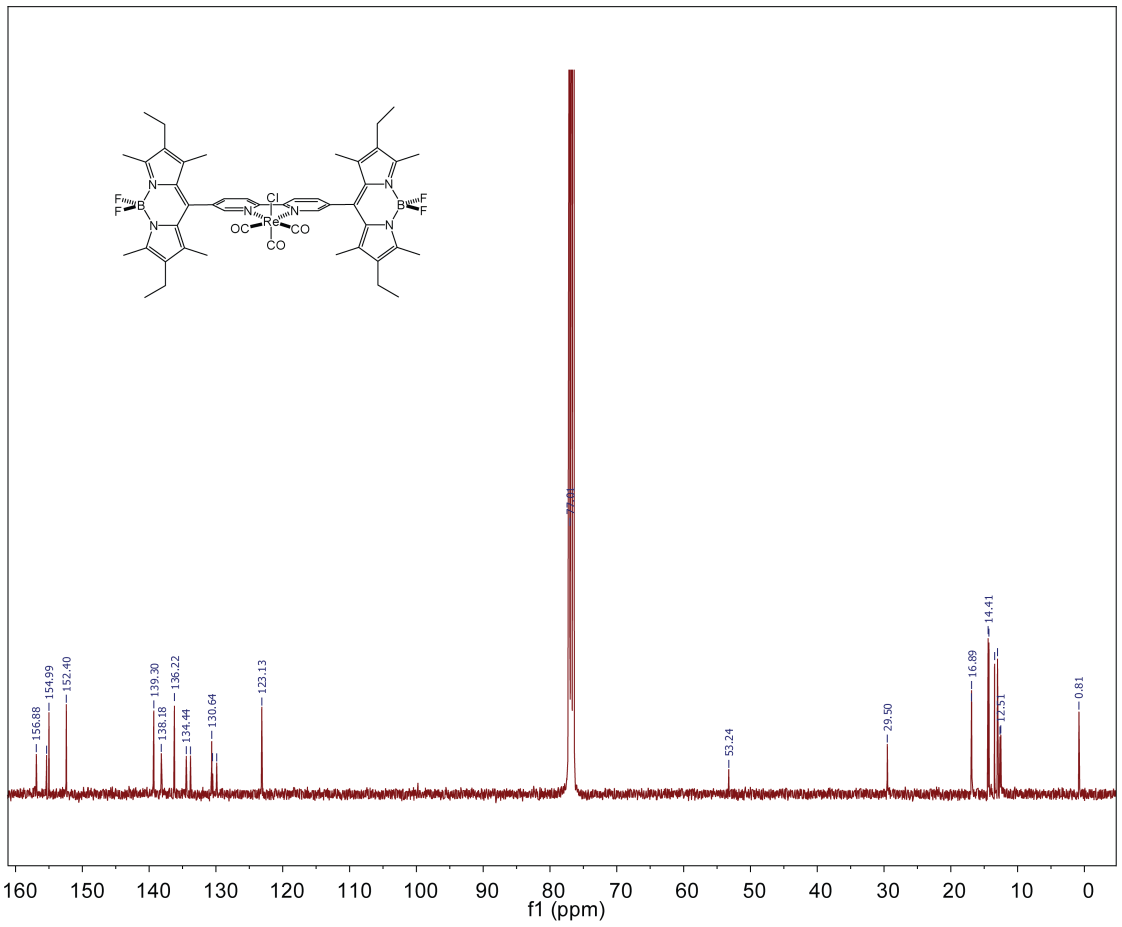
F
F
B
N
N
Cl
N
N
Re
OC
CO
CO
F
F
B
N
N
77.01
156.88
154.99
152.40
139.30
138.18
136.22
134.44
130.64
123.13
53.24
29.50
16.89
14.41
12.51
0.81
160
150
140
130
120
110
100
90
80
70
60
50
40
30
20
10
0
f1 (ppm)

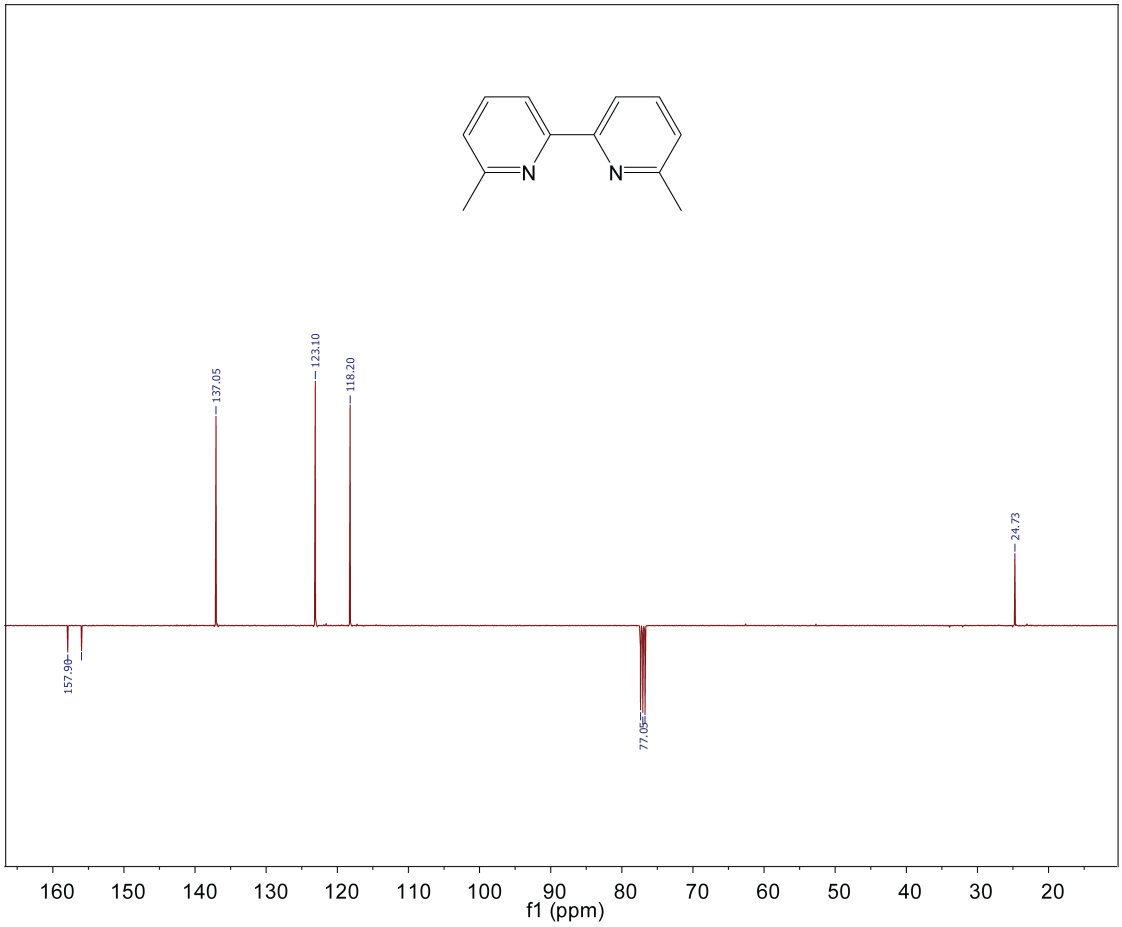
N
N
137.05
123.10
118.20
24.73
157.90
77.05
160
150
140
130
120
110
100
90
80
70
60
50
40
30
20
f1 (ppm)

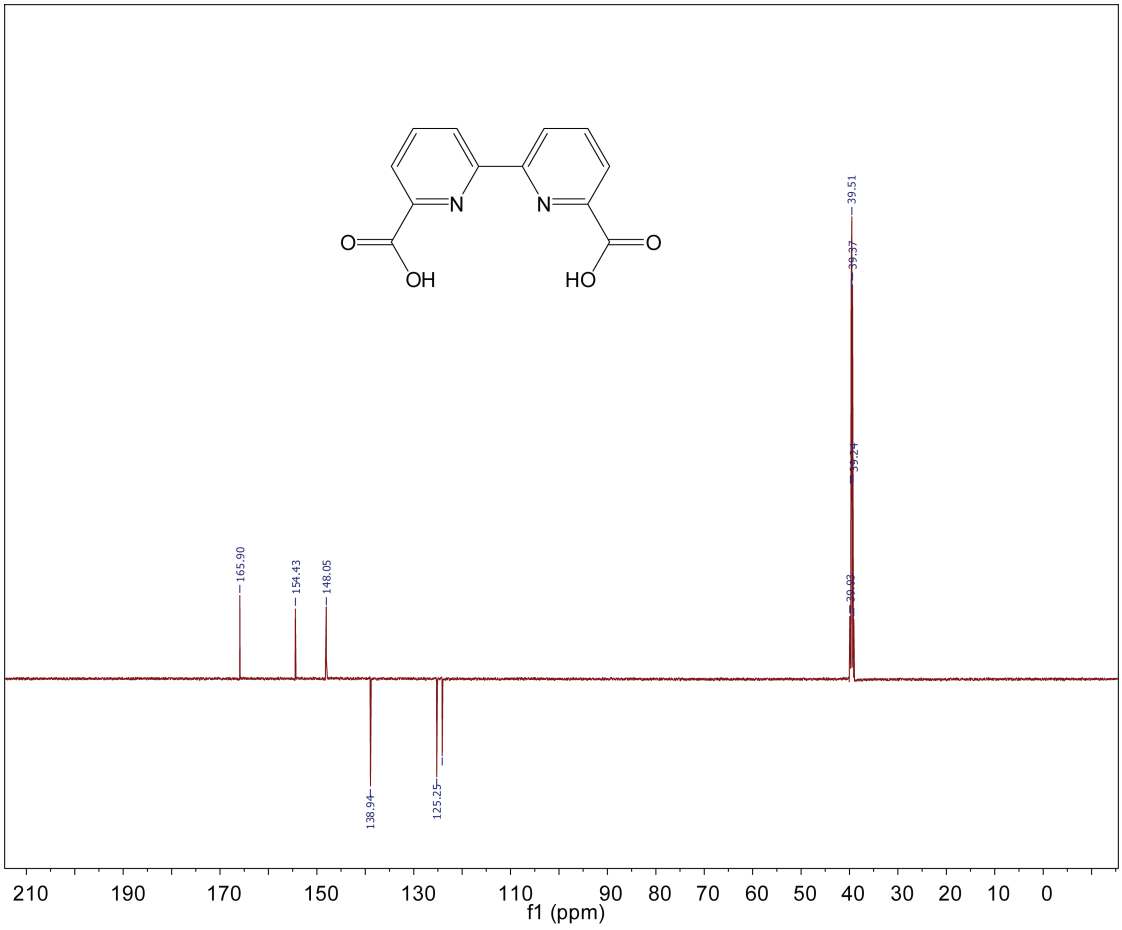
N
N
O
OH
HO
O
165.90
154.43
148.05
138.94
125.25
39.51
39.37
39.24
39.08
210
190
170
150
130
110
90
80
70
60
50
40
30
20
10
0
f1 (ppm)

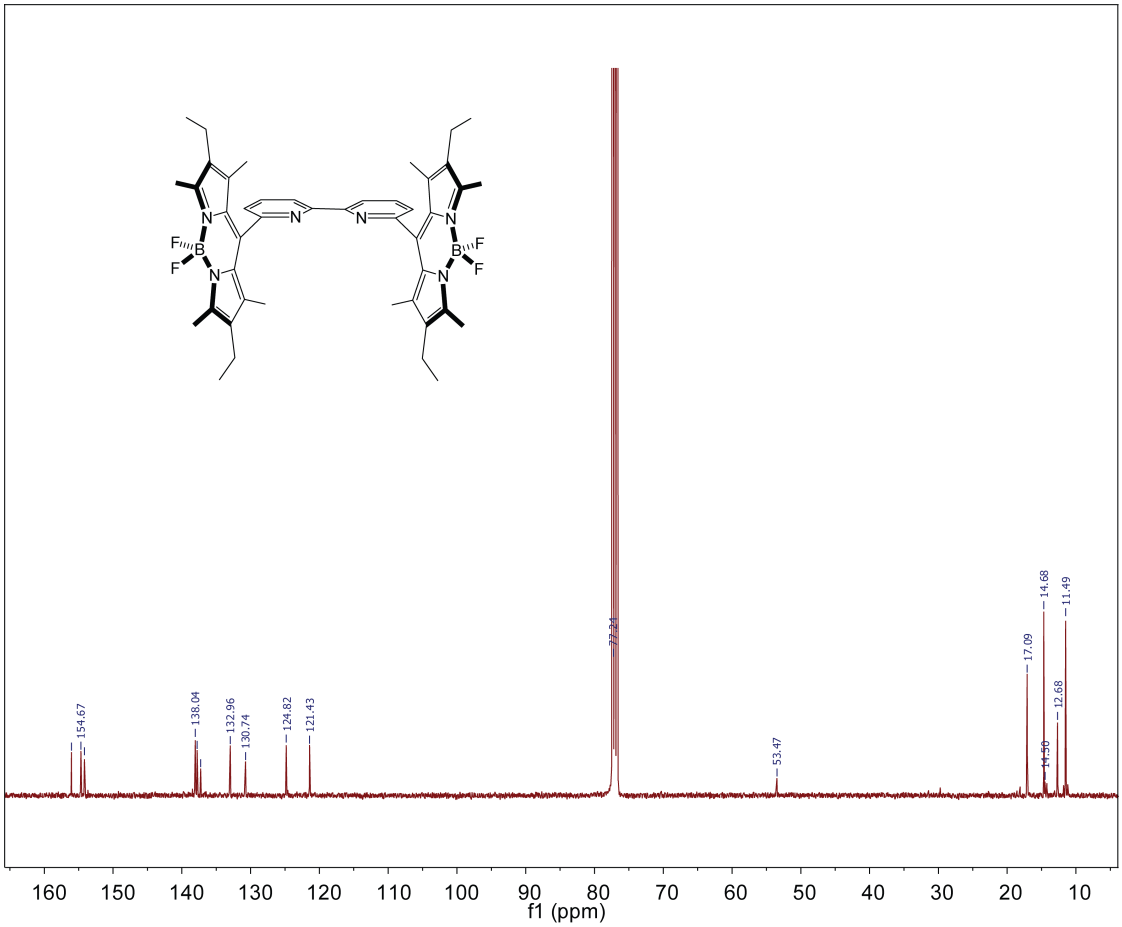

Appendix C

CRYSTALLOGRAPHIC DATA

Key Parameters	**Re(BB2)(CO)$_3$Cl**
Formula	$C_{47.5}H_{51}B_2Cl_2F_4N_6O_3Re$
F_W	1108.66
Crystal System	Triclinic
Space Group	P_{-1}
a	14.4395(8) Å
b	16.3930(9) Å

c	22.5783(12) Å
α	82.748(4) °
β	89.828(4) °
γ	73.525(4) °
V	5081.0(5) Å^3
Z	4
Temp	200(2) K
D_{calcd}	1.449 g cm^{-3}
2θ range	144.86°
μ (Cu Kα)	6.141 mm^{-1}
Reflections	49241
Unique	14814
R (int)	0.2102
R_1	0.0801
wR_2	0.1746

Bond Lengths for Re(BB2)(CO)$_3$Cl

Atom1	Atom2	Length
Re1	Cl1	2.459(5)
Re1	N1	2.13(1)
Re1	N4	2.14(1)
Re1	C1	1.87(2)
Re1	C2	1.86(2)
Re1	C3	1.84(2)
B1	F1	1.36(2)
B1	F2	1.43(2)
B1	N2	1.59(2)
B1	N3	1.50(3)
B2	F3	1.38(3)
B2	F4	1.43(2)
B2	N5	1.60(3)
B2	N6	1.48(3)
N1	C4	1.34(2)
N1	C8	1.34(2)
N2	C10	1.40(2)

N2	C13	1.35(3)
N3	C18	1.41(2)
N3	C21	1.35(2)
N4	C26	1.35(2)
N4	C30	1.34(2)
N5	C32	1.37(2)
N5	C35	1.34(3)
N6	C40	1.42(2)
N6	C43	1.35(3)
O1	C1	1.14(2)
O2	C2	1.16(2)
O3	C3	1.20(2)
C4	H4	0.95(2)
C4	C5	1.39(3)
C5	H5	0.95(2)
C5	C6	1.41(2)
C6	C7	1.37(2)
C6	C9	1.50(2)
C7	H7	0.95(2)
C7	C8	1.42(2)
C8	C26	1.46(2)
C9	C10	1.38(3)
C9	C18	1.37(2)
C10	C11	1.41(2)
C11	C12	1.38(3)
C11	C14	1.50(2)
C12	C13	1.43(3)
C12	C15	1.54(3)
C13	C17	1.52(3)
C14	H14A	0.98(2)
C14	H14B	0.98(2)
C14	H14C	0.98(2)
C15	H15A	0.99(2)
C15	H15B	0.99(2)
C15	C16	1.52(3)
C16	H16A	0.98(2)
C16	H16B	0.98(2)

C16	H16C	0.98(2)
C17	H17A	0.98(2)
C17	H17B	0.98(2)
C17	H17C	0.98(2)
C18	C19	1.41(3)
C19	C20	1.39(2)
C19	C22	1.47(3)
C20	C21	1.39(3)
C20	C23	1.53(3)
C21	C25	1.52(2)
C22	H22A	0.98(2)
C22	H22B	0.98(2)
C22	H22C	0.98(2)
C23	H23A	0.99(2)
C23	H23B	0.99(2)
C23	C24	1.52(2)
C24	H24A	0.98(2)
C24	H24B	0.98(2)
C24	H24C	0.98(2)
C25	H25A	0.98(2)
C25	H25B	0.98(2)
C25	H25C	0.98(2)
C26	C27	1.39(2)
C27	H27	0.95(2)
C27	C28	1.41(2)
C28	C29	1.36(3)
C28	C31	1.48(2)
C29	H29	0.95(2)
C29	C30	1.38(2)
C30	H30	0.95(2)
C31	C32	1.38(3)
C31	C40	1.39(3)
C32	C33	1.40(3)
C33	C34	1.43(3)
C33	C36	1.50(3)
C34	C35	1.40(3)
C34	C37	1.56(4)

C35	C39	1.49(3)
C36	H36A	0.98(2)
C36	H36B	0.98(2)
C36	H36C	0.98(2)
C37	H37C	0.99(2)
C37	H37D	0.99(3)
C37	C38	1.51(4)
C38	H38A	0.97(3)
C38	H38B	0.98(3)
C38	H38C	0.99(3)
C39	H39A	0.98(3)
C39	H39B	0.98(3)
C39	H39C	0.98(3)
C40	C41	1.44(3)
C41	C42	1.37(3)
C41	C44	1.48(2)
C42	C43	1.39(3)
C42	C45	1.48(3)
C43	C47	1.48(3)
C44	H44A	0.98(2)
C44	H44B	0.98(2)
C44	H44C	0.98(2)
C45	H45A	0.99(2)
C45	H45B	0.99(3)
C45	C46	1.59(4)
C46	H46A	0.98(3)
C46	H46B	0.98(3)
C46	H46C	0.98(3)
C47	H47A	0.98(2)
C47	H47B	0.98(2)
C47	H47C	0.98(2)

Bond Angles for Re(BB2)(CO)$_3$Cl

Atom1	Atom2	Atom3	Angle
Cl1	Re1	N1	83.2(4)
Cl1	Re1	N4	83.1(4)
Cl1	Re1	C1	95.5(6)

Cl1	Re1	C2	175.8(6)
Cl1	Re1	C3	91.9(6)
N1	Re1	N4	74.2(5)
N1	Re1	C1	98.5(7)
N1	Re1	C2	94.8(7)
N1	Re1	C3	172.2(7)
N4	Re1	C1	172.7(7)
N4	Re1	C2	92.8(7)
N4	Re1	C3	99.2(7)
C1	Re1	C2	88.5(8)
C1	Re1	C3	88.0(8)
C2	Re1	C3	89.7(8)
F1	B1	F2	110(2)
F1	B1	N2	107(2)
F1	B1	N3	115(2)
F2	B1	N2	108(1)
F2	B1	N3	112(2)
N2	B1	N3	105(1)
F3	B2	F4	105(2)
F3	B2	N5	110(2)
F3	B2	N6	113(2)
F4	B2	N5	106(2)
F4	B2	N6	111(2)
N5	B2	N6	110(2)
Re1	N1	C4	125(1)
Re1	N1	C8	118(1)
C4	N1	C8	117(1)
B1	N2	C10	125(1)
B1	N2	C13	126(1)
C10	N2	C13	108(1)
B1	N3	C18	129(1)
B1	N3	C21	125(2)
C18	N3	C21	106(1)
Re1	N4	C26	117(1)
Re1	N4	C30	126(1)
C26	N4	C30	117(1)
B2	N5	C32	122(2)

B2	N5	C35	127(2)
C32	N5	C35	111(2)
B2	N6	C40	123(2)
B2	N6	C43	129(2)
C40	N6	C43	108(2)
Re1	C1	O1	178(2)
Re1	C2	O2	177(2)
Re1	C3	O3	175(1)
N1	C4	H4	118(2)
N1	C4	C5	125(2)
H4	C4	C5	118(2)
C4	C5	H5	120(2)
C4	C5	C6	119(2)
H5	C5	C6	120(2)
C5	C6	C7	115(2)
C5	C6	C9	123(2)
C7	C6	C9	122(1)
C6	C7	H7	119(2)
C6	C7	C8	123(1)
H7	C7	C8	118(2)
N1	C8	C7	121(1)
N1	C8	C26	115(1)
C7	C8	C26	125(1)
C6	C9	C10	117(1)
C6	C9	C18	118(1)
C10	C9	C18	125(2)
N2	C10	C9	118(1)
N2	C10	C11	108(1)
C9	C10	C11	134(2)
C10	C11	C12	108(2)
C10	C11	C14	129(2)
C12	C11	C14	123(2)
C11	C12	C13	107(2)
C11	C12	C15	129(2)
C13	C12	C15	123(2)
N2	C13	C12	109(2)
N2	C13	C17	123(2)

C12	C13	C17	128(2)
C11	C14	H14A	110(2)
C11	C14	H14B	110(2)
C11	C14	H14C	109(2)
H14A	C14	H14B	109(2)
H14A	C14	H14C	109(2)
H14B	C14	H14C	109(2)
C12	C15	H15A	110(2)
C12	C15	H15B	110(2)
C12	C15	C16	110(2)
H15A	C15	H15B	108(2)
H15A	C15	C16	110(2)
H15B	C15	C16	110(2)
C15	C16	H16A	110(2)
C15	C16	H16B	109(2)
C15	C16	H16C	109(2)
H16A	C16	H16B	110(2)
H16A	C16	H16C	109(2)
H16B	C16	H16C	109(2)
C13	C17	H17A	109(2)
C13	C17	H17B	109(2)
C13	C17	H17C	109(2)
H17A	C17	H17B	110(2)
H17A	C17	H17C	109(2)
H17B	C17	H17C	109(2)
N3	C18	C9	117(1)
N3	C18	C19	110(1)
C9	C18	C19	134(2)
C18	C19	C20	105(1)
C18	C19	C22	130(2)
C20	C19	C22	125(2)
C19	C20	C21	108(2)
C19	C20	C23	125(2)
C21	C20	C23	127(2)
N3	C21	C20	111(2)
N3	C21	C25	121(2)
C20	C21	C25	128(2)

C19	C22	H22A	109(2)
C19	C22	H22B	109(2)
C19	C22	H22C	110(2)
H22A	C22	H22B	109(2)
H22A	C22	H22C	110(2)
H22B	C22	H22C	109(2)
C20	C23	H23A	109(2)
C20	C23	H23B	109(2)
C20	C23	C24	112(1)
H23A	C23	H23B	108(2)
H23A	C23	C24	109(2)
H23B	C23	C24	109(2)
C23	C24	H24A	109(2)
C23	C24	H24B	109(2)
C23	C24	H24C	109(2)
H24A	C24	H24B	110(2)
H24A	C24	H24C	109(2)
H24B	C24	H24C	109(2)
C21	C25	H25A	110(2)
C21	C25	H25B	110(2)
C21	C25	H25C	109(2)
H25A	C25	H25B	109(2)
H25A	C25	H25C	109(2)
H25B	C25	H25C	109(2)
N4	C26	C8	114(1)
N4	C26	C27	124(2)
C8	C26	C27	122(2)
C26	C27	H27	120(2)
C26	C27	C28	119(2)
H27	C27	C28	120(2)
C27	C28	C29	116(2)
C27	C28	C31	123(2)
C29	C28	C31	121(2)
C28	C29	H29	118(2)
C28	C29	C30	123(2)
H29	C29	C30	118(2)
N4	C30	C29	121(2)

N4	C30	H30	119(2)
C29	C30	H30	119(2)
C28	C31	C32	122(2)
C28	C31	C40	115(2)
C32	C31	C40	123(2)
N5	C32	C31	121(2)
N5	C32	C33	108(2)
C31	C32	C33	130(2)
C32	C33	C34	105(2)
C32	C33	C36	132(2)
C34	C33	C36	123(2)
C33	C34	C35	108(2)
C33	C34	C37	126(2)
C35	C34	C37	125(2)
N5	C35	C34	107(2)
N5	C35	C39	125(2)
C34	C35	C39	128(2)
C33	C36	H36A	109(2)
C33	C36	H36B	110(2)
C33	C36	H36C	110(2)
H36A	C36	H36B	109(2)
H36A	C36	H36C	109(2)
H36B	C36	H36C	110(2)
C34	C37	H37C	109(2)
C34	C37	H37D	109(2)
C34	C37	C38	113(2)
H37C	C37	H37D	108(2)
H37C	C37	C38	109(2)
H37D	C37	C38	109(2)
C37	C38	H38A	110(3)
C37	C38	H38B	109(3)
C37	C38	H38C	109(3)
H38A	C38	H38B	110(3)
H38A	C38	H38C	110(3)
H38B	C38	H38C	109(3)
C35	C39	H39A	110(2)
C35	C39	H39B	109(2)

C35	C39	H39C	109(2)
H39A	C39	H39B	110(2)
H39A	C39	H39C	109(2)
H39B	C39	H39C	109(2)
N6	C40	C31	120(2)
N6	C40	C41	106(2)
C31	C40	C41	134(2)
C40	C41	C42	107(2)
C40	C41	C44	128(2)
C42	C41	C44	124(2)
C41	C42	C43	109(2)
C41	C42	C45	128(2)
C43	C42	C45	123(2)
N6	C43	C42	110(2)
N6	C43	C47	119(2)
C42	C43	C47	132(2)
C41	C44	H44A	109(2)
C41	C44	H44B	109(2)
C41	C44	H44C	110(2)
H44A	C44	H44B	109(2)
H44A	C44	H44C	109(2)
H44B	C44	H44C	110(2)
C42	C45	H45A	109(2)
C42	C45	H45B	109(2)
C42	C45	C46	113(2)
H45A	C45	H45B	108(2)
H45A	C45	C46	109(2)
H45B	C45	C46	109(2)
C45	C46	H46A	109(2)
C45	C46	H46B	109(2)
C45	C46	H46C	110(2)
H46A	C46	H46B	109(3)
H46A	C46	H46C	110(3)
H46B	C46	H46C	110(3)
C43	C47	H47A	109(2)
C43	C47	H47B	109(2)
C43	C47	H47C	109(2)

H47A	C47	H47B	110(2)
H47A	C47	H47C	109(2)
H47B	C47	H47C	110(2)

Key Parameters	**Re(BB3)(CO)$_3$Cl**
Formula	$C_{49}H_{54}B_2Cl_3F_4N_6O_3Re$
F_W	1165.15
Crystal System	Triclinic
Space Group	P_{-1}
a	13.383(3) Å
b	14.555(3) Å
c	14.563(3) Å
α	88.305(4) °
β	81.330(4) °
γ	62.646(4) °
V	2488.1(5) Å^3
Z	2
Temp	200(2) K
D_{calcd}	1.555 g cm^{-3}
2θ range	53.16°
μ (Mo Kα)	2.666 mm^{-1}
Reflections	27844
Unique	12260
R (int)	0.0482
R_1	0.0598
wR_2	0.1336

Bond Lengths for Re(BB3)(CO)$_3$Cl		
Atom1	**Atom2**	**Length**
Re	Cl1	2.452(2)
Re	N3	2.194(7)
Re	N4	2.188(4)
Re	C1	1.924(7)
Re	C2	1.92(1)
Re	C3	1.937(6)
B1	F1	1.387(8)

B1	F2	1.39(1)
B1	N1	1.546(9)
B1	N2	1.55(1)
B2	F3	1.38(1)
B2	F4	1.393(8)
B2	N5	1.55(1)
B2	N6	1.554(8)
N1	C4	1.346(9)
N1	C7	1.40(1)
N2	C12	1.338(9)
N2	C15	1.40(1)
N3	C21	1.353(9)
N3	C25	1.351(8)
N4	C26	1.35(1)
N4	C30	1.354(9)
N5	C32	1.350(7)
N5	C35	1.40(1)
N6	C40	1.352(9)
N6	C43	1.39(1)
C1	O1	1.141(9)
C2	O2	1.13(1)
C3	O3	1.093(9)
C4	C5	1.42(1)
C4	C8	1.50(1)
C5	C6	1.39(1)
C5	C9	1.50(1)
C6	C7	1.432(8)
C6	C11	1.49(1)
C7	C20	1.40(1)
C8	H8A	0.980(6)
C8	H8B	0.98(1)
C8	H8C	0.979(7)
C9	H9A	0.99(1)
C9	H9B	0.991(9)
C9	C10	1.51(2)
C10	H10A	0.980(9)
C10	H10B	0.98(1)

C10	H10C	0.98(1)
C11	H11A	0.979(7)
C11	H11B	0.979(7)
C11	H11C	0.98(1)
C12	C13	1.39(2)
C12	C16	1.51(2)
C13	C14	1.39(1)
C13	C17	1.80(2)
C14	C15	1.43(1)
C14	C19	1.51(2)
C15	C20	1.392(9)
C16	H16A	0.98(1)
C16	H16B	0.981(9)
C16	H16C	0.98(1)
C17	H17A	0.99(2)
C17	H17B	0.99(1)
C17	C18	1.34(3)
C18	H18A	0.98(2)
C18	H18B	0.98(2)
C18	H18C	0.98(3)
C19	H19A	0.979(9)
C19	H19B	0.98(1)
C19	H19C	0.98(1)
C20	C22	1.49(1)
C21	H21A	0.949(6)
C21	C22	1.39(1)
C22	C23	1.37(1)
C23	H23A	0.95(1)
C23	C24	1.39(1)
C24	H24A	0.949(7)
C24	C25	1.39(1)
C25	C26	1.47(1)
C26	C27	1.395(8)
C27	H27A	0.95(1)
C27	C28	1.39(1)
C28	H28A	0.949(6)
C28	C29	1.37(1)

C29	C30	1.380(8)
C29	C31	1.49(1)
C30	H30A	0.949(8)
C31	C35	1.396(8)
C31	C43	1.40(1)
C32	C33	1.42(1)
C32	C36	1.50(1)
C33	C34	1.392(9)
C33	C37	1.504(9)
C34	C35	1.418(9)
C34	C39	1.51(1)
C36	H36A	0.979(9)
C36	H36B	0.980(7)
C36	H36C	0.980(7)
C37	H37A	0.990(8)
C37	H37B	0.99(1)
C37	C38	1.50(1)
C38	H38A	0.980(9)
C38	H38B	0.98(1)
C38	H38C	0.98(1)
C39	H39A	0.980(7)
C39	H39B	0.980(7)
C39	H39C	0.98(1)
C40	C41	1.40(1)
C40	C44	1.50(1)
C41	C42	1.40(1)
C41	C45	1.51(1)
C42	C43	1.418(9)
C42	C47	1.51(1)
C44	H44A	0.98(1)
C44	H44B	0.980(8)
C44	H44C	0.980(8)
C45	H45A	0.99(1)
C45	H45B	0.991(9)
C45	C46	1.50(2)
C46	H46A	0.98(1)
C46	H46B	0.98(1)

C46	H46C	0.98(2)
C47	H47A	0.980(7)
C47	H47B	0.98(1)
C47	H47C	0.981(7)

Bond Angles for Re(BB3)(CO)$_3$Cl			
Atom1	**Atom2**	**Atom3**	**Angle**
Cl1	Re	N3	83.4(1)
Cl1	Re	N4	83.2(1)
Cl1	Re	C1	93.5(2)
Cl1	Re	C2	92.6(2)
Cl1	Re	C3	178.1(2)
N3	Re	N4	74.7(2)
N3	Re	C1	100.5(3)
N3	Re	C2	172.0(3)
N3	Re	C3	95.6(3)
N4	Re	C1	174.5(3)
N4	Re	C2	98.0(3)
N4	Re	C3	94.9(3)
C1	Re	C2	86.6(3)
C1	Re	C3	88.2(3)
C2	Re	C3	88.2(3)
F1	B1	F2	109.6(6)
F1	B1	N1	110.8(6)
F1	B1	N2	110.2(6)
F2	B1	N1	109.9(6)
F2	B1	N2	109.5(6)
N1	B1	N2	106.9(6)
F3	B2	F4	109.3(6)
F3	B2	N5	111.0(6)
F3	B2	N6	110.4(6)
F4	B2	N5	109.7(6)
F4	B2	N6	109.8(6)
N5	B2	N6	106.6(6)
B1	N1	C4	127.0(6)

B1	N1	C7	125.4(6)
C4	N1	C7	107.5(6)
B1	N2	C12	126.7(7)
B1	N2	C15	125.3(6)
C12	N2	C15	108.0(7)
Re	N3	C21	125.6(4)
Re	N3	C25	116.2(4)
C21	N3	C25	118.1(6)
Re	N4	C26	116.7(4)
Re	N4	C30	125.2(4)
C26	N4	C30	118.0(5)
B2	N5	C32	126.1(6)
B2	N5	C35	125.8(6)
C32	N5	C35	107.9(6)
B2	N6	C40	125.9(6)
B2	N6	C43	126.0(6)
C40	N6	C43	108.0(6)
Re	C1	O1	177.9(7)
Re	C2	O2	177.9(8)
Re	C3	O3	172.6(8)
N1	C4	C5	110.5(7)
N1	C4	C8	122.4(7)
C5	C4	C8	127.1(7)
C4	C5	C6	107.0(7)
C4	C5	C9	124.5(7)
C6	C5	C9	128.4(7)
C5	C6	C7	106.8(7)
C5	C6	C11	124.6(7)
C7	C6	C11	128.6(7)
N1	C7	C6	108.1(6)
N1	C7	C20	119.9(6)
C6	C7	C20	131.9(7)
C4	C8	H8A	109.4(7)
C4	C8	H8B	109.5(7)
C4	C8	H8C	109.4(7)
H8A	C8	H8B	109.6(8)
H8A	C8	H8C	109.5(8)

H8B	C8	H8C	109.5(8)
C5	C9	H9A	108.8(8)
C5	C9	H9B	108.8(8)
C5	C9	C10	113.6(8)
H9A	C9	H9B	107.7(9)
H9A	C9	C10	108.8(9)
H9B	C9	C10	108.9(9)
C9	C10	H10A	109(1)
C9	C10	H10B	109(1)
C9	C10	H10C	109(1)
H10A	C10	H10B	109(1)
H10A	C10	H10C	109(1)
H10B	C10	H10C	110(1)
C6	C11	H11A	109.5(7)
C6	C11	H11B	109.5(7)
C6	C11	H11C	109.4(7)
H11A	C11	H11B	109.5(8)
H11A	C11	H11C	109.4(8)
H11B	C11	H11C	109.5(8)
N2	C12	C13	110.5(9)
N2	C12	C16	122.8(9)
C13	C12	C16	127(1)
C12	C13	C14	108(1)
C12	C13	C17	122(1)
C14	C13	C17	126(1)
C13	C14	C15	106.2(8)
C13	C14	C19	124.4(9)
C15	C14	C19	129.3(9)
N2	C15	C14	107.6(7)
N2	C15	C20	120.1(7)
C14	C15	C20	132.1(8)
C12	C16	H16A	109.5(9)
C12	C16	H16B	109.5(9)
C12	C16	H16C	109.4(9)
H16A	C16	H16B	109(1)
H16A	C16	H16C	109(1)
H16B	C16	H16C	109(1)

C13	C17	H17A	114(1)
C13	C17	H17B	114(1)
C13	C17	C18	85(1)
H17A	C17	H17B	112(1)
H17A	C17	C18	115(2)
H17B	C17	C18	114(2)
C17	C18	H18A	109(2)
C17	C18	H18B	109(2)
C17	C18	H18C	109(2)
H18A	C18	H18B	109(2)
H18A	C18	H18C	110(2)
H18B	C18	H18C	110(2)
C14	C19	H19A	109(1)
C14	C19	H19B	109(1)
C14	C19	H19C	109(1)
H19A	C19	H19B	110(1)
H19A	C19	H19C	110(1)
H19B	C19	H19C	110(1)
C7	C20	C15	121.9(7)
C7	C20	C22	119.2(6)
C15	C20	C22	118.7(6)
N3	C21	H21A	118.4(6)
N3	C21	C22	123.1(6)
H21A	C21	C22	118.5(6)
C20	C22	C21	121.5(6)
C20	C22	C23	119.9(6)
C21	C22	C23	118.6(6)
C22	C23	H23A	120.3(8)
C22	C23	C24	119.3(8)
H23A	C23	C24	120.4(8)
C23	C24	H24A	120.3(8)
C23	C24	C25	119.4(8)
H24A	C24	C25	120.3(8)
N3	C25	C24	121.6(7)
N3	C25	C26	116.2(6)
C24	C25	C26	122.2(7)
N4	C26	C25	115.9(6)

N4	C26	C27	122.2(6)
C25	C26	C27	121.9(6)
C26	C27	H27A	120.9(7)
C26	C27	C28	118.2(7)
H27A	C27	C28	120.8(7)
C27	C28	H28A	119.9(7)
C27	C28	C29	120.1(7)
H28A	C28	C29	120.0(7)
C28	C29	C30	118.4(7)
C28	C29	C31	120.5(6)
C30	C29	C31	121.1(6)
N4	C30	C29	123.1(6)
N4	C30	H30A	118.4(6)
C29	C30	H30A	118.5(7)
C29	C31	C35	117.2(6)
C29	C31	C43	119.8(6)
C35	C31	C43	122.9(7)
N5	C32	C33	110.0(6)
N5	C32	C36	123.9(6)
C33	C32	C36	126.1(7)
C32	C33	C34	106.8(6)
C32	C33	C37	123.8(7)
C34	C33	C37	129.4(7)
C33	C34	C35	107.4(6)
C33	C34	C39	123.4(7)
C35	C34	C39	129.1(7)
N5	C35	C31	118.8(6)
N5	C35	C34	107.9(6)
C31	C35	C34	133.2(7)
C32	C36	H36A	109.5(7)
C32	C36	H36B	109.5(7)
C32	C36	H36C	109.4(7)
H36A	C36	H36B	109.6(8)
H36A	C36	H36C	109.4(8)
H36B	C36	H36C	109.5(8)
C33	C37	H37A	109.2(7)
C33	C37	H37B	109.3(7)

C33	C37	C38	111.6(7)
H37A	C37	H37B	108.0(8)
H37A	C37	C38	109.3(8)
H37B	C37	C38	109.4(8)
C37	C38	H38A	109(1)
C37	C38	H38B	109(1)
C37	C38	H38C	109(1)
H38A	C38	H38B	109(1)
H38A	C38	H38C	109(1)
H38B	C38	H38C	110(1)
C34	C39	H39A	109.5(7)
C34	C39	H39B	109.5(7)
C34	C39	H39C	109.5(7)
H39A	C39	H39B	109.5(8)
H39A	C39	H39C	109.4(8)
H39B	C39	H39C	109.4(8)
N6	C40	C41	110.1(7)
N6	C40	C44	122.9(7)
C41	C40	C44	127.0(7)
C40	C41	C42	106.8(7)
C40	C41	C45	126.4(8)
C42	C41	C45	126.8(8)
C41	C42	C43	106.8(7)
C41	C42	C47	124.3(8)
C43	C42	C47	128.8(7)
N6	C43	C31	119.4(6)
N6	C43	C42	108.3(6)
C31	C43	C42	132.3(7)
C40	C44	H44A	109.6(8)
C40	C44	H44B	109.5(8)
C40	C44	H44C	109.5(8)
H44A	C44	H44B	109.4(9)
H44A	C44	H44C	109.5(9)
H44B	C44	H44C	109.4(9)
C41	C45	H45A	108.9(8)
C41	C45	H45B	108.8(8)
C41	C45	C46	113.6(9)

H45A	C45	H45B	107.8(9)
H45A	C45	C46	108.9(9)
H45B	C45	C46	108.8(9)
C45	C46	H46A	109(1)
C45	C46	H46B	109(1)
C45	C46	H46C	109(1)
H46A	C46	H46B	110(1)
H46A	C46	H46C	109(1)
H46B	C46	H46C	109(1)
C42	C47	H47A	109.5(7)
C42	C47	H47B	109.5(7)
C42	C47	H47C	109.4(7)
H47A	C47	H47B	109.5(8)
H47A	C47	H47C	109.5(8)
H47B	C47	H47C	109.4(8)
Cl2	C48	H48A	106(1)
Cl2	C48	H48B	106(1)
Cl2	C48	C49	123(1)
H48A	C48	H48B	106(2)
H48A	C48	C49	107(2)
H48B	C48	C49	106(2)
Cl3	C49	C48	125(1)
Cl3	C49	H49A	106(1)
Cl3	C49	H49B	106(1)
C48	C49	H49A	106(2)
C48	C49	H49B	106(2)
H49A	C49	H49B	106(2)

Key Parameters	**Re(BB4)(CO)$_3$Cl**
Formula	$C_{49}H_{54}B_2Cl_3F_4N_6O_3Re$
F_W	1165.15
Crystal System	Orthorhombic
Space Group	$Pmn2_1$
a	27.663(4) Å
b	11.5494(15) Å
c	8.0100(10) Å
α	90°

β	90°
γ	90°
V	2558.7(6) Å^3
Z	2
Temp	200(2) K
D_{calcd}	1.512 g cm^{-3}
2θ range	53.16°
μ (Mo Kα)	2.592 mm^{-1}
Reflections	29089
Unique	6513
R (int)	0.0716
R_1	0.0390
wR_2	0.0772

Bond Length for Re(BB4)(CO)$_3$Cl		
Atom1	**Atom2**	**Length**
Re	Cl1	2.481(2)
Re	N1	2.220(4)
Re	C23	1.924(5)
Re	C24	1.916(8)
Re	N1	2.220(4)
Re	C23	1.924(5)
B1	F1	1.397(6)
B1	F2	1.383(6)
B1	N2	1.547(7)
B1	N3	1.547(7)
N1	C1	1.355(6)
N1	C5	1.348(6)
N2	C7	1.393(6)
N2	C10	1.353(6)
N3	C15	1.350(6)
N3	C18	1.393(6)
O1	C23	1.143(7)
O2	C24	1.14(1)
C1	C2	1.390(7)
C1	C1	1.473(7)

C2	H2A	0.951(5)
C2	C3	1.389(7)
C3	H3A	0.949(5)
C3	C4	1.365(8)
C4	H4A	0.950(6)
C4	C5	1.376(7)
C5	C6	1.505(7)
C6	C7	1.399(6)
C6	C18	1.389(7)
C7	C8	1.430(7)
C8	C9	1.402(7)
C8	C11	1.482(8)
C9	C10	1.407(8)
C9	C12	1.492(8)
C10	C14	1.494(7)
C11	H11A	0.980(7)
C11	H11B	0.981(5)
C11	H11C	0.979(8)
C12	H12A	0.990(6)
C12	H12B	0.990(6)
C12	C13	1.507(8)
C13	H13A	0.980(6)
C13	H13B	0.980(6)
C13	H13C	0.980(6)
C14	H14A	0.980(6)
C14	H14B	0.981(6)
C14	H14C	0.980(5)
C15	C16	1.41(1)
C15	C19	1.490(9)
C16	C17	1.399(7)
C16	C20	1.484(8)
C17	C18	1.431(7)
C17	C22	1.491(7)
C19	H19A	0.981(8)
C19	H19B	0.980(6)
C19	H19C	0.981(7)
C20	H20A	0.991(8)

C20	H20B	0.989(6)
C20	C21	1.50(1)
C21	H21A	0.980(8)
C21	H21B	0.980(9)
C21	H21C	0.980(9)
C22	H22A	0.980(6)
C22	H22B	0.980(5)
C22	H22C	0.980(6)
B1	F1	1.397(6)
B1	F2	1.383(6)
B1	N2	1.547(7)
B1	N3	1.547(7)
N1	C1	1.355(6)
N1	C5	1.348(6)
N2	C7	1.393(6)
N2	C10	1.353(6)
N3	C15	1.350(6)
N3	C18	1.393(6)
C1	C2	1.390(7)
C2	H2A	0.951(5)
C2	C3	1.389(7)
C3	H3A	0.949(5)
C3	C4	1.365(8)
C4	H4A	0.950(6)
C4	C5	1.376(7)
C5	C6	1.505(7)
C6	C7	1.399(6)
C6	C18	1.389(7)
C7	C8	1.430(7)
C8	C9	1.402(7)
C8	C11	1.482(8)
C9	C10	1.407(8)
C9	C12	1.492(8)
C10	C14	1.494(7)
C11	H11A	0.980(7)
C11	H11B	0.981(5)
C11	H11C	0.979(8)

C12	H12A	0.990(6)
C12	H12B	0.990(6)
C12	C13	1.507(8)
C13	H13A	0.980(6)
C13	H13B	0.980(6)
C13	H13C	0.980(6)
C14	H14A	0.980(6)
C14	H14B	0.981(6)
C14	H14C	0.980(5)
C15	C16	1.41(1)
C15	C19	1.490(9)
C16	C17	1.399(7)
C16	C20	1.484(8)
C17	C18	1.431(7)
C17	C22	1.491(7)
C19	H19A	0.981(8)
C19	H19B	0.980(6)
C19	H19C	0.981(7)
C20	H20A	0.991(8)
C20	H20B	0.989(6)
C20	C21	1.50(1)
C21	H21A	0.980(8)
C21	H21B	0.980(9)
C21	H21C	0.980(9)
C22	H22A	0.980(6)
C22	H22B	0.980(5)
C22	H22C	0.980(6)
O1	C23	1.143(7)

Bond Angles for Re(BB4)(CO)$_3$Cl			
Atom1	**Atom2**	**Atom3**	**Angle**
Cl1	Re	N1	84.4(1)
Cl1	Re	C23	91.0(2)
Cl1	Re	C24	178.6(2)
Cl1	Re	N1	84.4(1)
Cl1	Re	C23	91.0(2)
N1	Re	C23	101.1(2)

N1	Re	C24	96.7(2)
N1	Re	N1	75.1(1)
N1	Re	C23	174.3(2)
C23	Re	C24	87.9(3)
C23	Re	N1	174.3(2)
C23	Re	C23	82.4(2)
C24	Re	N1	96.7(2)
C24	Re	C23	87.9(3)
N1	Re	C23	101.1(2)
F1	B1	F2	108.9(4)
F1	B1	N2	109.3(4)
F1	B1	N3	109.7(4)
F2	B1	N2	111.3(4)
F2	B1	N3	111.3(4)
N2	B1	N3	106.2(4)
Re	N1	C1	114.9(3)
Re	N1	C5	127.7(3)
C1	N1	C5	117.4(4)
B1	N2	C7	126.1(4)
B1	N2	C10	126.0(4)
C7	N2	C10	107.8(4)
B1	N3	C15	125.6(4)
B1	N3	C18	126.1(4)
C15	N3	C18	108.1(4)
N1	C1	C2	122.1(4)
N1	C1	C1	117.1(4)
C2	C1	C1	120.7(4)
C1	C2	H2A	120.4(5)
C1	C2	C3	119.0(5)
H2A	C2	C3	120.6(5)
C2	C3	H3A	120.6(5)
C2	C3	C4	118.8(5)
H3A	C3	C4	120.6(5)
C3	C4	H4A	120.1(5)
C3	C4	C5	119.6(5)
H4A	C4	C5	120.3(5)
N1	C5	C4	123.0(4)

N1	C5	C6	120.6(4)
C4	C5	C6	116.4(4)
C5	C6	C7	118.5(4)
C5	C6	C18	119.0(4)
C7	C6	C18	122.1(4)
N2	C7	C6	119.5(4)
N2	C7	C8	108.4(4)
C6	C7	C8	132.0(4)
C7	C8	C9	106.4(4)
C7	C8	C11	129.5(4)
C9	C8	C11	124.1(5)
C8	C9	C10	107.0(4)
C8	C9	C12	128.3(5)
C10	C9	C12	124.7(5)
N2	C10	C9	110.3(4)
N2	C10	C14	121.9(4)
C9	C10	C14	127.8(5)
C8	C11	H11A	109.5(5)
C8	C11	H11B	109.5(5)
C8	C11	H11C	109.5(5)
H11A	C11	H11B	109.4(6)
H11A	C11	H11C	109.5(6)
H11B	C11	H11C	109.4(6)
C9	C12	H12A	108.9(5)
C9	C12	H12B	108.9(5)
C9	C12	C13	113.5(5)
H12A	C12	H12B	107.7(5)
H12A	C12	C13	108.9(5)
H12B	C12	C13	108.9(5)
C12	C13	H13A	109.6(5)
C12	C13	H13B	109.5(5)
C12	C13	H13C	109.5(5)
H13A	C13	H13B	109.4(6)
H13A	C13	H13C	109.4(6)
H13B	C13	H13C	109.5(6)
C10	C14	H14A	109.4(5)
C10	C14	H14B	109.5(5)

C10	C14	H14C	109.5(5)
H14A	C14	H14B	109.5(5)
H14A	C14	H14C	109.5(5)
H14B	C14	H14C	109.4(5)
N3	C15	C16	110.0(5)
N3	C15	C19	123.1(5)
C16	C15	C19	126.8(6)
C15	C16	C17	107.1(5)
C15	C16	C20	124.9(5)
C17	C16	C20	128.0(5)
C16	C17	C18	106.5(4)
C16	C17	C22	124.7(5)
C18	C17	C22	128.7(4)
N3	C18	C6	119.7(4)
N3	C18	C17	108.3(4)
C6	C18	C17	132.0(4)
C15	C19	H19A	109.5(6)
C15	C19	H19B	109.5(6)
C15	C19	H19C	109.5(6)
H19A	C19	H19B	109.4(7)
H19A	C19	H19C	109.5(7)
H19B	C19	H19C	109.4(7)
C16	C20	H20A	108.7(6)
C16	C20	H20B	108.8(6)
C16	C20	C21	114.0(6)
H20A	C20	H20B	107.7(6)
H20A	C20	C21	108.7(6)
H20B	C20	C21	108.7(6)
C20	C21	H21A	109.4(7)
C20	C21	H21B	109.4(7)
C20	C21	H21C	109.5(7)
H21A	C21	H21B	109.5(8)
H21A	C21	H21C	109.4(8)
H21B	C21	H21C	109.5(8)
C17	C22	H22A	109.5(5)
C17	C22	H22B	109.5(5)
C17	C22	H22C	109.5(5)

H22A	C22	H22B	109.4(5)
H22A	C22	H22C	109.5(5)
H22B	C22	H22C	109.5(5)
Re	C23	O1	175.1(5)
Re	C24	O2	176.9(7)
F1	B1	F2	108.9(4)
F1	B1	N2	109.3(4)
F1	B1	N3	109.7(4)
F2	B1	N2	111.3(4)
F2	B1	N3	111.3(4)
N2	B1	N3	106.2(4)
Re	N1	C1	114.9(3)
Re	N1	C5	127.7(3)
C1	N1	C5	117.4(4)
B1	N2	C7	126.1(4)
B1	N2	C10	126.0(4)
C7	N2	C10	107.8(4)
B1	N3	C15	125.6(4)
B1	N3	C18	126.1(4)
C15	N3	C18	108.1(4)
C1	C1	N1	117.1(4)
C1	C1	C2	120.7(4)
N1	C1	C2	122.1(4)
C1	C2	H2A	120.4(5)
C1	C2	C3	119.0(5)
H2A	C2	C3	120.6(5)
C2	C3	H3A	120.6(5)
C2	C3	C4	118.8(5)
H3A	C3	C4	120.6(5)
C3	C4	H4A	120.1(5)
C3	C4	C5	119.6(5)
H4A	C4	C5	120.3(5)
N1	C5	C4	123.0(4)
N1	C5	C6	120.6(4)
C4	C5	C6	116.4(4)
C5	C6	C7	118.5(4)
C5	C6	C18	119.0(4)

C7	C6	C18	122.1(4)
N2	C7	C6	119.5(4)
N2	C7	C8	108.4(4)
C6	C7	C8	132.0(4)
C7	C8	C9	106.4(4)
C7	C8	C11	129.5(4)
C9	C8	C11	124.1(5)
C8	C9	C10	107.0(4)
C8	C9	C12	128.3(5)
C10	C9	C12	124.7(5)
N2	C10	C9	110.3(4)
N2	C10	C14	121.9(4)
C9	C10	C14	127.8(5)
C8	C11	H11A	109.5(5)
C8	C11	H11B	109.5(5)
C8	C11	H11C	109.5(5)
H11A	C11	H11B	109.4(6)
H11A	C11	H11C	109.5(6)
H11B	C11	H11C	109.4(6)
C9	C12	H12A	108.9(5)
C9	C12	H12B	108.9(5)
C9	C12	C13	113.5(5)
H12A	C12	H12B	107.7(5)
H12A	C12	C13	108.9(5)
H12B	C12	C13	108.9(5)
C12	C13	H13A	109.6(5)
C12	C13	H13B	109.5(5)
C12	C13	H13C	109.5(5)
H13A	C13	H13B	109.4(6)
H13A	C13	H13C	109.4(6)
H13B	C13	H13C	109.5(6)
C10	C14	H14A	109.4(5)
C10	C14	H14B	109.5(5)
C10	C14	H14C	109.5(5)
H14A	C14	H14B	109.5(5)
H14A	C14	H14C	109.5(5)
H14B	C14	H14C	109.4(5)

N3	C15	C16	110.0(5)
N3	C15	C19	123.1(5)
C16	C15	C19	126.8(6)
C15	C16	C17	107.1(5)
C15	C16	C20	124.9(5)
C17	C16	C20	128.0(5)
C16	C17	C18	106.5(4)
C16	C17	C22	124.7(5)
C18	C17	C22	128.7(4)
N3	C18	C6	119.7(4)
N3	C18	C17	108.3(4)
C6	C18	C17	132.0(4)
C15	C19	H19A	109.5(6)
C15	C19	H19B	109.5(6)
C15	C19	H19C	109.5(6)
H19A	C19	H19B	109.4(7)
H19A	C19	H19C	109.5(7)
H19B	C19	H19C	109.4(7)
C16	C20	H20A	108.7(6)
C16	C20	H20B	108.8(6)
C16	C20	C21	114.0(6)
H20A	C20	H20B	107.7(6)
H20A	C20	C21	108.7(6)
H20B	C20	C21	108.7(6)
C20	C21	H21A	109.4(7)
C20	C21	H21B	109.4(7)
C20	C21	H21C	109.5(7)
H21A	C21	H21B	109.5(8)
H21A	C21	H21C	109.4(8)
H21B	C21	H21C	109.5(8)
C17	C22	H22A	109.5(5)
C17	C22	H22B	109.5(5)
C17	C22	H22C	109.5(5)
H22A	C22	H22B	109.4(5)
H22A	C22	H22C	109.5(5)
H22B	C22	H22C	109.5(5)
Re	C23	O1	175.1(5)

H25A	C25	H25B	109(2)
H25A	C25	Cl2	110(2)
H25A	C25	C25	78(2)
H25A	C25	C26	147(3)
H25A	C25	H26B	137(2)
H25A	C25	Cl3	103(2)
H25B	C25	Cl2	110(2)
H25B	C25	C25	121(2)
H25B	C25	C26	92(2)
H25B	C25	H26B	43(1)
H25B	C25	Cl3	112(2)
Cl2	C25	C25	122(2)
Cl2	C25	C26	85(2)
Cl2	C25	H26B	110(2)
Cl2	C25	Cl3	7.8(9)
C25	C25	C26	69(2)
C25	C25	H26B	92(2)
C25	C25	Cl3	123(2)
C26	C25	H26B	50(2)
C26	C25	Cl3	92(2)
H26B	C25	Cl3	117(2)
H26A	C26	H26B	108(2)
H26A	C26	Cl3	110(2)
H26A	C26	C25	162(3)
H26A	C26	C26	79(2)
H26A	C26	H26A	31.2(6)
H26A	C26	Cl2	98(1)
H26B	C26	Cl3	110(2)
H26B	C26	C25	82(2)
H26B	C26	C26	113(2)
H26B	C26	H26A	117(2)
H26B	C26	Cl2	114(1)
Cl3	C26	C25	52(2)
Cl3	C26	C26	130(2)
Cl3	C26	H26A	127(2)
Cl3	C26	Cl2	12.3(7)
C25	C26	C26	111(3)

C25	C26	H26A	155(2)
C25	C26	Cl2	64(2)
C26	C26	H26A	48(1)
C26	C26	Cl2	131(2)
H26A	C26	Cl2	117(1)
C26	H26A	C26	53(1)
C26	H26B	C25	48(2)
C25	Cl2	C26	31(1)
C26	Cl3	C25	35(1)
C25	C25	C26	69(2)
C25	C25	H26B	92(2)
C25	C25	Cl3	123(2)
C25	C25	H25A	78(2)
C25	C25	H25B	121(2)
C25	C25	Cl2	122(2)
C26	C25	H26B	50(2)
C26	C25	Cl3	92(2)
C26	C25	H25A	147(3)
C26	C25	H25B	92(2)
C26	C25	Cl2	85(2)
H26B	C25	Cl3	117(2)
H26B	C25	H25A	137(2)
H26B	C25	H25B	43(1)
H26B	C25	Cl2	110(2)
Cl3	C25	H25A	103(2)
Cl3	C25	H25B	112(2)
Cl3	C25	Cl2	7.8(9)
H25A	C25	H25B	109(2)
H25A	C25	Cl2	110(2)
H25B	C25	Cl2	110(2)
C25	C26	C26	111(3)
C25	C26	H26A	155(2)
C25	C26	Cl2	64(2)
C25	C26	H26A	162(3)
C25	C26	H26B	82(2)
C25	C26	Cl3	52(2)
C26	C26	H26A	48(1)

C26	C26	Cl2	131(2)
C26	C26	H26A	79(2)
C26	C26	H26B	113(2)
C26	C26	Cl3	130(2)
H26A	C26	Cl2	117(1)
H26A	C26	H26A	31.2(6)
H26A	C26	H26B	117(2)
H26A	C26	Cl3	127(2)
Cl2	C26	H26A	98(1)
Cl2	C26	H26B	114(1)
Cl2	C26	Cl3	12.3(7)
H26A	C26	H26B	108(2)
H26A	C26	Cl3	110(2)
H26B	C26	Cl3	110(2)
C26	H26A	C26	53(1)
C25	H26B	C26	48(2)
C26	Cl2	C25	31(1)
C25	Cl3	C26	35(1)